UNIVERSITAT DE BARCELONA

Study of immune population infiltrated in white adipose tissue: Novel target genes in obesity and metabolic diseases

Marjorie Reyes Farías

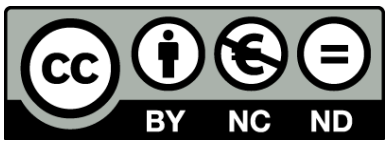

Aquesta tesi doctoral està subjecta a la llicència ***Reconeixement- NoComercial – SenseObraDerivada 4.0. Espanya de Creative Commons***.

Esta tesis doctoral está sujeta a la licencia ***Reconocimiento - NoComercial – SinObraDerivada 4.0. España de Creative* Commons**.

This doctoral thesis is licensed under the ***Creative Commons Attribution-NonCommercial-NoDerivs 4.0. Spain License***.

UNIVERSITAT DE BARCELONA

Facultat de Farmàcia
i Ciències de l'Alimentació

Programa de Doctorat en Alimentació i Nutrició

Dpt. Bioquímica i Fisiologia

Study of immune population infiltrated in white adipose tissue: Novel target genes in obesity and metabolic diseases.

Marjorie Reyes Farias

Barcelona, 2023

UNIVERSITAT DE BARCELONA
Facultat de Farmàcia
i Ciències de l'Alimentació

Programa de Doctorat en Alimentació i Nutrició

Study of immune population infiltrated in white adipose tissue: Novel target genes in obesity and metabolic diseases.

Memòria presentada per Marjorie Reyes Farias per optar al títol de doctor per la Universitat de Barcelona

David Sánchez Infantes Laura Herrero Rodríguez

Xavier Remesar

Marjorie Reyes Farias

Barcelona, 2023

"Lo que caracteriza al hombre de ciencia

no es la posesión del conocimiento o

de verdades irrefutables, sino la búsqueda

desinteresada e incesante de la verdad."

Karl Popper

AGRADECIMIENTOS

RESUMEN

La obesidad es una condición crónica cuya incidencia se ha triplicado en las últimas cuatro décadas. Esta condición está asociada a una activación de la respuesta proinflamatoria de las células inmunes infiltradas en el WAT, lo que puede conducir a diferentes comorbilidades, afectando directamente la esperanza de vida.

El WAT es órgano principal de almacenamiento de lípidos, pero también actúa como un órgano endocrino pudiendo responder a cambios metabólicos. Por lo tanto, cambios en este tejido puede conducir el desarrollo de comorbilidades asociadas a obesidad. El WAT se distribuye en dos depósitos: SAT y VAT, cada uno con sus propias funciones metabólicas. Se ha descrito que la SAT tiene un papel protector y se asocia inversamente con el desarrollo de IR y T2D. Al mismo tiempo, el VAT está relacionado con un empeoramiento del estado metabólico.

Este tejido, está compuesto por una población heterogénea de células que incluyen preadipocitos, fibroblastos, células endoteliales, células madre y células inmunitarias que cambian según el estado metabólico. Las células inmunitarias regulan la función del WAT, que, en condición de obesidad, promueven la activación de la una señalización inflamatoria, hipóxica y fibrótica en este tejido. Debido a que los ATMs son la población inmune más abundante contribuyen en una proporción más alta a la alteración de la homeostasis en WAT en sujetos obesos.

Actualmente existe poca información respecto a vías de señalización alteradas en VAT en respecto a SAT asociadas al desarrollo de enfermedades metabólicas. Por ello, el objetivo de este trabajo fue determinar dianas genéticas

que contribuyan a un peor pronóstico metabólico para encontrar su posible papel en el desarrollo de la obesidad.

Nuestro trabajo muestra por primera vez que el fenotipo de ATMs tienen un perfil de expresión génica diferente según el depósito estudiado. Nuestro trabajo propone nuevas dianas implicadas en la obesidad y enfermedades metabólicas relacionadas.

ABSTRACT

Obesity is a chronic condition with a multifactorial etiology whose incidence has tripled in the last four decades. This condition is associated with a low-grade inflammation caused by an activation of the proinflammatory response of the immune cells infiltrated in the white adipose tissue (WAT), which can lead to different comorbidities, directly affecting life expectancy.

WAT is the main organ responsible for energy storage in the form of lipids, and due to its heterogeneous composition, it acts as an endocrine organ able to respond to metabolic changes. Therefore, obesity promotes changes in metabolism, leading to inflammatory, hypoxic, and fibrotic events in WAT that trigger the development of metabolic diseases. WAT is distributed into two depots: subcutaneous adipose tissue (SAT) and visceral adipose tissue (VAT), each one with its biochemical features and metabolic role. SAT has been reported to be protective in overall metabolism, while VAT has been linked to worsening metabolic status. However, little is known about which genes or pathways are altered in VAT compared to SAT, promoting the development of metabolic diseases. Thus, this work aimed to identify novel target genes contributing to a worse metabolic prognosis to find their potential role in obesity-related development with each depot and inflammatory state.

First, we found that IL-16, a cytokine linked to airway pathologies, is expressed in human WAT and that its expression changes between SAT and VAT in patients with obesity. Bioinformatic analyses showed that this cytokine is related to activating pro-inflammatory pathways and T cells activation. Our *in vitro* models

showed that during adipogenesis and in mature adipocytes, IL-16 seems to modulate lipid metabolism, fibrosis, and inflammatory signaling, suggesting a role in obesity.

Because adipose tissue macrophages (ATMs) are the most abundant immune cell population in WAT, we evaluated its phenotype in both SAT and VAT depots. We showed for the first time that the phenotype of macrophages infiltrated in human WAT has a different gene expression profile according to the depot. We described two target genes overexpressed in SAT compared to VAT in individuals with obesity: MYO1E and NCEH1, suggesting that these genes are related with the protective role of SAT in metabolism. Our results showed that silencing of *Myo1e* is associated with activating the inflammatory signalling from macrophages, reducing their migratory capacity. At the same time, *Nceh1* knockdown is also related with a pro-inflammatory profile of the cells and might have a role in lipid accumulation in obesity.

In conclusion, this study proposes novel target genes involved in the development of obesity and its related metabolic diseases.

TABLE OF CONTENTS

FIGURES INDEX

TABLES INDEX

ABBREVIATIONS

7-AAD	:	7-Aminoactinomycin D (Live Dead Dye)
ACAT1	:	Acetyl-CoA acetyltransferase 1
ACP5	:	Acid phosphatase 5
ADIPOQ	:	Adiponectin
AIF1	:	Allograft inflammatory factor 1
ANLN	:	Anillin, Actin Binding Protein
APOC1	:	Apolipoprotein C1
ARG1	:	Arginase 1
AT	:	Adipose tissue
ATGL	:	Adipose triglyceride lipase
ATM	:	Adipose tissue infiltrated macrophages
ATP	:	Adenosine triphosphate
BAT	:	Brown adipose tissue
BIRC5	:	Baculoviral IAP Repeat Containing 5
BMI	:	Body mass index
BP	:	Biological process
BSA	:	Bovine serum albumin
C/EBP	:	CCAAT-enhancer-binding protein
C1Q	:	Complement C1q
CBS	:	Newborn calf bovine serum
CC	:	Celullar component
CCL2	:	Chemokine (C-C motif) ligand 2 (also called MCP1)
CCL20	:	Chemokine (C-C motif) ligand 20

CD11b	:	Integrin alpha M, also known as ITGAM
CD14	:	Cluster of differentiation 14
CD16	:	Cluster of differentiation 16, also known as FcγRIII
CD206	:	Cluster of differentiation 206, also known as Mannose Receptor C-Type 1 (MRC1)
CD300E	:	Cluster of differentiation 300e, also know as CLM-2
CD36	:	Cluster of differentiation 36, also known as fatty acid translocase (FAT)
CD99	:	Cluster of differentiation 99, also known as MIC2
CDK1	:	Cyclin Dependent Kinase 1
cDNA	:	Complementary DNA
CLS	:	Crown like structures
COL4A	:	Collagen Type IV Alpha
COLA6	:	Collagen Type VI Alpha
CPT1	:	Carnitine Palmitoyltransferase 1
CSF3R	:	Colony Stimulating Factor 3 Receptor
CTSD	:	Cathepsin D
CVD	:	Cardiovascular disease
CXCL2	:	C-X-C Motif Chemokine Ligand 2
CXCL3	:	C-X-C Motif Chemokine Ligand 3
CXCL8	:	C-X-C Motif Chemokine Ligand 8, also known as IL-8
CYP27A1	:	Cytochrome P450 Family 27 Subfamily A Member 1
DAMP	:	Damage-associated molecular pattern
DMEM	:	Dulbecco's Modified Eagle Medium
DMSO	:	Dimethyl Sulfoxide

ECM	:	Extracellular matrix
ER	:	Endoplasmic reticulum
EREG	:	Epiregulin
FA	:	Fatty acid
FABP4	:	Fatty acid binding protein 4
FAO	:	Fatty acid oxidation
FBS	:	Fetal bovine serum
FC	:	Free cholesterol
FCGR3A	:	Low affinity immunoglobulin gamma Fc region receptor III-A
FCN1	:	Ficolin-1, also termed M-ficolin
FDR	:	False discovery rate
FFA	:	Free fatty acid
FPR1	:	Formyl peptide receptor 1
G0S2	:	G0/G1 switch 2 protein
GLUT4	:	Glucose transporter type 4
GO	:	Gene ontology
GPD1	:	Glycerol-3-Phosphate Dehydrogenase 1
GSEA	:	Gene set enrichment analysis
HEA	:	Healthy
HFD	:	High fat diet
HIF1a	:	Hypoxia Inducible Factor 1 Subunit Alpha
iBAT	:	Beige/brite adipose tissue or Inducible brown adipose tissue
IBMX	:	3-isobutyl-1-methylxanthine

IFITM2	:	Interferon Induced Transmembrane Protein 2
IFITM3	:	Interferon Induced Transmembrane Protein 3
IL-16	:	Interleukin 16
IL-1b	:	Interleukin 1 beta
IL-4	:	Interleukin 4
IL-6	:	Interleukin 6
IR	:	Insulin resistance
IRS-1	:	Insulin receptor substrate 1
ITNL1	:	Intelectin 1, also known as omentin
ITNL2	:	Intelectin 2
KPNA2	:	Karyopherin Subunit Alpha 2
LAL	:	Lipase A, Lysosomal Acid Type
LCN2	:	Lipocalin 2
LD	:	Lipid droplet
LEP	:	Leptin
LPS	:	Lipopolysacaride
LST1	:	Leukocyte Specific Transcript 1
MANOVA	:	Multivariate analysis of variance
MARCO	:	Macrophage Receptor With Collagenous Structure
MF	:	Molecular function
MMPs	:	Matris metalloproteases
MMP9	:	Matrix metallopeptidase 9
MNDA	:	Myeloid Cell Nuclear Differentiation Antigen
MS4A6A	:	Membrane Spanning 4-Domains A6A
MS4A7	:	Membrane Spanning 4-Domains A7

MSR1	:	Macrophage Scavenger Receptor 1
MYO1E	:	Myosin IE
MYO1F	:	Myosin IF
NAAA	:	N-Acylethanolamine acid amidase
NAFLD	:	Non-alcoholic fatty liver disease
NCEH1	:	Neutral cholesterol ester hydrolase 1
NLRP3	:	NLR family pyrin domain containing 3
NUSAP1	:	Nucleolar And Spindle Associated Protein 1
OECD	:	Organization for Economic Co-operation and Development
OLR1	:	Oxidized low density lipoprotein receptor 1
OXPHOS	:	Oxidative phosphorylation
P/S	:	Penicillin-Streptomycin
PA	:	Palmitate
PCA	:	Principal component analysis
PCR	:	Polymerase chain reaction
PFA	:	Paraformaldehyde
PGC1α	:	PPARγ coactivator 1-α
PLIN	:	Perilipin
PPARγ	:	Peroxisome proliferator-activated receptor-γ
PREF1	:	Delta Like Non-Canonical Notch Ligand 1, also called Dlk1/FA1
PSAP	:	Prosaposin
PTPRC	:	Protein Tyrosine Phosphatase Receptor Type C
qPCR	:	Quantitative polymerase chain reaction

RHEB	:	Ras homolog, MTORC1 binding
RHOC	:	Ras homolog family member C
RIN	:	RNA integrity number
RPS19	:	Ribosomal protein S19
S100A8	:	S100 calcium binding protein A8
S100A9	:	S100 calcium binding protein A9
S100A12	:	S100 calcium binding protein A12
SAT	:	Subcutaneous adipose tissue
SAT1	:	Spermidine/Spermine N1-Acetyltransferase 1
SELL	:	Selectin L
SERPINA1	:	Serpin Family A Member 1
siRNA	:	Small interfering RNA
SPN	:	Sialophorin
SR-A1	:	Macrophage Scavenger Receptor 1, also known as MSR1
SRGN	:	Serglycin
SVF	:	Stromalvascular fraction
T2D	:	Type II diabetes
TCF7L2	:	Transcription factor 7 like 2
TGF-β	:	Transforming growth factor beta
TIMP1	:	TIMP metallopeptidase inhibitor 1
TLR4	:	Toll like receptor 4
TNF-α	:	Tumor Necrosis Factor alpha
TPM	:	Transcripts per million
TPX2	:	TPX2 Microtubule Nucleation Factor

TYMS	:	Thymidylate synthetase
UBE2C	:	Ubiquitin conjugating enzyme E2 C
UCP1	:	Uncoupling protein-1
UNH	:	Unhealthy
VAT	:	Visceral adipose tissue
VCAN	:	Versican
VEGF	:	Vascular endothelial growth factor
WAT	:	White adipose tissue
WHO	:	World health organization
YBX1	:	Y-Box binding protein 1
ZFP36L2	:	ZFP36 ring finger protein like 2

1. INTRODUCTION

1.1 Obesity: Prevalence, causes and consequences

Obesity is a chronic relapsing progressive disease with a multifactorial etiology [1, 2]. The worldwide incidence of this disease has tripled in the last four decades, becoming one of the most prevalent diseases worldwide [3]. In this context, the World Health Organization (WHO) reported that in 2016, 13% of the worldwide adult population was overweight or obese [4]. Additionally, the Organization for Economic Co-operation and Development (OECD) indicates that 56% of people over 15-years old has overweight and obesity [5]. Here in Spain, the European Health Survey registered that the prevalence of overweight and obesity reached 61.4% in men and 46.1% in women [6].

Obesity is characterized by the excessive or abnormal accumulation of adipose tissue in the body, caused by a long-term energy imbalance between calorie intake and expenditure [7]. Obesity is defined as an increase in body weight above 20% of the ideal weight, according it age and sex [8]. However, in clinical practice, obesity degree is defined according to the Body Mass Index (BMI) [9]. BMI alloy to classify the weight of a person into different categories according to their nutritional status (Table 1). This index is calculated by dividing the weight of a person (expressed in kilograms) by its height (in meters squared) (kg/m^2).

Obesity is a significant risk factor for several chronic diseases, such as cardiovascular disease (CVD), insulin resistance (IR), type II diabetes (T2D), non-alcoholic fatty liver disease (NAFLD), and degenerative disorders, including

dementia, airway disease, and some types of cancers [10-12]. In addition, adult obesity is related to a reduction in life expectancy [13-17].

Table 1. WHO classification of metabolic status according to BMI.

Classification	BMI (kg/m^2)
Underweight (severe thinness)	< 16.0
Underweight (moderate thinness)	16.0 – 16.9
Underweight (mild thinness)	17.0 – 18.4
Normal range	18.5 – 24.9
Overweight (Pre-obese)	25.0 – 29.9
Obese (Class I)	30.0 – 34.9
Obese (Class II)	35.0 – 39.9
Obese (Class III)	≥ 40.0

1.2 Adipose tissue classification and distribution

Adipose tissue (AT) is classified into brown (BAT), pink, beige/brite, and white adipose tissue (WAT) [18-20] (Figure 1). BAT is a tissue mainly characterized by multilocular lipid droplets and a large number of mitochondria, which confer the ability to produce heat through non-shivering thermogenesis to maintain body temperature [21]. Beige/brite AT (or inducible BAT, iBAT) arises from WAT exposed to chronic cold exposure having an intermediate phenotype between BAT and WAT, which stores triglycerides and contributes to heat production [22].

Pink adipose tissue, present during pregnancy and lactation phases, comprises milk-secreting alveolar cells with a high lipid droplet content and milk-containing granules [23]. Similarly, this tissue could change into WAT and BAT post-lactation [24].

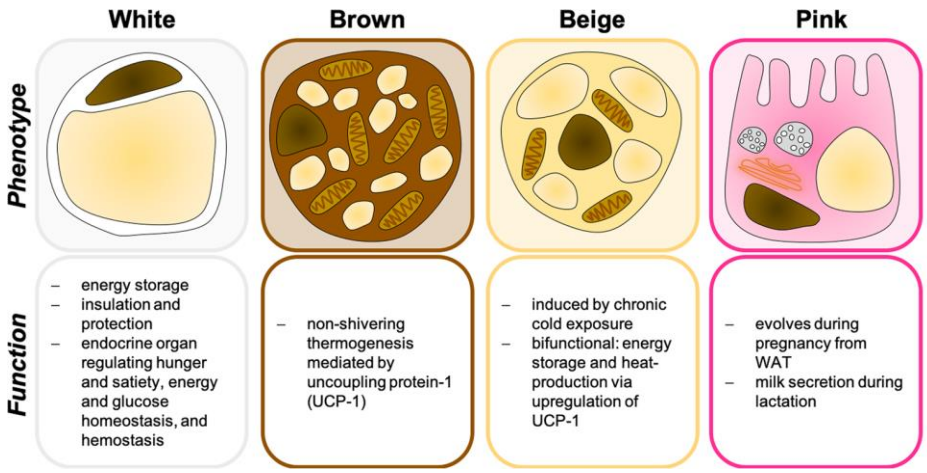

Figure 1. Types of adipocytes.

(From Zinngrebe, *et* al. [20])

Finally, WAT is composed mainly of large adipocytes with a single lipid droplet and less mitochondria than BAT, which confers the capacity for energy storage, through the accumulation of lipids [25]. Although WAT is composed mainly of adipocytes, this organ is also a source of heterogeneous cell populations such as pre-adipocytes, fibroblasts, or immune cells [26]. For this reason, even though the primary function of WAT is lipid storage, it also has a crucial endocrine role, being able to respond to metabolic changes [27, 28]. Furthermore, in humans, WAT could be classified according to its distribution into two main depots: visceral WAT (VAT), which includes omental, mesenteric, retroperitoneal, gonadal, and pericardial WAT, and subcutaneous WAT (SAT), which is located under the skin. Both depots are broadly studied for their association with insulin resistance (IR) development and cardiometabolic risk [29, 30]. However, each depot has different biochemical features and metabolic functions. For example, it has been described that WAT distribution has a direct effect on overall metabolism [31, 32], and some studies

demonstrate that a high VAT amount is associated with metabolic dysregulation [33, 34], promoting glucose intolerance and IR [35].

Furthermore, *in vitro* assays have shown that adipocytes isolated from VAT have higher lipid synthesis and lipolysis than SAT adipocytes [36, 37]. Additionally, portal theory explains that all metabolites of VAT are released into the portal vein; therefore, an increase in VAT size could be responsible for metabolic complications associated with liver status [38, 39]. Consequently, increased VAT mass is an independent factor in metabolism deterioration, and the size of this depot is directly related with a poor prognosis of metabolic diseases [40]. On the other hand, some studies propose that an increase in SAT mass has a protective role and is inversely associated with glucose intolerance, IR, and risk of T2D diagnosis [35, 41]. A decrease in triglyceride accumulation in SAT results in increased lipid deposition in VAT, leading to metabolic complications [37, 42, 43].

1.3 Changes of WAT during obesity development

During obesity development, all depots increase in weight and size, strongly correlating with the metabolic status (Figure 2). In fact, in humans, the percentage of VAT in obese subjects strongly correlates with IR and poor glycemic control [41, 44, 45]. In animal models, surgical removal of this tissue prevents IR and delays T2D development [46]. Furthermore, obese subjects have less SAT, contributing to further deterioration of insulin response and promoting T2D establishment [44, 47]. In addition, insulin-sensitive obesity is linked to a smaller VAT under the same BMI, suggesting SAT increase [48]. All that evidence indicates that both SAT and VAT contribute to the development of IR, however, their roles are contrary. While SAT

increase is associated with better metabolic status, VAT increase is linked with worsening metabolic status.

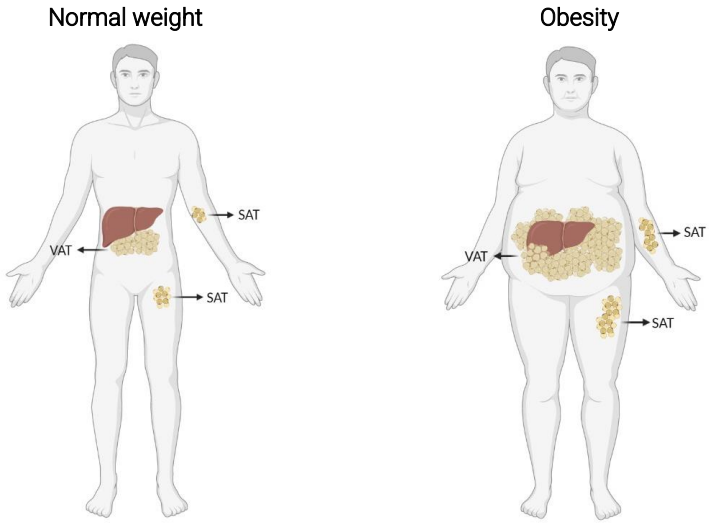

Figure 2. Changes in the distribution of adipose tissue changes with obesity.
Distribution of WAT is associated with development of metabolic dysregulation. In obesity status an increase of SAT, VAT, and VAT/SAT ratio worsen the metabolic status observe in obese subjects. (From Reyes-Farias, *et* al. [26])

1.4 Meta-inflammation: The onset of metabolic diseases

WAT is a highly active organ involved in numerous metabolic, hormonal, and immune processes [49, 50]. It has been described that an increase in hypertrophy and hyperplasia causes local and systemic low-grade chronic inflammation, or meta-inflammation, that triggers the development of severe metabolic diseases [51, 52].

Adipokines, such as Adiponectin, Leptin, IL-6, TNF-α, or CCL2, among others, are secreted by the WAT and contribute to the structural and functional rearrangement of this tissue [53]. It is broadly described that in obesity, an increase

in triglyceride accumulation in the adipocyte causes an enlargement of WAT and, consequently, a dysregulation in the secretion of adipokines In addition, the secretion of pro-inflammatory cytokines by WAT promotes the migration and infiltration of immune cells into the WAT that will that will also contribute to the inflammation process [54], thus, promoting a chronic and self-maintained low-grade inflammation associated with several obesity-related pathologies [55] (Figure 4).

As previously evidenced, the number of adipocytes in the WAT of an individual remains mainly constant throughout life [56]. Therefore, an increase in WAT translates into an increase in the hypertrophy of adipocytes [57]. The consequent triglyceride release activates TRL4 receptors in macrophages, promoting a TNF-α secretion [57-59]. Both triglycerides and TNF-α are crucial to IR development because they inhibit the IRS-1 signaling cascade, affecting glucose uptake into the WAT [60-63]. Furthermore, WAT inflammation directly affects insulin sensitivity and is associated with T2D and CVD development. Thus, WAT increase promotes infiltration of pro-inflammatory immune cells, which secretes cytokines that promotes an inflammatory phenotype and worse prognosis in related metabolic illness [64, 65].

1.4.1 ATMs: The main immune cells that control the meta-inflammation

Despite adipocytes are the main cell type present in WAT, immune cells play a broad role in both local and systemic metabolism. Processes like the expansion of adipose tissue mass or the activation of lipolysis lead to the recruitment and activation of immune cells in WAT [66].

Each WAT subpopulation changes according to its metabolic status. In this context, WAT-resident macrophages were the first immune cell population described to infiltrate the WAT. Interestingly, in 2003 some researchers found differences in WAT-infiltrated macrophages (ATM) and their surface markers between lean and obese subjects in mice and humans [67]. ATM could be broadly classified as M1, which has a pro-inflammatory phenotype, and M2, characterized by an immunosuppressive phenotype. Both subpopulations are present in WAT at different rates. M1 phenotype is predominantly found in dysfunctional/obese WAT and has a high proportion in subjects with metabolic complications [68]. In this context, hypertrophy of WAT increases CCL2 expression in adipocytes, secretion of adipokines, adipocyte death, and recruitment of macrophages [69]. On the other hand, M2 phenotype ATM promotes AT homeostasis, tissue remodeling, and insulin sensitivity, and they are predominantly found in healthy/lean WAT [68].

Studies with human and animal models showed increased BMI accompanied by higher macrophage infiltration in WAT and a deterioration in insulin sensitivity [70]. Conversely, weight loss raises WAT macrophage recruitment at the initial step. However, the pro-inflammatory phenotype could be maintained or decreased according to interventions and models of study. [71-76].

For this reason, an increase in adipose tissue due to obesity results in a hyperactive organ able to secrete several pro-inflammatory molecules, driving alterations in metabolic and endocrine functions, which contribute to the development of metabolic syndrome [133-135]. Furthermore, this pathology is characterized by low-grade chronic inflammation or meta-inflammation [136]. Thus,

in obesity status, the increased adipose tissue drives meta-inflammation, the beginning of the development of comorbidities associated with obesity [136, 137].

1.4.2 Lipid-laden macrophages and lipotoxicity

As described above, obesity promotes the remodeling and release of lipids by adipocytes engulfed by ATM [77]. ATM lipid content correlates with BMI in human and animal models and is significantly more visceral than subcutaneous ATM [71, 78, 79]. Fatty acid exposure promotes pro-inflammatory phenotype in ATM [80-82]. Extracellular free fatty acids (FFA) exert their effects in Toll-like receptor (TLR)-dependent and -independent manner [83, 84]. On the other hand, intracellular FA promotes endoplasmic reticulum and oxidative stress, which exacerbates proinflammatory signaling in the macrophages [85, 86]. FFA also acts as danger-associated molecular patterns (DAMP), leading to an NLRP3 inflammasome-mediated inflammation [87, 88]. This pro-inflammatory environment FA translates into a pathogenic mechanism underlying lipotoxicity in obesity-associated diseases [89] (Figure 3).

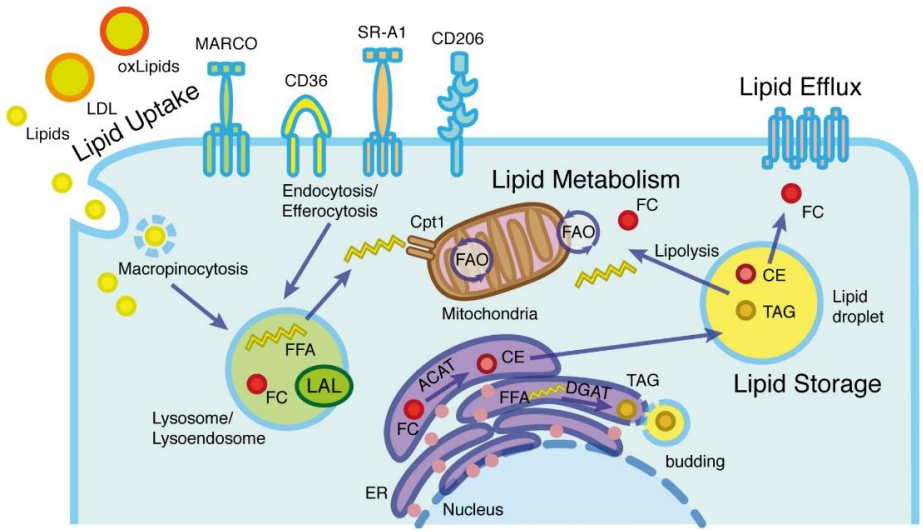

Figure 3. Mechanisms of lipid handling of macrophages.
The Uptake of different lipid species, such as native LDL, oxidized LDL particles, or free fatty acids, is facilitated by different scavenger receptors (CD36, MARCO, SR-A1, CD206). Lipids are trafficked to lysosomes and endo-lysosomes, in which complex lipids are degraded into free cholesterol (FC) and fatty acids (FFA) by the lysosomal acid lipase (LAL). Then, FC and FFA are transported to the endoplasmic reticulum (ER), where the acyl-coenzyme cholesterol acyltransferase-1 (ACAT1) converts deleterious FC to cholesteryl esters (CE). TAG and CE are shuttled into budding lipid droplets (LD), which represent the major lipid storage mechanism. Upon energy demand, macrophages can either directly shuttle lysosomal-derived FFA to mitochondria or derive FC and FFA from LD, which is subsequently transported into the mitochondria via carnitine palmitoyl-transferase I (CPT1). FC and FFA are further used as fuel for FAO and ATP production. Alternatively, lipid droplet-derived FC can be exported via ATP-binding cassette (ABC) transporters. (From Vogel, *et* al. [88]).

1.4.3 MYO1E a regulatory protein related with macrophages pro-inflammatory phenotype

Myo1E is widely expressed in humans mostly in immune cells, like dendritic cells, macrophages and B lymphocytes, participate in the clathrin-mediated endocytosis [90-92] and plays an important role in the major histocompatibility complex II (MHCII) presentation process [93]. Although its role in macrophages is not completely described, there some evidence that participates in the phagosome

closure cups [94]. Additionally, in LPS-stimulated macrophages, MYO1E reduces cell spreading, chemokine secretion and antigen presentation [94] and its deficiency is related with an increased secretion of CCL2 [93].

1.4.4 NCEH1 alleviates lipid accumulation in foam cells.

NCEH1 is a key regulator of hydrolysis of intracellular CE and in macrophages is expressed mainly in foam cells during atherosclerosis [95]. This enzyme participates in the reverse cholesterol transport, meaning that NCEH1 reduce the lipid droplet size in macrophages supporting the hydrolysis of CE and participating in the FC efflux from macrophages, stimulating the remotion of atherosclerotic lesions [96-98]. Currently, no evidence of the role of this enzyme in ATM or obese WAT has been reported.

1.5 WAT remodeling: A hallmark of obesity-related pathologies

One of the changes in adipose tissue in response to nutrient deprivation and excess is the remodeling of the WAT, which involves modifications in shape, size, structure, and composition due to a physiological, adaptive, or pathological mechanism [71, 99-103]. During remodeling, changes in adipocyte hypertrophy and hyperplasia have been observed, as well as in the extracellular matrix of the tissue and its angiogenesis [104]. However, Arner, *et* al. found that hypertrophy negatively correlates with hyperplasia of WAT independently of BMI [105]. They classified the subjects as having either hyperplasia or hypertrophy and found that the number of new adipocytes per year was 70% less in hypertrophic compared with hyperplasic classified subjects [105]. Impaired adipogenesis is present in hypertrophic obesity and contributes to the development of IR in obesity [106, 107]. Moreover, obesity-

associated metabolic complications are linked to a decreased lifespan [108]. Metabolic interventions driving weight loss also increase life expectancy [109-111]. Additionally, rapamycin-treated, and knock-out mice with limited adipogenesis show an increase in lifespan [112-115].

1.5.1 ECM: A driver of WAT-fibrosis

Seminal studies demonstrated that in the late stages of obesity, there is an accumulation of extracellular matrix (ECM) proteins, and, consequently, WAT fibrosis, which is related to the pro-inflammatory phenotype observed in obesity [102, 116, 117]. An *in vitro* model of adipocytes treated with macrophages-conditioned media shows increased gene expression of metalloproteinases (MMPs) [118]. Additionally, when transcriptomic analysis in AT from obese subjects was performed, it has found that an increase in ECM components (which decreased after bariatric surgery) was accompanied by an increased expression of some enzymes responsible for ECM degradation [119]. Both results indicate that WAT continuously undergoes fibrotic remodeling in response to weight changes in individuals [120]. Additionally, obese humans and murine models show that WAT collagen gene expression increases in obese subjects and correlates with insulin resistance, inflammatory markers, fibrotic size areas, and the number of infiltrated macrophages [121-125]. Moreover, collagen knock-out mice showed less AT fibrosis and inflammation and improved glucose metabolism [125].

1.5.2 Apoptosis in WAT-remodeling

It has been reported that adipocyte apoptosis and fibrosis are crucial events promoting WAT macrophage infiltration and obesity-associated metabolic diseases

[126, 127]. AT from mice fed with HFD showed more hypertrophy and inflammation, typically associated with a pro-apoptotic phenotype [127]. Moreover, in obese mice and humans, intrinsic apoptosis pathways were activated, and inhibition of adipocyte apoptosis in mice protects from macrophage infiltration and the development of fatty liver and IR [127]. WAT-macrophages infiltration is characterized by the presence of crown-like structures (CLS) surrounding dead adipocytes [128, 129] and promoting pro-inflammatory signaling, a hallmark of obesity-related diseases [130, 131]. However, the inducible elimination of adipocytes in a mouse model, through targeted activation of caspase-8, promotes the influx of alternative-activated M2 macrophages [132]. Altogether, adipocyte apoptosis might be the origin of AT macrophage infiltration, thus triggering obesity-related diseases.

1.5.3 WAT-mitochondrial dysfunction

It has been described that mitochondria are responsible of the metabolic control of WAT, being the main source of ATP, similarly than other tissues [133]. WAT mitochondria participate in differentiation, lipogenesis, lipolysis, and fatty acid oxidation from adipocytes [134] (Figure 4). In this context, Forner *et* al., found that mitochondria from WAT express higher levels of proteins with lipogenic function and with ability to degrade xenobiotics [135].

In fact, mitochondria are responsible of the maintaining WAT function and health, being its dysfunction a hallmark of obesity [136]. Thus, obesity status is characterized by an altered mitochondrial metabolism in WAT, which is linked with impaired glucose homeostasis [137]. Animal models, show that obesity status is linked with a reduced WAT-OXPHOS, mainly in VAT depot [136]. This characteristic

is having been described such an adaptive mechanism to energy excess, adipocyte hypertrophy, and WAT enlargement during obesity development [134]. Additionally, an excessive expansion of WAT leads a local hypoxia, which switch the WAT-mitochondrial activity from aerobic OXPHOS to anaerobic glycolysis, which in turns leads a loss of mitochondrial mass [138-141]. Because an overloading of fatty acids into WAT, this tissue also shows a diminution of *de novo* lipogenesis in obesity [142, 143].

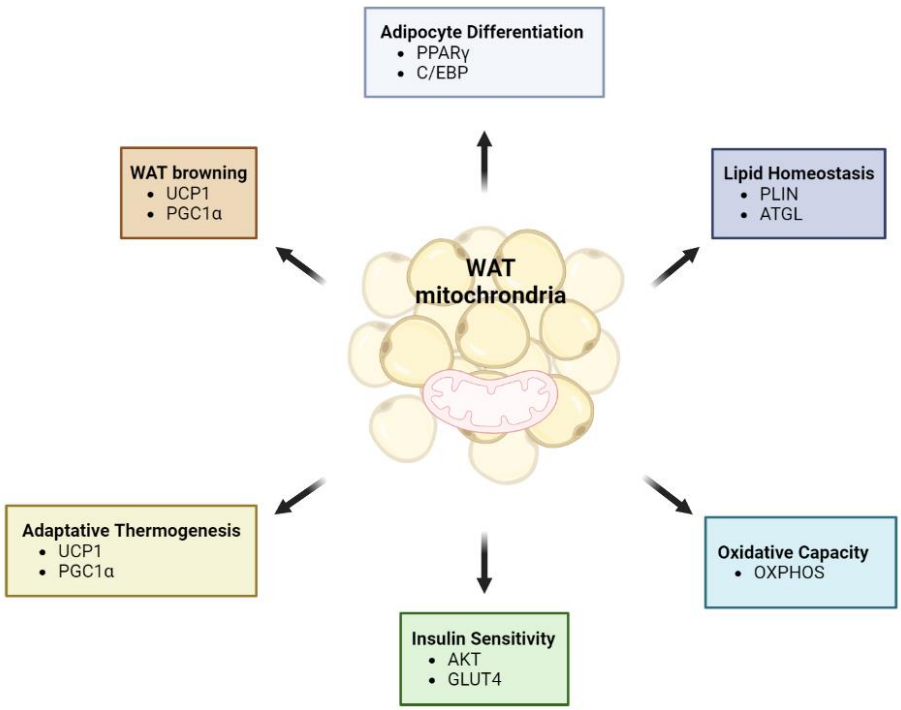

Figure 4. The physiological role of WAT-mitochondria.
Mitochondria in adipocytes regulates adipocyte differentiation, lipid homeostasis, oxidative capacity, insulin sensitivity, adaptive thermogenesis, and browning of WAT. Peroxisome proliferator-activated receptor-γ (PPARγ); CCAAT-enhancer-binding protein (C/EBP); Perilipin (PLIN); Adipose triglyceride lipase (ATGL); Oxidative phosphorylation (OXPHOS); Glucose transporter type 4 (GLUT4); Uncoupling protein-1 (UCP1); PPARγ coactivator 1-α (PGC1α). (From Lee, *et* al. [125])

1.5.4 IL-16: A new cytokine involved in obesity and its co-morbidities

IL-16 is a pro-inflammatory cytokine that acts as a leukocyte chemoattractant factor secreted by several immune cell populations [144]. While the expression of the IL-16 pro-molecule is constitutive in T cells, mast cells, eosinophils, epithelial cells, fibroblasts, and dendritic cells [144], it requires processing and activation by caspase-3 cleavage [145].

Although its role in the peripheral proinflammatory immune response has been widely studied [144, 146-149], there is little evidence of its role in adipose tissue. In this context, it has been described that overweight adolescents have higher plasma levels of IL-16 compared to normal weight controls. Also, IL-16 levels correlate significantly with weight, BMI, and waist circumference [150]. Moreover, children with autoimmune diabetes show a significant increase of IL-16 circulating levels [151]. Additionally, non-obese mice genetically prone to diabetes treated with an IL-16 neutralizing antibody protect from diabetes development [152]. Furthermore, when WAT expression was analyzed IL-16 is upregulated in obese compared with lean mice and caloric restriction further increased these levels [153].

2. OBJECTIVES

To identify new genes and metabolic pathways involved in the development of obesity-induced insulin resistance.

1. To perform a transcriptomic analysis of WAT and WAT-macrophages in subjects with obesity according to anatomical location of WAT-depot.

2. To identify candidate genes involved in metabolic changes between study groups.

3. To determine the metabolic impact of candidate genes.

3. MATERIAL AND METHODS

3.1 Human WAT samples

SAT and VAT biopsies were collected from normal weight controls and obese patients. The samples were maintained in a solution composed by PBS + 1%FBS at room temperature, until its processing. For the development of this project, we work with two independent cohort of patients.

The cohort 1 was composed by complete SAT and VAT from normal weight and obese subject (Table 2). Then an RNA-seq was performed to determine a possible target related with the function of its depot in obesity development. The cohort 2, was composed by WAT-infiltrated macrophages from SAT and VAT, from obese patients, and its posterior analysis using a Clariom D transcriptomic platform (Table 2).Table 2. Clinical data of cohorts of patients

	Cohort 1		Cohort 2
	Control group (n=14)	Patients with obesity (n=13)	Patients with obesity (n=18)
Age	48.6 ± 8.22	46.2 ± 10.09	50.7 ± 9.9
Weight	64.9 ± 9.40	112.2 ± 12.02	112.1 ± 25.6
BMI (kg/m2)	24.7 ± 2.55	43.5 ± 3.89	42.3 ± 6.7

Table 2. Clinical data of cohorts of patients

	Cohort 1		Cohort 2
	Control group (n=14)	Patients with obesity (n=13)	Patients with obesity (n=18)
Age	48.6 ± 8.22	46.2 ± 10.09	50.7 ± 9.9
Weight	64.9 ± 9.40	112.2 ± 12.02	112.1 ± 25.6
BMI (kg/m^2)	24.7 ± 2.55	43.5 ± 3.89	42.3 ± 6.7

3.1.1 RNA isolation of WAT

Total RNA from SAT and VAT was isolated using Nucleospin RNA mini kit (Macherey-Nagel, 740955.250), according to manufacturer instructions. For thus, 30-50 mg of each depot was disrupted using a TissueLyser at 50Hz for 2 min, with 500 µl of RA1 Buffer + 5 µL of β-mercaptoethanol (Sigma-Aldrich, M3148). Then, the lysate was filtrate with the objective to reduce viscosity and clear the lysate by filtration through NucleoSpin Filter and centrifugated for 1 min at 11000g. Then, the eluted was mixed with 500 µl of 70% ethanol and mixed by vortex. This mix was loaded into NucleoSpin RNA Column and centrifugated 30 seg at 11000g and flow through was discarded. To inactive, the column was desalted using MBD buffer and centrifugated at 11000g for 1 min to dry the membrane. Next, column was treated with 95 µL of rDNase mix and incubated at room temperature for 15 minutes. To inactivate rDNase 200 µL of RAW2 buffer was added and the column was centrifugated for 30 seg at 11000g. A second wash was performed using 600 µL of RA3 buffer, and centrifugated again at 11000g for 30 seg. Finally, a third wash was performed adding 250 µl of the RA3 buffer and column was centrifugated during 2 min at 11000g to dry the membrane completely. After those washes, the RNA was eluted using 50 µl of RNase-free H_2O and centrifugated at 11000g for 1 min. The eluted RNA was storage at -80ºC until the RNA-seq were done.

3.1.2 WAT-infiltrated macrophages isolation

Immediately after surgical extraction, the isolation of SVF from SAT and VAT biopsies were performed in sterile conditions. First, SAT and VAT samples were washed with Hank's Buffer (*Capricorn Scientific, HBSS-2A*), minced with scalpel, and

digested into 50 ml conical tubes with 5 mL of a collagenase digestion solution (Table 3). The digestion was performed at 37°C, for one hour with vortex every ten minutes. Once the tissue was totally digested, the digestion was stopped by putting the samples in ice. Then, solution that contains SVF was filtered through 100 µm filter and centrifuged at 500g for 5 minutes at 4ºC and the supernatant was discarded. The obtained pellet was washed twice by resuspension in 5 mL of PBS+FBS (Table 3) and centrifugation at 500g for 5 minutes at 4ºC.

After those washes, the resulting pellet, that contains SVF, was resuspended in 500 µL of cold MACS buffer (Table 3), to proceed to magnetic labeling of $CD11b^+$ cells.

3.1.3 $CD11b^+$ magnetic labeling and separation

First, the cell suspension was centrifuged at 300g for 10 minutes and the supernatant was completely discarded. Second, the pellet was resuspended in 82 µL of MACS buffer () and 2 µL was taken, diluted by adding 18 µl of MACS buffer and reserved at 4ºC to evaluate percentage of $CD11b^+$ cells. Then, 20 µL of CD11b MicroBeads (Miltenyi, 130-126-725) was added to 80 µL of cell suspension, mixed and incubated for 15 minutes in ice. Next, the cells were washed by adding 2 mL of MACS buffer and centrifugated at 300g for 10 minutes at 4ºC. Then the pellet was resuspended in 500 µL of MACS buffer and maintained in ice.

Table 3. Solutions for SVF isolation and magnetic labeling

Buffer	Reagent	Reference	Final concentration
PBS + FBS	PBS 1x	Sigma-Aldrich, P3813	1X
	FBS	Capricorn Scientific, FBS-12A	2%
Collagenase digestion solution	Hanks' Balanced Salt Solution (HBSS)	Capricorn Scientific, HBSS-2A	1X
	Collagenase NB 4 Standard Grade	SERVA, S1745401	1 mg/mL
MACS buffer	PBS 1x	Sigma-Aldrich, P3813	
	BSA	Sigma-Aldrich, A8531	0.5%

Meanwhile, the separation column is prepared. For this, the LS column (Miltenyi, 130-042-401) was placed in the magnetic field, on the MidiMACS™ Separator (Miltenyi, 130-042-302), and rinsed with 3 mL of MACS buffer. Once the column reservoir is empty, the cell suspension was added into the column. When all the suspension passed, the column was washed by adding 3 mL of MACS buffer, twice. After that, the column was removed from the magnetic field, and placed onto a new 15 mL conical tube (collection tube). Then, 5 mL of MACS buffer was added and the fraction with the magnetically labeled cells was immediately flushed out applying the plunger supplied with the column. 20 µL of the eluted fraction was reserved in ice.

Next, the $CD11b^+$ fraction of cells was centrifuged at 300g for 7 minutes at 4ºC, 4 mL of the supernatant was discarded, and the pellet was resuspended in the remaining volume, which was transferred into 1.5 mL conical tube (Eppendorf™, 0030119460) and centrifuged at 11000g for 5 min, the resulting pellet was used to perform RNA extraction.

3.1.4 Evaluation of the enrichment of CD11b$^+$ cells

The reserved aliquots from SAT and VAT were labeled to quantify the viability and the number of infiltrated CD11b$^+$ cells, respectively. For this purpose, 10 µL of cell sample was mixed with 48 µL of MACS Buffer, 2 µL of 7-AAD (Miltenyi, 130-111-568) and 0.5 µL of CD11b (Miltenyi, 130-113-797), the prepared mix was incubated in darkness for 10 min and then 10 µL of CountBright counting beads (Invitrogen, C36950) was added. Data acquisition was performed in a FACSCanto™ II system (BD Biosciences) using the FACSDIVA™ software (BD Biosciences) and analyzed in FlowJo version X.0.7. (FlowJo LLC).

3.1.5 RNA isolation from CD11b$^+$ cells

The obtained pellet after CD11b$^+$ magnetic separation, was used to extract total RNA, using Single Cell RNA Purification Kit (Norgen Biotek Corp., 51800). For this, a mixture composed of 100 µL Buffer RL + 1 µL β-mercaptoethanol (Sigma-Aldrich, M3148) was added to each pellet to lyse the cells. Then, 100 µL of 70% ethanol was added and the tubes were vortex. The mix of cell lysis and ethanol was transferred onto the column and centrifuged for 1 minute at 3500g and the flow through was discarded. Next, 400 µL of Wash Solution was added to the column and centrifuged for 2 minutes at 14000g, again discarding the flow trough.

To eliminate DNA contamination, 115 µL of a mixture of DNase I + Enzyme Incubation Buffer was added, and the columns were centrifuge at 14000g for 1 minute, to ensure that the entire DNase I solution passes through the column. Then the flow through was pipetted onto the top of the column and the columns was incubated for 15 minutes at 25-30ºC.

After, two washes with 400 µL of Wash Solution were perform, and the flow through was again discarded. Finally, the column was centrifuged for 2 minutes at 14000g to thoroughly dry the resin. Once this was done, the RNA was eluted, for this 12 µL of Elution Solution A was added onto the column and centrifuged for 1 minute at 200g, followed by a new centrifugation for 1 minute at 14000g. The eluted RNA was storage at -80ºC until the transcriptomic assays were done.

3.2 Transcriptomic Assays

3.2.1 RNA-Seq

Before sequencing, the RNA integrity number (RIN) of each sample was determined using an Agilent Bioanalyzer 2100; samples with RIN ≥ 7.5 were used for RNA-sequencing. The cDNA library quality and quantity were further analyzed as previously described [154]. Libraries yielding satisfactory results were sequenced on an Illumina HiSeq 2000 sequencer (NIM Genetics, Madrid, Spain). The average reads per sample was 45 million; this level of coverage was previously shown to provide sufficient sequencing depth for gene expression quantification and transcript detection [155, 156]. Quality control of reads was performed using FastQC (version 0.11.8; https://bioinformatics.babraham.ac.uk/projects/fastqc).

3.2.2 Clariom D assay

The total quantity and integrity of RNA extracted was evaluated using Bioanalyzer system. RNA of each sample was undergone to microarray hybridization using Affymetrix (Thermofisher) arrays (Clariom-D Assay, human;

https://www.thermofisher.com/order/catalog/product/902922#/902922), processed on an Applied Biosystems GeneChip 3000 system.

Sample processing was performed by the High Technology Unit (UAT) facility at Vall d'Hebron Institut de Recerca (VIHR), selecting those samples with RNA concentrations ≥3 µg and RIN >7. Cohort of patients was clusterized by glycemia levels, initially we group the samples such healthy (Glycemia≤100 mg/dL) and unhealthy (Glycemia>100mg/dL).

Experimental design for hybridization processing: 4 batches of 8-12 samples each with balancing among different batches between all four conditions: subcutaneous healthy (SUB.HEA), subcutaneous unhealthy (SUB.UNH), visceral healthy (VIS.HEA), and visceral unhealthy (VIS.UNH).

To validate the selected genes in the transcriptomic analyses, *in vitro* experiments were performed.

3.3 In vitro assays

3.3.1 Reagent preparation

3.3.1.1. IL-16 stock solution

Mouse IL-16 recombinant protein (Invitrogen, RP-8610) was prepared at 100 ng/µL concentration. Briefly, the entire lyophilized content of the vial was resuspended in 100 µL of a solution of 0.1% BSA in a sterile condition, aliquoted in smaller volumes, and stored at -20ºC.

3.3.1.2. Dexametashone stock solution

Dexamethasone (Sigma Aldrich, D4902) was prepared in ethanol (Merck, 1.07017.2511) at 0.25 mM concentration. For this purpose, 98.115 mg of dexamethasone was dissolving in 1 mL of ethanol, aliquoted into smaller volumes and then stored at -20ºC.

3.3.1.3. 3-isobutyl-1-methylxanthine (IBMX) stock solution

IBMX (Sigma Aldrich, I7018) was prepared in DMSO at 0.5 M concentration. Briefly, 111.12 mg of IBMX was dissolved in 1 mL of DMSO (Sigma Aldrich, D2438), aliquoted into smaller volumes and then stored at -20ºC.

3.3.1.4. Palmitate-BSA 10mM stock solution

Because palmitate, a long-chain FFAs, has low solubility in aqueous solutions, it was conjugated to bovine serum album (BSA) [157], in 5:1 ratio at a concentration of 10 mM. For this purpose, 1.3 g of defatted BSA (Sigma-Aldrich, A6003) were dissolved on a beaker in 9 mL of a 0.9% NaCl solution (Sigma-Aldrich, S7653) by stirring and heating in a water bath to 35-45ºC. Simultaneously, 27.88g of sodium palmitate (Sigma-Aldrich, P9767) were dissolved in 1 mL of a 0.1N NaOH solution (PanReac-AppliChem, 211687.1211), heated at 80°C until a clear solution was obtained. Next, the palmitate in NaOH solution was added drop by drop into the BSA solution, this step should be performed under stirring at 40ºC, to avoid the formation of aggregates. Finally, the obtained solution, that contains Palmitate-BSA conjugated (PA), was filtered through 0.45 µm syringe filters (Merck Millipore, SLHUD33RB), aliquoted in smaller volumes and stored at -20ºC.

For control group, a BSA solution was prepared at the same concentration than in PA solution, adding 1 mL of 0.1N NaOH in 9 mL of a 0.9% NaCl solution.

3.3.1.5. Oil-Red-O stock solution

Stock solution was prepared by adding 300 mg of Oil Red O powder (Sigma Aldrich, O0625) to 100 ml of 2-propanol (Alfa Aesar, 36644). The solution was protected from light and stirred overnight. The final solution was filter through Whatman paper, to remove dye precipitates.

3.3.1.6. LPS and IL-4 stock solution

Both LPS (Sigma-Aldrich, L2880) and lyophilized IL-4 (PeproTech, 200-04) stocks solutions were prepared in sterile milliQH_2O. LPS was prepared at 5 mg/mL, while IL-4 at 10 mg/mL concentration. Then, each stock solution was subsequently aliquoted into small volumes and stored at -20°C.

3.3.1.7. siRNA stock solutions

Lyophilized siRNAs for *Nceh1* (Dharmacon™, L-058031-01-0005), *Myo1e* (Dhamacon™, L-055283-01-0005) and Non-targeting pool (Dharmacon™, D001810-01-05) were resuspended in RNAse-free water in a final concentration of 20 µM in a sterile condition, aliquoted in smaller volumes, and stored at -20ºC.

3.3.1.8. Nile red stock solution

Nile red (Sigma Aldrich, 72485) stock was prepared at 1 mg/mL in DMSO (Sigma Aldrich, D2438), aliquoted into smaller volumes and then stored at -20ºC.

3.4 Cell Culture

All procedures carried out in the cell culture room were performed under a laminar flow hood. Cell lines were grown at 37°C with an atmosphere of 95% air, 5% CO_2. All the reagents used during cell culture procedures was heated to 37ºC in a water bath before its use.

3.4.1 Cell counting

Cells were counted using Countess® Automated Cell Counter (Life Technologies, C10227). Accordingly, 10 µL of cell suspension and 10 µL of Trypan Blue Stain (Life Technologies, T10282) were gently mixed. Then, 10 µL of the mix were added into a Cell counter chamber slide (Life Technologies, C10228) and this was introduced in the equipment. The total amount of cells per mL, the number of live cells and the number of dead cells, as well as the percentage of viability was obtained.

3.5 *In vitro* obesity model of adipocytes

3.5.1 3T3-L1 maintenance

3T3-L1 cell line (CL-173, ATCC) at passage 7, was provided by Dr. David Sebastian (Institute for Research in Biomedicine). Cells were seeded, subcultured and stored at passage 10. All the experiments were done with cells between passages 13 and 15. Cells were washed with sterile PBS 1X (Sigma-Aldrich, D1408 (diluted with sterile milliQH2O)) in each media renewal.

To seed, freeze 3T3-L1 fibroblasts were resuspended in growth medium (Table 4) and seeded in 75cm^2 flasks (Corning®, 430641). Subcultures of the cells were done when flasks reached 70-80% confluence for this, plated cells were washed with sterile PBS 1X and incubated with 3 mL of Trypsin – 0.53 mM EDTA (Life Technologies, 25300-062) for 5 min at 37ºC. Once all the cells were lifted, 7 mL of growth media was added to trypsin action, the total volume was mixed, transferred into a new 15 mL conical tube (Fisher Scientific, 431042) and centrifuged at 1200g for 5 min. The supernatant was discarded, and the pellet resuspended in fresh growth media. Thereafter, cells were counted and, then seeded at a concentration of 2x10^3 cells/cm^2 in growth media to subculture them, or frozen at 1x10^6 cell/mL in freezing medium (Table 4).

3.5.2 3T3-L1 differentiation to mature adipocyte phenotype

To obtain a matures adipocytes from 3T3L1, cells were plated into 12-well plate and grown to 100% confluency, renewing the growth medium every other day. Two days after 100% confluence, induction medium was added, and cells were incubated for 48h. After that time, induction medium was changed for differentiation medium (Table 4) and cells were incubated for an additional 48h. Finally, after this time, differentiation media was changed for maintenance medium (Table 4) until the cells acquired a mature adipocyte phenotype.

Table 4. 3T3-L1 culture media

Medium	Reagent	Reference	Final concentration
Growth medium	DMEM	Gibco™, 41966-029	
	Newborn Calf Serum (CBS)	Gibco™, 1803780	10%
	Penicillin-Streptomycin antibiotics (P/S)	Sigma-Aldrich, 15140-122	1%
Maintenance medium	DMEM	Gibco™, 41966-029	
	Fetal Bovine Serum (FBS)	Gibco™, 10270-106	10%
	Penicillin-Streptomycin antibiotics (P/S)	Sigma-Aldrich, 15140-122	1%
Induction medium	Maintenance medium		
	Insulin	Sigma-Aldrich, I9278	10 µg/mL
	Dexamethasone	Sigma-Aldrich, D4902	0.25 µM
	IBMX	Sigma-Aldrich, I7018	500 µM
Differentiation medium	Maintenance medium		
	Insulin	Sigma-Aldrich, I9278	10 µg/mL
Freezing Medium	CBS	Gibco™, 1803780	90%
	DMSO	Sigma-Aldrich, D2438	10%

3.5.3 IL-16 treatment

IL-16 was used at concentration 1,10 and 100 ng/mL during 3T3-L1 differentiation to evaluate the effect of this cytokine during *in vitro* adipogenesis. Moreover, differentiated adipocytes was treated for 24h with the same concentrations of IL-16.

3.5.4 Mature adipocyte palmitate treatment

To simulate an *in vitro* obesity condition, mature adipocytes were treated with palmitate. For this, PA 10 mM, was diluted in maintenance medium at 1 mM concentration. Then, mature adipocytes were treated for 24h with this media.

3.5.5 Adipocyte lipid staining using Oil Red-O

To stain lipid accumulation in 3T3-L1 cells, plated cells were carefully washed with PBS 1X, avoiding disruption of the cell monolayer. Next cells were fixed with 500 µl of PFA 4% (Sigma-Aldrich, 47608 (diluted in PBS 1X)) and incubated for 30 minutes at room temperature. During this step, a fresh Oil Red-O working solution was prepared mixing 3 parts of the Oil Red-O stock solution with 2 parts of distilled water and incubated for 10 minutes at room temperature, protected from light. Then the working solution was filtered through syringe filter unit (Merck, SLHV033RB), to discard any precipitate.

Once the cell monolayer was fixed, it was washed twice with distilled water and, then incubated for 5 minutes with 500 µl of a 60% isopropanol solution. Next, 500 µl of Oil Red-O working solution was added and incubated for 15 minutes to stain intracellular lipids. After, the staining solution was removed, and the cell monolayer was washed three times with distilled water. Cell monolayer was photographed using a microscope (Leica DM IL LED, Leica Biosystems) to check the lipid vesicles in mature adipocytes. In addition, the staining was quantified by extracting the stain with 1000 µL of 100% isopropanol, 200 µL of this solution were placed in a 96-well plate (Greiner Bio-one, 655101) to read the absorbance at 492 nm in Varioskan LUX equipment (Thermo Scientific).

3.6 *In vitro* macrophages experiments

3.6.1 RAW264.7 maintenance

RAW264.7 cells (ATCC ref# TIB-71) at passage 8 were obtained from our laboratory (Regulation of lipid metabolism in obesity and diabetes group).

Cells were seeded, subcultured and stored at passage 10. All the experiments were done with cells between passages 12 and 13. In each media renewal, cells were washed with sterile PBS 1X (Sigma-Aldrich, D1408 (diluted with sterile milliQH_2O)).

To seed, freeze RAW264.7 macrophages were resuspended in growth medium, which contain DMEM (Gibco™, 41966-029), 10%FBS (Gibco™, 10270-106) and 1%P/S (Sigma-Aldrich, 15140-122). The cell suspension was seeded in 100mm plate dish (Corning®, 430167). When cells reached 70-80% confluence, they were harvested and expanded in more plates. Briefly, plated cells were washed with sterile PBS 1X and 5 mL of growth medium was added, then cells were mechanically lifted using a cell scraper (SPL Life Science, 90020), cell suspension was transferred into a 15mL conical tube (Fisher Scientific, 431042) and centrifuged at 1200g for 5 min. The supernatant was discarded, and the pellet resuspended in fresh growth media. Thereafter, cells were counted and seeded at a concentration of $1x10^6$ cells/plate in growth media to subculture them, or frozen at the same concentration in FBS with 10%DMSO (Sigma-Aldrich, D2438). For the experiments, cells were seeding in 12-well plates at $2x10^5$ cells/well.

3.6.2 Gene silencing using siRNAs

The day before silencing, $2x10^5$ cells per well were seeded in 12-well plates, with 1mL of growth media, and were cultured for 24h. The transduction was performed using Lipofectamine™ RNAiMAX, according to manufacture instructions. For this purpose, cells were washed with sterile PBS 1X and 900 µL of transduction media were added in each well (Table 5). Cells were then transducted with 25 nM of siRNA or non-targeting pool, as a Scrambled control. For this, siRNAs Media and Lipofectamine Media was prepared (Table 5) and incubated for 20 min at room temperature. Thereafter, siRNA media was added drop by drop to the Lipofectamine Media. The final mix of siRNA attached to lipofectamine was added to the wells and the total volume was mixed gently by rocking the plate and cells were incubated cells for 24h. After incubation, the medium was removed, and cells were washed with sterile PBS 1X and treated for the next experiments.

Table 5. siRNA silencing media

Media Name	Volume (µL)	Reagent	Reference
Transduction Medium	855	OptiMEM	Gibco™, 31985070
	45	Fetal Bovine Serum (FBS)	Gibco™, 10270-106
siRNAs Medium	1.25	siRNAs or Non-targeting pool	
	50	OptiMEM	Gibco™, 31985070
Lipofectamine Medium	3	Lipofectamine™ RNAiMAX	Thermo Fisher, 13778075
	50	OptiMEM	Gibco™, 31985070

3.6.3 LPS and IL-4 treatment

Macrophages were treated in 12-well plates, with LPS (60 ng/mL) diluting stock solution of each activating molecule in starvation medium composed by DMEM + 1% P/S and 0.05% BSA. Then, 1mL of the corresponding medium mix was added to each well, a control only with starvation medium was added to each experiment. Cells were incubated during 2, 4 and 8 h.

3.6.4 Palmitate treatment

Macrophages were treated in 12-well plates, with 1 mM of PA. Briefly, 10 mM stock solution of PA-BSA was diluted in DMEM + 1% P/S and pH was adjusted at 7.4. Then medium was filtered and 1mL was added to each well, using as control medium with the same volume of BSA diluted in DMEM + 1% P/S. Cells were incubated during 2, 4 and 8 h.

3.6.5 Wound healing assay

After 24h of *Myo1e* silencing, the medium was removed, the cells were washed with sterile PBS 1X and cell monolayer were cross-shape scratched with a 10 µL micropipette tip attached to a glass pipette. Thereafter, cells were washed again with sterile PBS 1X, to remove detached cells and then 1 mL of RAW264.7 growth media, but with 5% FBS, was added. Each well was photographed to record scratch distance and then incubated for 24h at 37°C in a humidified, 5% CO_2 incubator. Each well was photographed again the next day, in the same site that day before to quantify cell migration after 24h. The photograph was taken with ZOE™ fluorescent cell imager (Biorad). The obtained images were analyzed by ImageJ software (REF)

and the MRI wound healing tool plugin [158]. These experiments were repeated with 4 replicates per group.

3.6.6 Lipid dye using Nile red

First, treated cells were fixed with 500 µl of PFA 4% (REF, (diluted in PBS 1X)) and incubated for 30 minutes at room temperature. A fresh Nile red working solution was prepared during this step, diluting stock solution 1/10 in PBS 1x. Then, cells were incubated with 0.5 mL of working solution for 30 minutes at room temperature, protected from light. Finally, the staining solution was removed, and three PBS 1x washes were performed. The last wash was kept, and a photograph was taken using a fluorescence microscope to check the lipid vesicles into macrophages. Lipid accumulation was quantified usin ImageJ (REF).

3.7 Molecular biology techniques

3.7.1 RNA extraction and quantification

RNA extraction was performed using the Chomczynsky method [134] using Trizol™ Reagent (Invitrogen, 15596026), according to manufacturer indications. Briefly, 500 µL of Trizol™ reagent were added to each well and plates were gently shaken for 5 min to dissolve the cell monolayer and allow the complete dissociation of the nucleoproteins complex, then the volume was transferred into 1.5 mL conical tubes (Fisher Scientific, 15537741). Next, 100 µL of chloroform (Merck, 102445) was added, the tubes were shaken for 15 seconds and subsequently incubated for 3 min at room temperature followed by a centrifugation for 15 minutes at 12000g at 4ºC. After this, the aqueous phase, of each sample, was transferred into a new

1.5 mL conical tube and RNA was precipitated by adding 250 µL of isopropanol (Merck. 100995) and 1 µL of GlycoBlue® (ThermoFisher, AM9515). To increase RNA yield, samples were left to precipitate overnight at -20°C, and then centrifuged for 10 min at 12000g at 4°C. Hereafter, the supernatant was discarded, and the pellet was washed twice with 75% ethanol (Sigma-Aldrich, 1.00983 (Diluted in DEPC water)), making a vortex each time and centrifuged for 5 min at 12000g at 4ºC. Finally, the pellet was vaccum dry using a SpeedVac at 'low power' (Savant SpeedVac® Plus SC110A Concentrator) and resuspended in 30 µL nuclease-free water. The resuspended RNA was then heated for 10 min at 56ºC in a heat block before its quantification. Then, the samples were stored at -80ºC.

For RNA quantification, 2 µL of resuspended RNA sample was added into Nanodrop ND-1000 Spectrophotometer to obtain concentration and purity of RNA samples.

3.7.2 cDNA synthesis by reverse transcription

cDNA retrosynthesis was performed from 1000 ng of RNA samples using M-MLV reverse transcriptase (Invitrogen, 28025-013). To this, 10 µL of 100 ng/µL of each RNA sample was combined with 2 µL of Mix 1 (Table 6) and samples were incubated for 5 minutes at 65ºC and then immediately chilled on ice. After, 7 µL of Mix 2 (Table 6) was added and samples were incubated at 37ºC for 2 minutes. Finally, 1 µL of M-MLV RT enzyme (Invitrogen, 28025-013) was added and samples were incubated 2 minutes at 37ºC, 10 minutes at 25ºC, 50 minutes at 37ºC and 15 minutes at 70ºC.

Table 6. Reagents used in retrosynthesis.

	Reagent	Reference	Volume for each sample
Mix 1	Oligo d(T)16 (50 µM)	Invitrogen, 100023441	0.5 µL
	Random Hexamer (50 µM)	Invitrogen, 100026484	0.5 µL
	10 mM dNTPs Mix	Invitrogen, 100004893	1 µL
Mix 2	5X First-Strand buffer	Invitrogen, Y02321	4 µL
	0.1M DTT	Invitrogen, Y00147	2 µL
	RNAseOUT™ (40 U/µL)	Invitrogen, 100000840	1 µL

Once retrosynthesis was done, the resulting cDNA was diluted 1:20 with nuclease-free water at a 2.5 ng/µl concentration. In each reverse transcription performed, two negative controls were included: RT1, a pool of RNA samples with nuclease-free water instead of MMLV RT and RT2, where nuclease-free water was used instead of sample.

3.7.3 Quantitative real-time polymerase chain reaction

To quantify gene expression for each sample a quantitative real-time polymerase chain reaction (qRT-PCR) was performed. For this purpose, 8 µL of Mastermix (Table 7) was mixed with 2 µL of diluted cDNA samples in 384-well plate (Fisher scientific, 04729749001) additionally, a qRT-PCR negative control with nuclease-free water instead of sample was included.

The qRT-PCR was carried out on LightCycler® 480 Instrument II (Roche, 05015243001) and the gene expression was normalized by *Ppia,* housekeeping gene and expressed as relative quantification respect to the control group, using $2^{-\Delta\Delta Ct}$ method [159]. The list of used primers can be found on Supplementary Table 1 (Table S1).

Table 7. qPCR Master Mix

Reagent	Reference	Volume for each sample
LightCycler 480 SYBR Green I Master	Roche, *4887352001*	5 µL
Primer mix (For + Rev) 10 uM		0.5 µL
Nuclease-free H_2O	Invitrogen, 100004893	2.5 µL

3.8 Bioinformatics analysis

3.8.1 Cohort 1

To complete WAT, gene expression was quantified in TPM units (transcripts per million) using Salmon version 1.1.0 [160] with the additional parameters "–seqBias – gcBias – validateMappings". GENCODE version 31 (GRCh38.p12) was used as the reference genome [161] and indexed using default parameters. This resulted in 175775 transcripts corresponding to 35183 genes. Differential expression analysis was separately conducted for SAT and VAT, between controls and patients with obesity using DESeq2 version 1.24.0 [162]. For each gene and transcript isoform, $\log_2$ fold change (log2(FC)) values were calculated, and unpaired Wald's test were used to evaluate differential expression. A gene was differentially expressed between the groups when it met the criteria of $\log_2(FC) > |0.585|$ (i.e., FC = |1.5|) and adjusted p-value < 0.05 with Benjamini-Hochberg correction. All the bioinformatics analysis were performed by Dr. Rubén Cereijo (Universitat de Barcelona).

3.8.2 Cohort 2

To WAT-infiltrated macrophages, whole transcriptomic profiling data were generated using Clariom D. For exploratory purposes, standard analysis with default settings was run with the Transcript Analysis Console (TAC v4.0) software from Affymetrix Thermofisher. Bioinformatic analysis was performed using the R open-source statistical analysis software by High Content Genomics and Bioinformatics Facility (IGTP). Raw data files in *.cel* format were used as input for processing with the oligo package which performs background subtraction, probe set level summarization and normalization using up to date genome annotation from Bioconductor.

Quality control was performed using the *arrayQualityMetrics* package. Principal component analysis was used to explore data consistency and possible presence of outliers before and after normalization. All samples were included in subsequent differential expression analysis using the limma package at the gene level taking the average of all probe sets for a particular gene and focusing on known genes (with assigned gene symbols). Five contrasts were performed.

Inference of biological functions affected was performed using Gene ontology (GO) enrichment analysis using GOrilla web tool (with default settings) [163] and Gene Set Enrichment Analysis (GSEA) [164]. For GO analysis, unranked significant gene lists (using $|FC|>1.2$ and $p_{adj}<0.05$ as cutoff thresholds) of the different overlapped subsets were compared to the background list of all genes profiled by microarray hybridization. In case of GSEA analysis, permutation-based testing using log2intensity values, with a FDR>0.05 and grouping assignments to compute

enrichment and gene list ranked by log2FoldChange is tested for significance in enrichment were performed. The following gene set collections were analyzed:

H – Hallmark collections (robust gene sets for major signaling processes)

C2 – Curated gene perturbation (CGP) and Canonical Pathway (CP) gene set collections (including Reactome, KEGG and wikipathways).

C3 – Gene sets sharing transcription factor binding site to their promoters (TFT)

C5 – Gene Ontology, including: biological process (GOBP), molecular function (GOMF), cellular component (GOCC), as well as human pathologies (HP).

C7 – Immunology gene set collection

C8 – Cell types, based on single cell gene expression profiling datasets.

3.9 Statistical analysis

The statistical analyses performed indicate a comparison between controls and treatments of each experimental model. Two-way ANOVA was performed when more than two groups were compared, followed by uncorrected Fisher LSD. Student's t test statistical analysis was used when two groups were compared. Statistically significant differences were considered when the level of confidence was above 95% (p-value < 0.05). Figures represent data expressed as mean ± standard error of mean (SEM). The number of samples per group used in each experiment is specified in each figure legend. All statistical analyses and figures have been generated using the GraphPad Prism 9.5.1 (GraphPad Software).

4. RESULTS

As mentioned above, two cohorts of patients were used to develop this work (Table 2).

4.1 Cohort 1

The first cohort were composing by healthy subjects and patients with obesity. SAT and VAT extracted to perform a complete tissue RNAseq transcriptomic analysis. When clinical parameters were compared between control and obese subjects from Cohort 1, both groups did not present significant differences in age or fasting glycemia levels (Table 8). However, as expected, there are substantial differences in weight and BMI. Surprisingly, we also found significant differences in total cholesterol and HbA1c levels.

Table 8. Comparison of clinical data of control and obese subject from cohort 1.

	Normal weight			Obese			
	Mean	SD	N	Mean	SD	N	p-value
Age (years)	48,6	8,22	14	46,2	10,09	13	ns
Weight (Kg)	64,9	9,4	14	112,2	12,02	13	****
BMI (kg/m²)	24,7	2,55	14	43,5	3,89	13	****
Glucose (mg/dL)	92,7	15,43	14	106,5	23,5	13	ns
Total cholesterol (mg/dL)	190	33,6	14	158	18	13	**
HbA1c (mmol/mol)	31,5	1,79	14	44,9	11,17	13	***

Data were analyzed by unpaired t-test. BMI, Body Mass Index. *p<0.05, **p<0.01, ***p<0.001, ****p<0.0001.

4.1.1 RNA-seq of WAT

The raw transcriptomic data from SAT and VAT of obese patients and controls were analyzed using the Salmon tool [160] and carried out by Dr. Rubén Cereijo. This

tool allows for quantifying transcripts from RNA-seq data. Next, the DESeq2 and PCAtools packages from R were used to obtain the principal component analysis (PCA) to simplify the dimensions and determine if the transcriptomics output of the clustering of the samples according to BMI, WAT-depot or the interaction of BMI and WAT-depot [162, 165] (Figure 5A-C). Surprisingly, the PCA plots showed that the transcriptome of the samples does not vary according to the BMI (Figure 5A). However, there is a cluster when using the WAT-depot as grouping criteria (Figure 5B), which is maintained when evaluated with the interaction of BMI (Figure 5C).

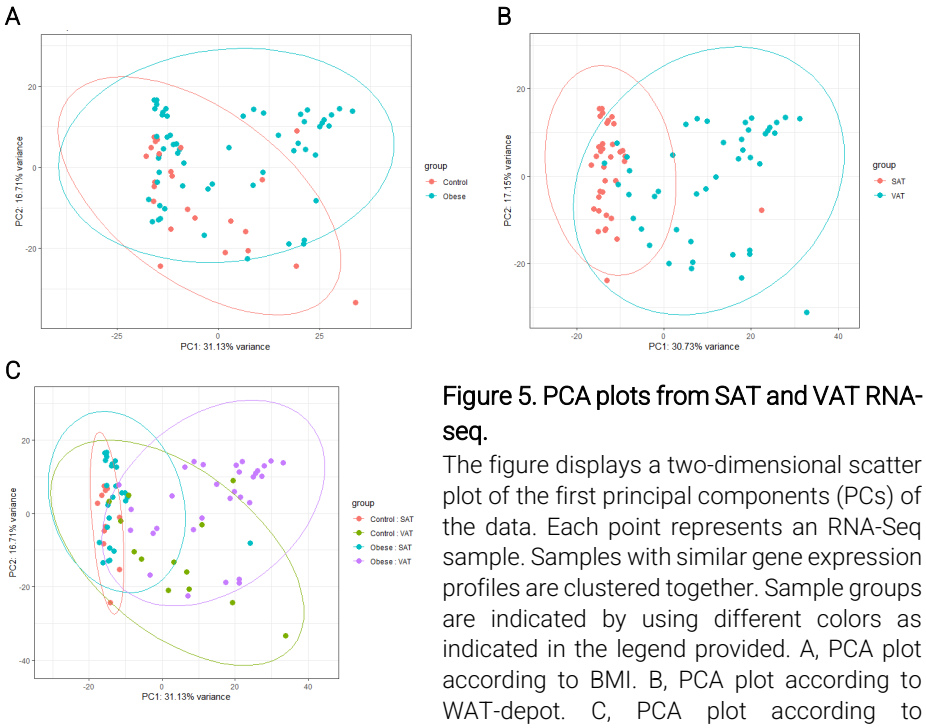

Figure 5. PCA plots from SAT and VAT RNA-seq.
The figure displays a two-dimensional scatter plot of the first principal components (PCs) of the data. Each point represents an RNA-Seq sample. Samples with similar gene expression profiles are clustered together. Sample groups are indicated by using different colors as indicated in the legend provided. A, PCA plot according to BMI. B, PCA plot according to WAT-depot. C, PCA plot according to interaction of BMI and WAT-depot.

Then we evaluated genes of biological interest in the database described in the literature to validate the results. For this purpose, a preliminary expression of ITLN1, ITLN2, ADIPOQ, and LEP was evaluated (Figure 6A-D).

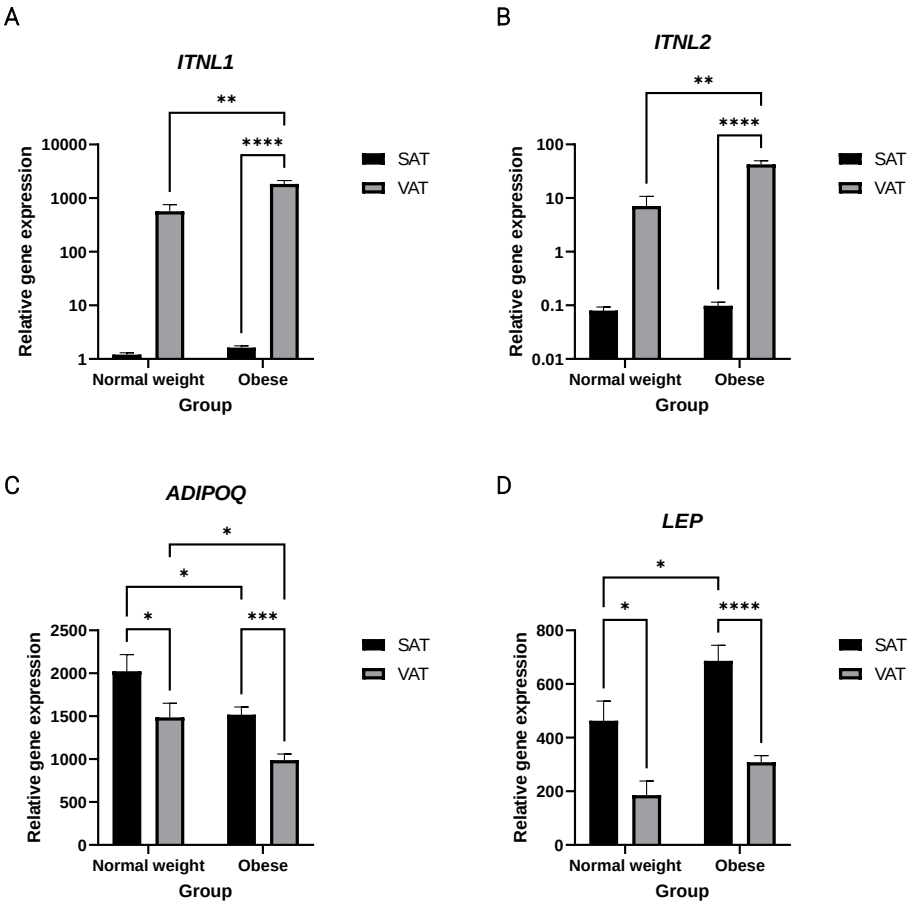

Figure 6. Validation of the RNA-seq outcome.

Gene expression of genes of biological interest described in the literature. Levels of mRNA (transcripts per million [TPM] aggregated on the gene level, produced with Salmon). Data are represented as mean±SEM. Data were analyzed by two-way ANOVA followed by Tukey post-hoc. *p<0.05, **p<0.01, ***p<0.001, ****p<0.0001.

Differential expression results show that ITLN1 and ITLN2 are differentially expressed between SAT and VAT (Figure 6A-B), ADIPOQ and LEP between control and obese patients (Figure 6C-D), indicating that results are biologically consistent. Then we proceeded to perform further analyses.

4.1.2 IL-16 as a novel gene induced in obesity and related with COVID prognosis in patients

Then we begin the analysis of the data to find our target gene. Within the criteria used to select a target gene to study, we searched the literature for genes of high biological interest in obesity which were poorly described in the literature to determine the role of using *in vitro* assays. In this context, an association between obesity and the worst prognosis of the COVID disease began to be described [166-168]. Additionally, a positive correlation between the severity of the disease and the plasmatic levels of IL-16 was described [169-171]. Given the pandemic's impact, we decided to evaluate the expression of IL-16 in our cohort. Surprisingly, the expression of IL-16 was increased in VAT from obese patients compared to its standard weight counterpart (Figure 7A).

Before carrying out other assays, the literature was searched for information associating IL-16 and metabolism or WAT. In this context, the little evidence that exists in this regard associates this cytokine with obesity in adolescents [150], the presence of childhood diabetes [151], and the remodeling of adipose tissue under conditions of caloric restriction in an animal model [153]. For this reason, we decided to determine the serum levels of this interleukin before and after bariatric surgery (Figure 7B), observing higher circulating levels of IL- in obese compared with

normal-weight subjects (Figure 7B). Additionally, these values are increased at 6-months and restored at 12-months after bariatric intervention (Figure 7B).

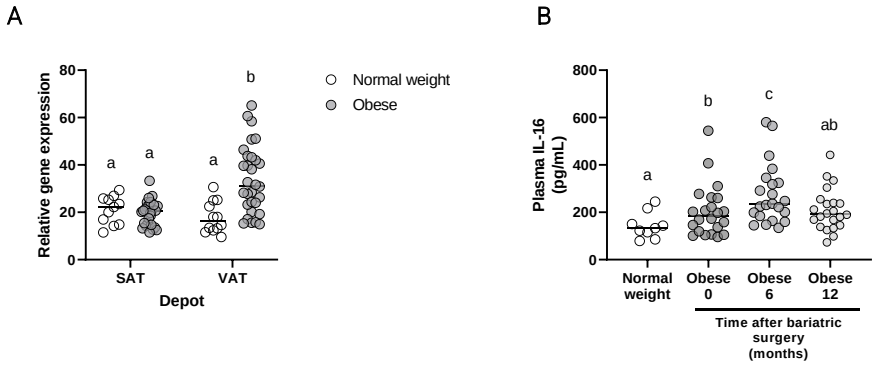

Figure 7 . SAT and VAT IL-16 gene expression and serum levels.

A, Levels of transcripts per million [TPM]. B, Plasma levels of IL-16 before and after bariatric surgery and comparison with normal weight subject. Data are represented as mean±SEM. Data were analyzed by ordinary one-way ANOVA followed by uncorrected Fisher LSD, different letters indicate statistically significant difference at $p<0.05$ within each compared group.

4.1.3 IL-16 gene expression is related with markers of inflammation and immune cell activation

To determine which signaling pathways could be related to IL-16 in WAT, correlations were made between the expression levels of this gene and the rest of the genes obtained from RNA-seq. For this, a Shapiro-Wilk analysis was performed to determine normality in the expression values of each gene, and later a Pearson or Spearman analysis was was performed as appropriate (Table S2). All the genes that have a moderate correlation coefficient (≥0.6) and a significant p-value (<0.05) were selected. To obtain a deeper analysis, this list of the genes was processed

using GOrilla analysis [154], to find the process involved in IL-16 signalling. Genes correlating positively with IL-16 mainly engage in immune signalling and cell activation (Figure 8A and Table S2). An Azimuth analysis was performed to identify the cell identity of genes that correlate with IL-16 [163], indicating that these genes are mainly described in T lymphocytes (Figure 8B and Table S2).

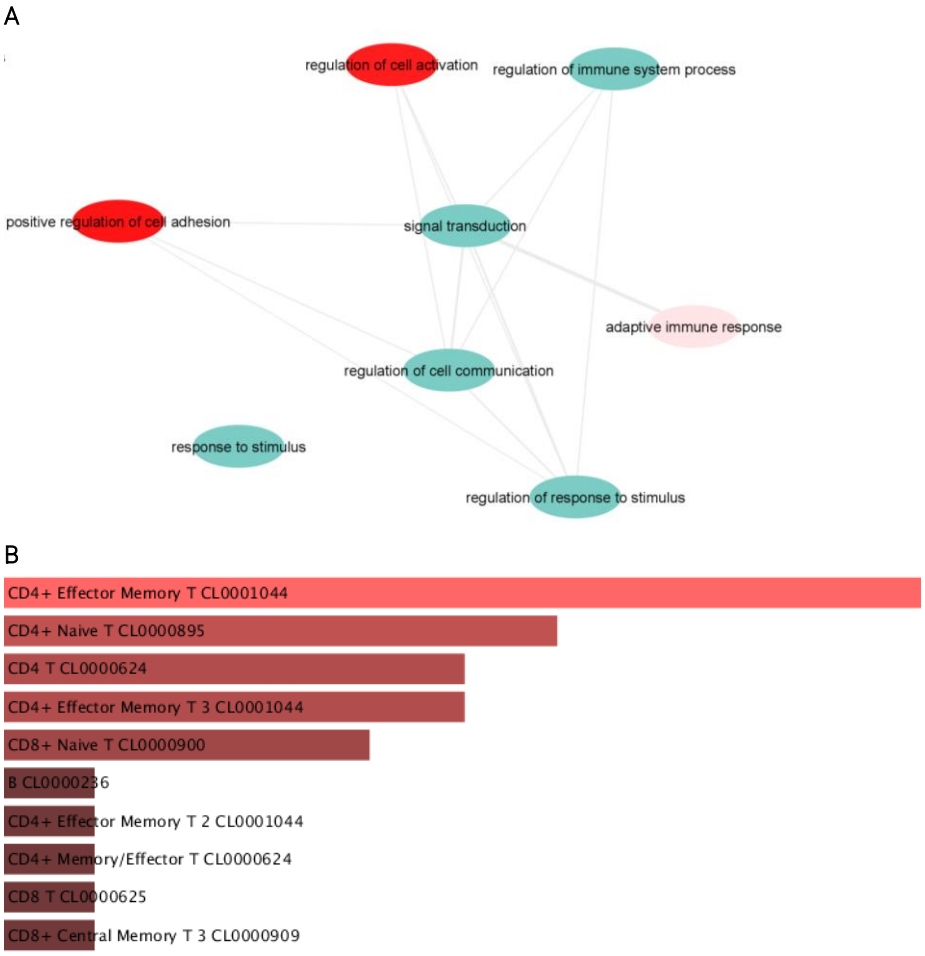

Figure 8. Pathways enriched in genes that correlate with IL-16.

To identify the function and role of the selected targets, we decided to use in vitro assays with murine cell lines. For this purpose, we used 3T3-L1 murine adipocyte to study the IL-16 potential role over adipose tissue.

To identify the function and role of the selected targets, we decided to use in vitro assays with murine cell lines. For this purpose, we used 3T3-L1 murine adipocyte to study the IL-16 potential role over adipose tissue.

4.2 Evaluation of IL-16 over adipogenesis and mature adipocytes

4.2.1 Differentiation of 3T3-L1 towards adipocytes and characterization of the mature phenotype

Briefly 3T3-L1 cell line was cultured, and hormonal differentiation was induced. Then, the time where a mature adipocyte phenotype is observed was evaluated. For this purpose, lipid accumulation and gene expression of differentiation markers during the differentiation process (Figure 9) were evaluated. As can be seen, lipid accumulation (Figure 9A) and gene expression of *Plin1, Glut4,* and *Pref1* show significant changes at day 4 of differentiation (Figure 9B). However, other markers such as *AdipoQ*, *Pparg,* and *Fabp4* begin to show significance from day 7 of differentiation (Figure 9B).

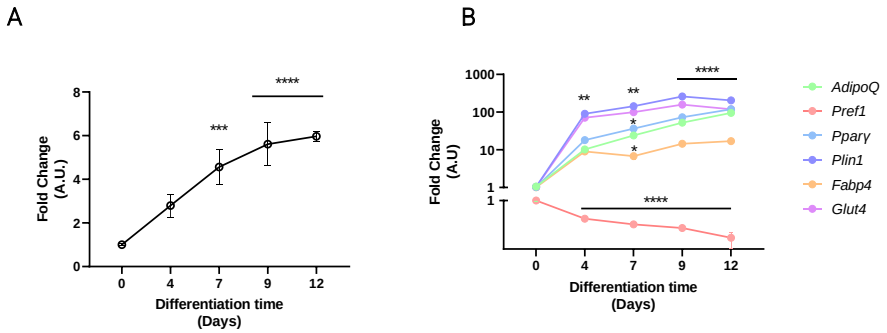

Figure 9. Lipid accumulation and differentiation markers of 3T3-L1.
3T3-L1 were differentiated to evaluate mature phenotype. A.Lipid accumulation were determined using Oil Red O assay. B, Levels of mRNA. Data are represented as Fold Change (arbitrary units (A.U.)), relative to day 0 of differentiation, and expressed as mean±SEM; n=3-4. Data were analyzed by ordinary one-way ANOVA followed by uncorrected Fisher LSD, *p<0.05, **p<0.01, ***p<0.001, ****p<0.0001.

To determine with greater certainty the day of differentiation where there are significant changes in the adipocytes markers, a multivariate analysis (MANOVA) was then performed to combine all variables resulting from gene expression and lipid accumulation (Table 9) with a Dunnet post to compare each differentiation time with the day 0. This analysis indicates again that the adipocytes have a mature phenotype from day 4. Because the differentiation protocol uses 3 different culture media, it has been decided to work with day 7 adipocytes, which no longer have a culture medium with hormonal stimulation.

Table 9. Manova analysis of gene expression and lipid accumulation markers.

Contrast	Estimate	Lower	Upper	p-value
Day 4	105.330	33.20815	177.4518	0.0097
Day 7	166.914	50.46846	283.3595	0.0103
Day 9	275.016	166.95209	383.0799	0.0013
Day 12	349.959	135.14478	564.7732	0.0064

4.2.2 IL-16 modulates the expression of genes related with fibrosis, and metabolism

To evaluate the effect of IL-16 over *in vitro* adipogenesis, this cytokine was added during differentiation at every change of culture medium. Briefly, the 3T3-L1 cell line was cultured and treated to promote differentiation (Section 3.5.2). In this case, cells were collected at different differentiation times to evaluate changes at the gene expression level produced by adding IL-16. On this occasion, 1 ng/mL and 10 ng/mL of IL-16 were used. It can be observed that the addition of IL-16 doesn't affect the lipid accumulation profile during the differentiation process, compared with no treated group (Figure 10).

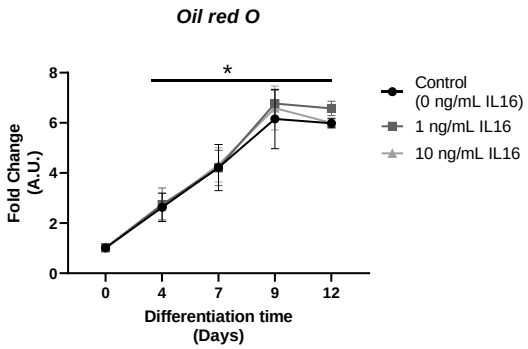

Figure 10. Effect of IL-16 over lipid accumulation during adipogenesis. 3T3-L1 differentiated in presence of 1 or 10 ng/mL of IL-16 and lipid accumulation were determined using Oil Red O assay. Data are represented as Fold Change (arbitrary units (A.U.)), relative to day 0 of differentiation and expressed as mean±SEM; n=4. Data were analyzed by ordinary one-way ANOVA followed by uncorrected Fisher LSD, *p<0.05.

Next, to evaluate if the addition of IL-16 affects the gene expression in the adipogenesis process, the expression of *AdipoQ and Pref1* was assessed (Figure 11). Although the addition of IL-16 during the adipogenesis process does not affect the expression of *AdipoQ* (Figure 11A), it affects the expression of *Pref1* at day 12 of differentiation (Figure 11B).

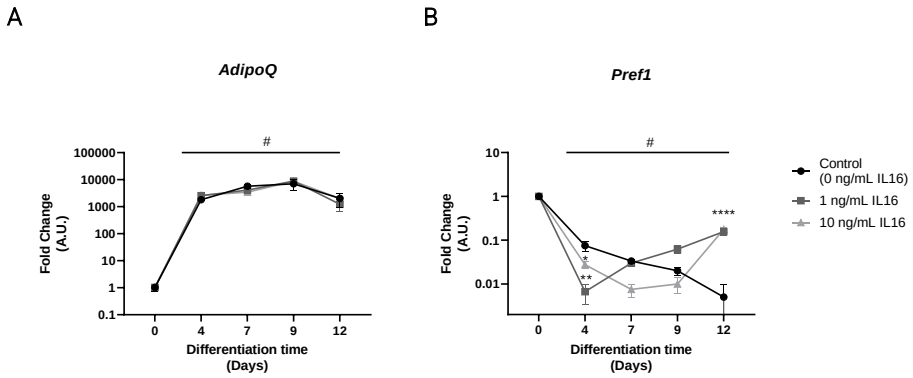

Figure 11. Effect of IL-16 over differentiation markers of 3T3-L1.

3T3-L1 were differentiated in presence of 1 or 10 ng/mL of IL-16. A, *AdipoQ*. B, *Pref1*. Data are represented as relative mRNA level (arbitrary units (A.U.)), relative to day 0 of differentiation, and expressed as mean±SEM; n=4. Data were analyzed by ordinary one-way ANOVA followed by uncorrected Fisher LSD, *p<0.05, **p<0.01, ***p<0.001, ****p<0.0001.

Because *Pref1* gene expression is related to adipose tissue fibrosis [116], the expression of fibrosis gene markers was measured. For this purpose, we evaluate the expression of *ColA6 and Hif1*a when IL-16 was added to the adipogenesis process. We found that 10 ng/mL of IL-16 promotes the expression of *ColA6* on days 9 and 12 (Figure 12A). However, no changes in *Hif1a* expression were observed (Figure 12B).

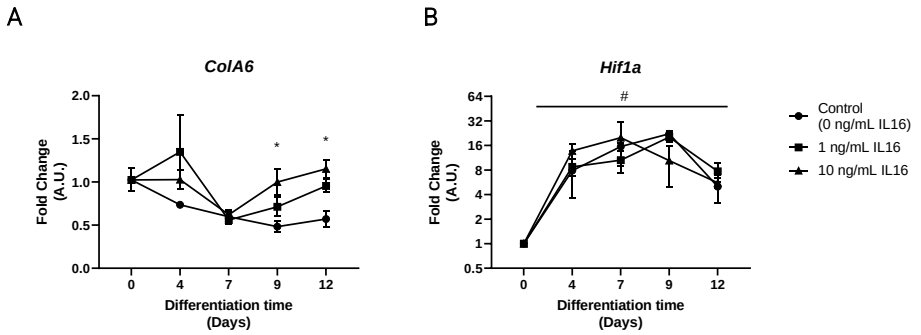

Figure 12. Effect of IL-16 over fibrosis gene markers of 3T3-L1.
3T3-L1 were differentiated in presence of 1 or 10 ng/mL of IL-16. A, *AdipoQ*. B, *Pref1*. Data are represented as relative mRNA level (arbitrary units (A.U.)), relative to day 0 of differentiation, and expressed as mean±SEM; n=4. Data were analyzed by ordinary one-way ANOVA followed by uncorrected Fisher LSD, *p<0.05, **p<0.01, ***p<0.001, ****p<0.0001.

Finally, to evaluate the effect of lipid and glucose metabolism gene expression during adipogenesis, *Cd36*, *Plin1*, *Fabp4* and *Glut4* were measured (Figure 13). Adding IL-16 promotes the expression of genes associated with lipid and glucose metabolism. Both doses of IL-16 (1 ng/mL and 10 ng/mL) reduce the expression of *Cd36*, *Fabp4* and *Plin1* at the latter stages of differentiation, thus at days 9 and 12 (Figure 13A-C). However, it promotes the expression of *Glut4* (Figure 13D) at the early stages of differentiation (days 4 and 7).

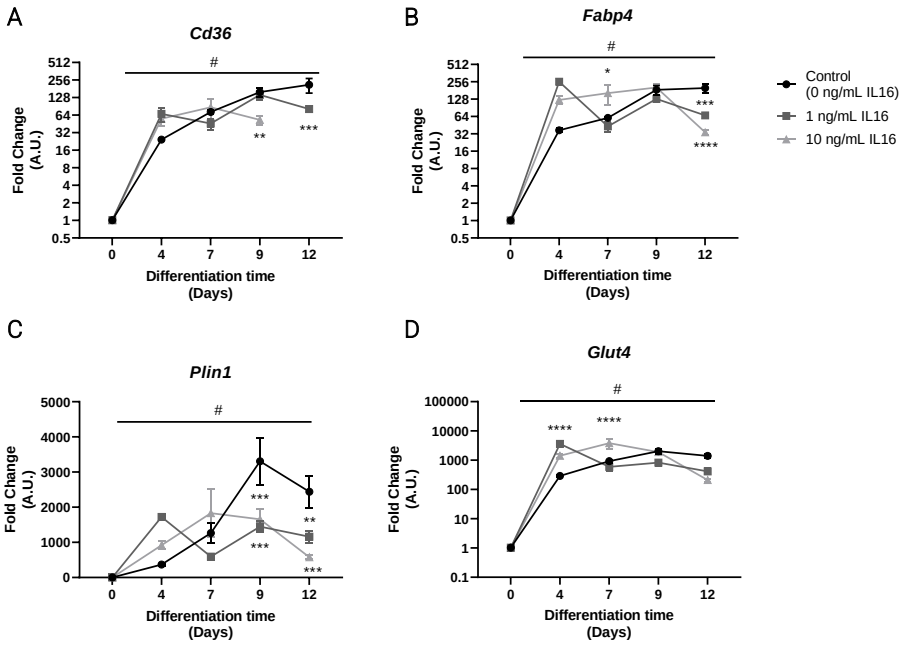

Figure 13. Effect of IL-16 over lipid and glucose metabolism gene markers of 3T3-L1. 3T3-L1 were differentiated in presence of 1 or 10 ng/mL of IL-16. A, *AdipoQ*. B, *Pref1*. Data are represented as relative mRNA level (arbitrary units (A.U.)), relative to day 0 of differentiation, and expressed as mean±SEM; n=4. Data were analyzed by ordinary one-way ANOVA followed by uncorrected Fisher LSD, *p<0.05, **p<0.01, ***p<0.001, ****p<0.0001.

4.2.3 IL-16 modulates inflammation, lipid metabolism and fibrosis gene expression in mature adipocytes

Since there is no evidence of IL-16 levels in adipose tissue, a first approximation was made with different concentrations of IL-16 to determine which concentration range induced a change in gene expression in mature adipocytes. To start, canonical markers of adipocytes were measured (Figure 14). No changes are observable in *Adipoq* gene expression (Figure 14A). Meanwhile, *Leptin* and *Pref1* show a decrease in its expression at 1 and 10 ng/mL of IL-16 (Figure 14B-C).

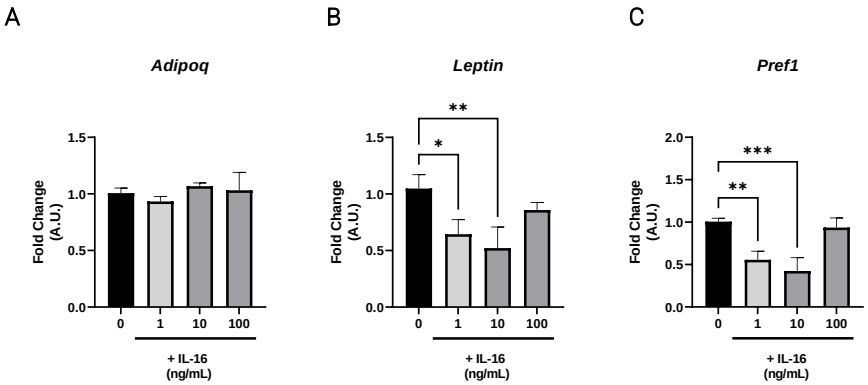

Figure 14. Adipocyte differentiation markers.

3T3-L1 mature adipocytes were treated with increasing doses of IL-16. A, *Adipoq*. B, *Pref1*. Data are represented as relative mRNA level (arbitrary units (A.U.)), relative to dose 0 ng/mL of IL-16, and expressed as mean±SEM; n=4. Data were analyzed by ordinary one-way ANOVA followed by uncorrected Fisher LSD, *p<0.05, **p<0.01, ***p<0.001, ****p<0.0001.

To assess whether the addition of IL-16 affects the pro-inflammatory signaling of adipocytes, the expression of *Ccl2*, *Tnfa*, and *Il6* were evaluated (Figure 15). First, it is observed that only the highest dose of IL-16 produces a significant increase in the expression of *Ccl2* (Figure 15A) and a downregulation in the expression of *Tnfa* (Figure 15B). Gene expression of *Il6* is decreased with the 10 ng/mL and this effect was loosened with 100 ng/mL of IL-16 (Figure 15C).

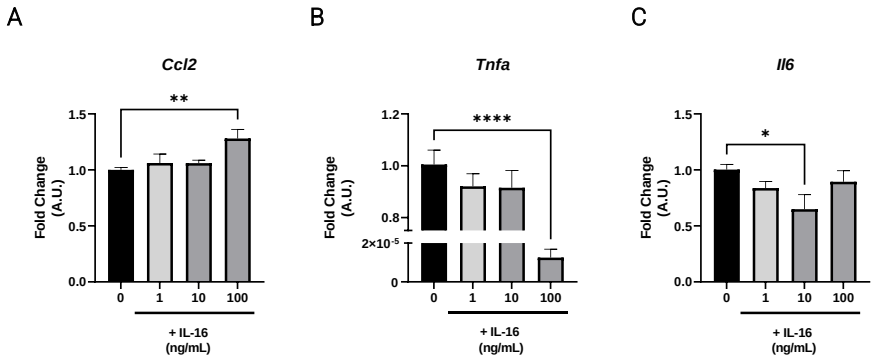

Figure 15. Inflammation markers of adipocytes treated with IL-16.

3T3-L1 mature adipocytes were treated with increasing doses of IL-16. A, *Ccl2*. B, *Tnfa*. C, *Il6*. Data are represented as relative mRNA level (arbitrary units (A.U.)), relative to dose 0 ng/mL of IL-16, and expressed as mean±SEM; n=4. Data were analyzed by ordinary one-way ANOVA followed by uncorrected Fisher LSD, *p<0.05, **p<0.01, ***p<0.001, ****p<0.0001.

Then, genes associated with lipid metabolism were determined to evaluate the IL-16 role over mature adipocytes. For this, the gene expression *Pparg*, *Pgc1a*, *Plin1* and *Cd36* were measured (Figure 16). First, *Pparg* gene expression increases with 100 ng/mL of IL-16 (Figure 16A). *Plin1* and *Cd36* show a dose response effect (Figure 16B-C). Additionally, the *Glut4* expression was evaluated, and a significant reduction was observed with the dose of 10 ng/mL (D).

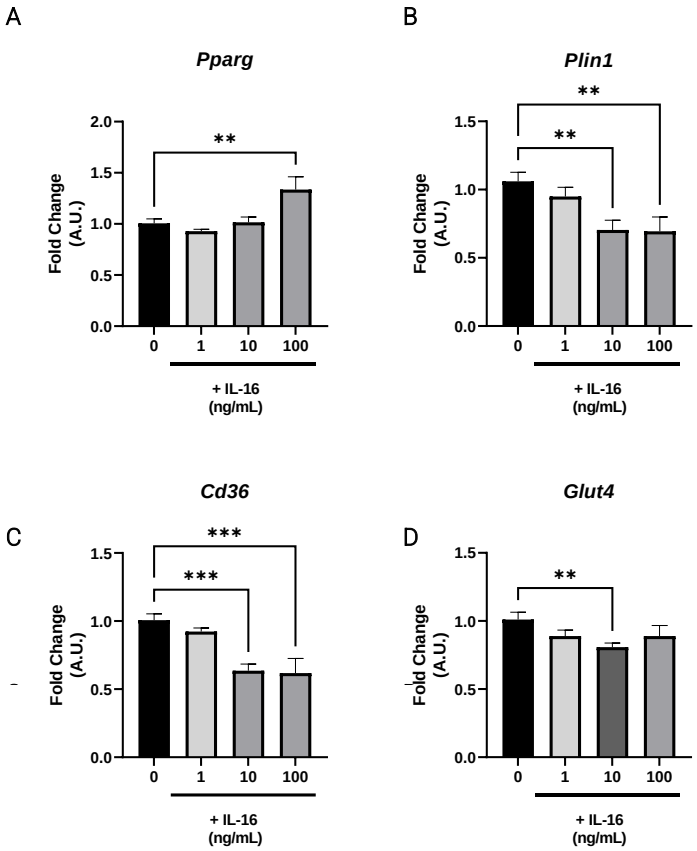

Figure 16. Genes related with lipid and glucose metabolism.

3T3-L1 mature adipocytes were treated with increasing doses of IL-16. A, *Pparg*. B,, *Plin1*. C, *Cd36*. C, *Glut4*. Data are represented as relative mRNA level (arbitrary units (A.U.)), relative to dose 0 ng/mL of IL-16, and expressed as mean±SEM; n=4. Data were analyzed by ordinary one-way ANOVA followed by uncorrected Fisher LSD, *p<0.05, **p<0.01, ***p<0.001, ****p<0.0001.

To assess the role of IL-16 on adipocyte remodeling, *Hif1a*, *Vegf*, *Col4a*, *Mmp9* and *Timp1* genes were measured (Figure 17). It can be observed that IL-16 decreases significatively the expression of *Hif1a* and *Vegf* in a dose-dependent manner (Figure 17A-B). Similarly, in a less thoughtful way, *Col4a* and *Col6a* expression also decreases with the addition of IL-16, up to a dose of 10 ng/mL, the effect that is reversed when using the dose of 100 ng/mL (Figure 17C). Since changes in genes associated with ECM remodeling are observed, it was decided to

evaluate the expression of *Mmp9* and its inhibitor *Timp1*. IL-16 promotes *Mmp9* and decreases *Timp1* expression, increasing the dose-dependent Mmp9/Timp1 ratio in mature adipocytes (Figure 17D-F and Figure S1).

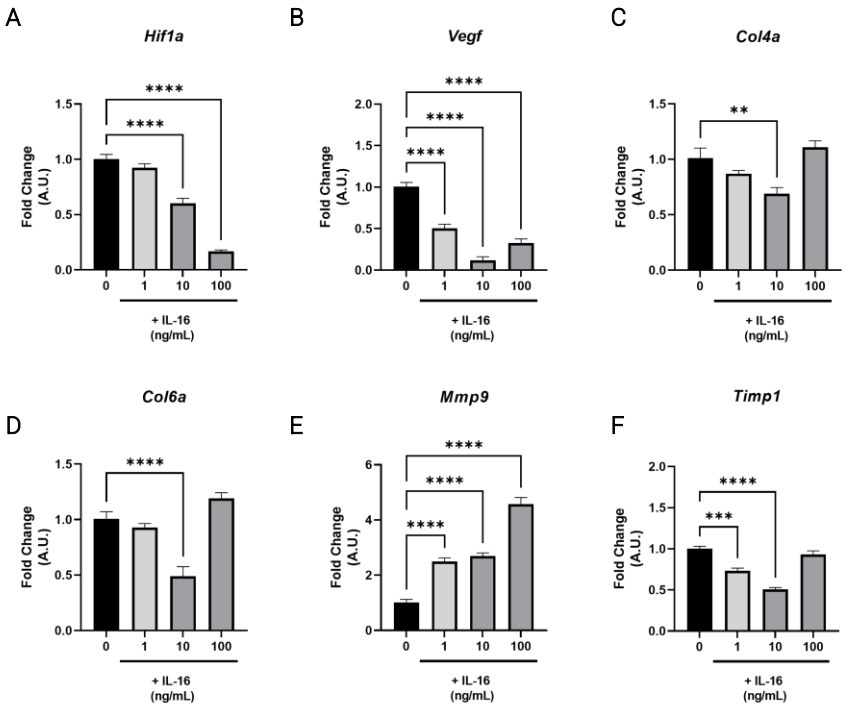

Figure 17. Remodeling markers of adipocytes treated with IL-16.
3T3-L1 mature adipocytes were treated with increasing doses of IL-16. A, *Hif1a*. B, *Vegf*. C, *Col4a*.D, Col6a. E, *Mmp9*. F, *Timp1*. Data are represented as relative mRNA level (arbitrary units (A.U.)), relative to dose 0 ng/mL of IL-16, and expressed as mean±SEM; n=4. Data were analyzed by ordinary one-way ANOVA followed by uncorrected Fisher LSD, *p<0.05, **p<0.01, ***p<0.001, ****p<0.0001.

4.3 Evaluation of IL-16 on an *in vitro* obesity model

4.3.1 Induction of obesity signalling on 3T3-L1 mature adipocytes using palmitate

It has been described that in obese patients, there is a high level of FFAs in circulation, one of the molecules that associate obesity with the development of co-morbidities [172]. Palmitate (C16:0) is one of the most abundant FFAs in plasma and *in vitro* models, enhancing adipocyte differentiation and hypertrophy of mature phenotype, mimicking the obesity signaling in *vitro* models [173-175]. For this, mature adipocytes on day 7 were treated with 1 mM of Palmitate conjugated to BSA (PA) for 24h, according to previous results in our laboratory [176]. Additionally, inflammation markers were measured through qPCR (Figure 18). It can be observed that PA treatment promoted the inflammatory gene expression, increasing *Ccl2*, *Il6* and *Tgfb* and decreasing *Leptin* expression without affecting *AdipoQ* gene levels (Figure 18).

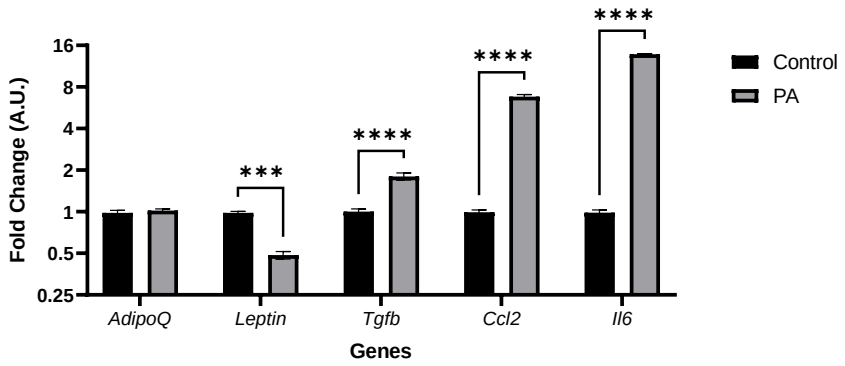

Figure 18. Inflammation and hypertrophy markers on Adipocytes treated with PA.
Mature adipocytes were treated for 24 hours with PA and gene expression were measured. Data are represented as mean±SEM. Data were analyzed by unpaired t-test. *p<0.05, **p<0.01, ***p<0.001, ****p<0.0001.

Then, Oil-Red O and secreted glycerol were measured for lipid accumulation and lipolysis, respectively (Figure 19). Treatment with 1mM PA on mature adipocytes increases both, lipid accumulation (Figure 19A) and glycerol secretion (Figure 19B).

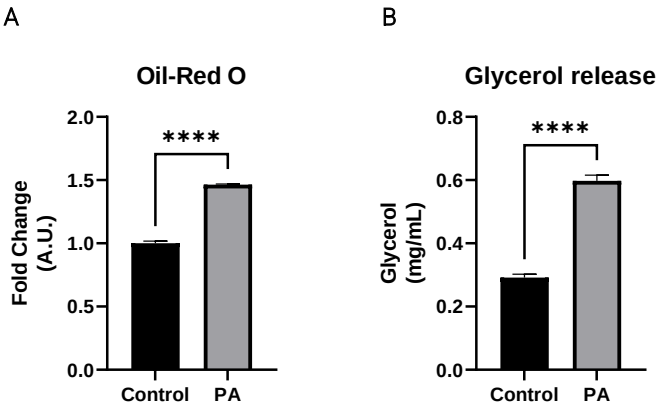

Figure 19. Hypertrophic and lipolytic effect of PA-treatment over mature adipocytes. Mature adipocytes were treated for 24 hours with PA. A, Lipid accumulation was measured by Oil-Red O staining. B, Glycerol secretion. Data are represented as mean±SEM. Data were analyzed by unpaired t-test. *p<0.05, **p<0.01, ***p<0.001, ****p<0.0001.

Then, we decide to treat mature adipocytes simultaneously with IL-16 and PA to simulate an obesity context.

4.3.2 IL-16 blunts the PA-induced lipid accumulation and lipolysis

To evaluate the effect of IL-16 in obesity context, mature adipocytes were treated simultaneously with 1,10 and 100 ng/mL oof IL-16 and PA (1mM) for 24h, using as control cells without PA treatment. Then, lipid accumulation and glycerol release were measured (Figure 20).

First, we could observe that PA treatment promotes lipid accumulation and lipolysis, effect partially reverted with the presence of IL-16. Furthermore, 10 ng/mL of IL-16 blunts significatively the PA-induced lipid accumulation (Figure 20A), and reduce the glycerol released (Figure 20B). The highest dose de IL-16 show an effect comparable with control group (Figure 20).

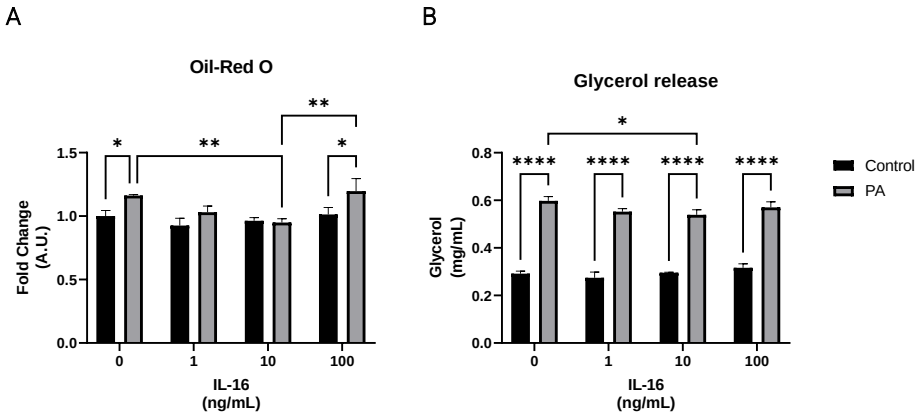

Figure 20. Hypertrophic and lipolytic effect of IL-16 in obesity context.
Mature adipocytes were treated for 24 hours with PA and IL-16. A, Lipid accumulation was measured by Oil-Red O staining. B, Glycerol secretion. Data are represented as mean±SEM. Data were analyzed by two-way ANOVA followed by uncorrected Fisher LSD. *p<0.05, **p<0.01, ***p<0.001, ****p<0.0001.

4.3.3 IL-16 modulate the PA signaling over mature adipocytes

Because an interaction of PA and IL-16 were observed in the lipid profile of mature adipocytes a gene expression were measured. First, we evaluate the effect of IL-16 over adipocytes differentiation gene markers in an obesity context (Figure 21). We could observe that PA addition decrease significatively the expression of *AdipoQ* (Figure 21A) and *Pref1* (Figure 21C) and the addition of IL-16 blunts the PA

effect, and rise the expression of *AdipoQ*, *Leptin* and *Pref1* in a dose dependent manner.

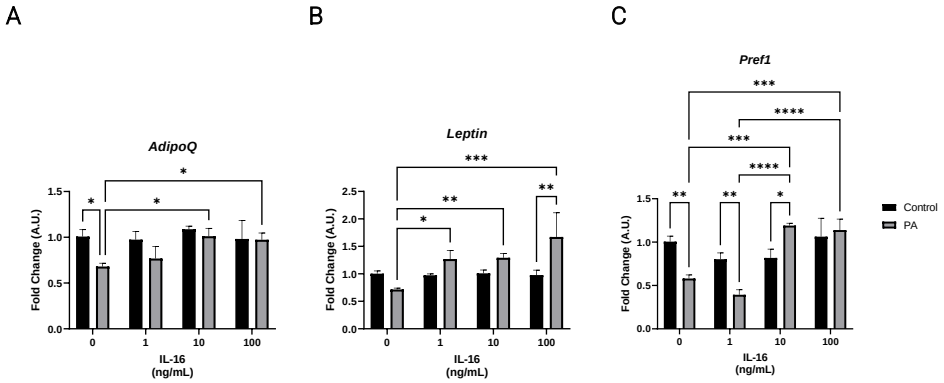

Figure 21. Effect of IL-16 on adipocyte markers in PA-treated adipocytes.
3T3-L1 mature adipocytes were treated simultaneously with PA and increasing doses of IL-16. A, *AdipoQ*. B, *Leptin*. C, *Pref1*. Data are represented as relative mRNA level (arbitrary units (A.U.)), relative to control group and expressed as mean±SEM; n=4. Data were analyzed by two-way ANOVA followed by uncorrected Fisher LSD, *p<0.05, **p<0.01, ***p<0.001, ****p<0.0001.

Then, the pro-inflammatory signaling was evaluated. First, PA promotes the expression of *Ccl2* and *Il6*, the addition of IL-16 increases the effect of PA, rising significatively the expression of *Ccl2* and *Il6* in a dose dependent manner (Figure 22). The expression of *Tnfa* also was evaluated failing to detect its levels (data not shown).

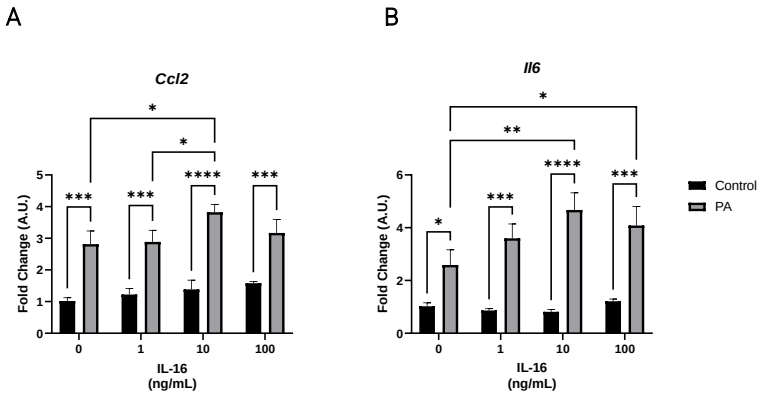

Figure 22. Effect of IL-16 on inflammatory markers in PA-treated adipocytes.
3T3-L1 mature adipocytes were treated simultaneously with PA and increasing doses of IL-16. A, *Ccl2*. B, *Il6*. Data are represented as relative mRNA level (arbitrary units (A.U.)), relative to control group and expressed as mean±SEM; n=4. Data were analyzed by two-way ANOVA followed by uncorrected Fisher LSD, *p<0.05, **p<0.01, ***p<0.001, ****p<0.0001.

Then, genes associated with lipid and glucose metabolism were determined to evaluate the IL-16 effect in cells with an obesity context. For this, the gene expression *Pparg*, *Plin1*, *Cd36* and *Glut4* were measured. IL-16 (Figure 23).

It has been observed that PA addition decrease the expression of *Pparg*, *Plin1*, *Cd36*, and *Glut4* (Figure 23A-D) like reported previously [177]. When IL-16 effect was evaluated we observed that 1 ng/mL and 10 ng/ml doses can blunt the effect of PA on *Pparg* expression (Figure 23A), in *Plin1*, *Cd36* and *Glut4* IL-16 inhibits the effect of PA in a dose-dependent manner (Figure 23B-D).

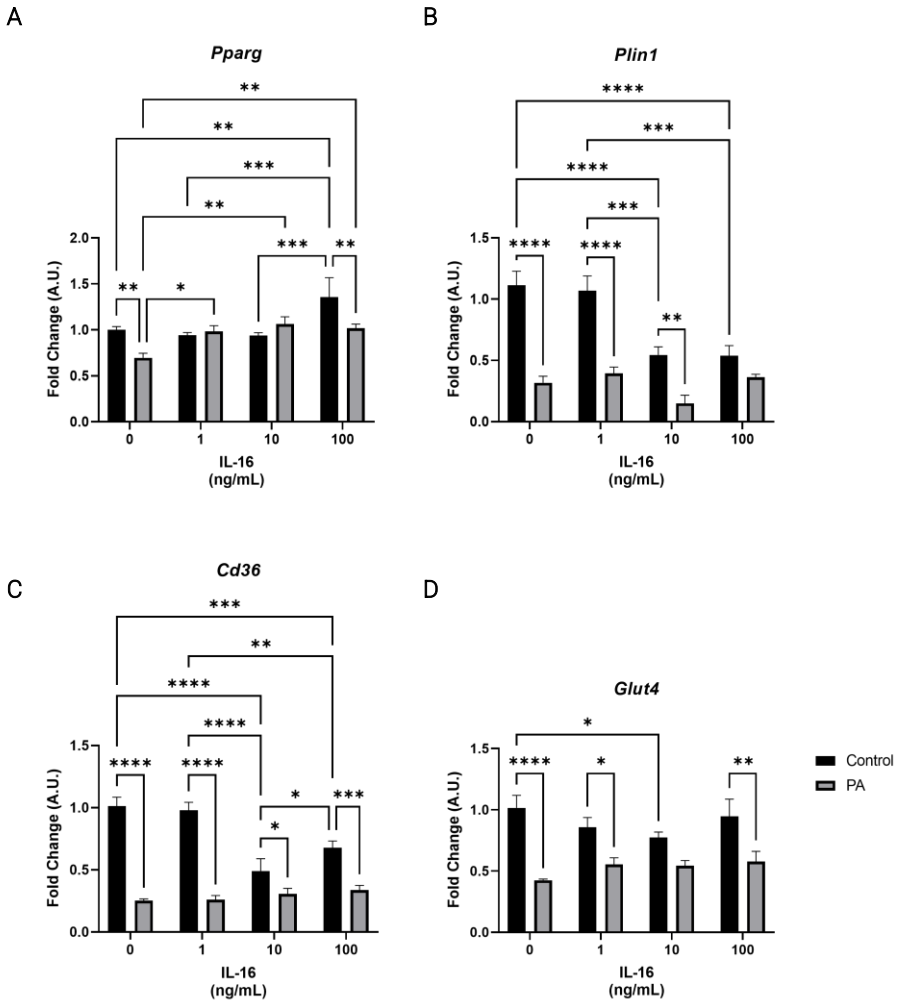

Figure 23. Effect of IL-16 on genes related with lipid and glucose metabolism.
3T3-L1 mature adipocytes were treated simultaneously with PA and increasing doses of IL-16. A, P*parg*. B, *Plin1*. C, *Cd36*. D, *Glut4*. Data are represented as relative mRNA level (arbitrary units (A.U.)), relative to control group and expressed as mean±SEM; n=4. Data were analyzed by two-way ANOVA followed by uncorrected Fisher LSD, *p<0.05, **p<0.01, ***p<0.001, ****p<0.0001.

4.4 Cohort 2

The second cohort were composing by patients with obesity underwent to bariatric surgery (Table 10). SAT and VAT extracted to perform an isolation of $CD11b^+$ cells and then, RNA isolation to perform a Clariom D transcriptomic analysis.

Table 10. Clinical data of cohort 2

	Patients with obesity (n=18)
Age	50.7 ± 9.9
Weight	112.1 ± 25.6
BMI (kg/m^2)	42.3 ± 6.7
Glycemia (mg/dL)	103.2 ± 21.0
Total cholesterol (mg/dL)	191.1 ± 48.0
HbA1c (mmol/mol)	39.5 ± 6.0

4.4.1 WAT-resident macrophages enrichment

To evaluate the CD11b+ enrichment before the transcriptomic analysis, a Flow cytometry was performed (Section 3.1.4). After SVF isolation the viability was over 90% (Figure 24B), and around 3% correspond to $CD11b^+$ cells (Figure 24C). After the MACS enrichment, the purity of CD11b+ cells correspond over 95% (Figure 24D).

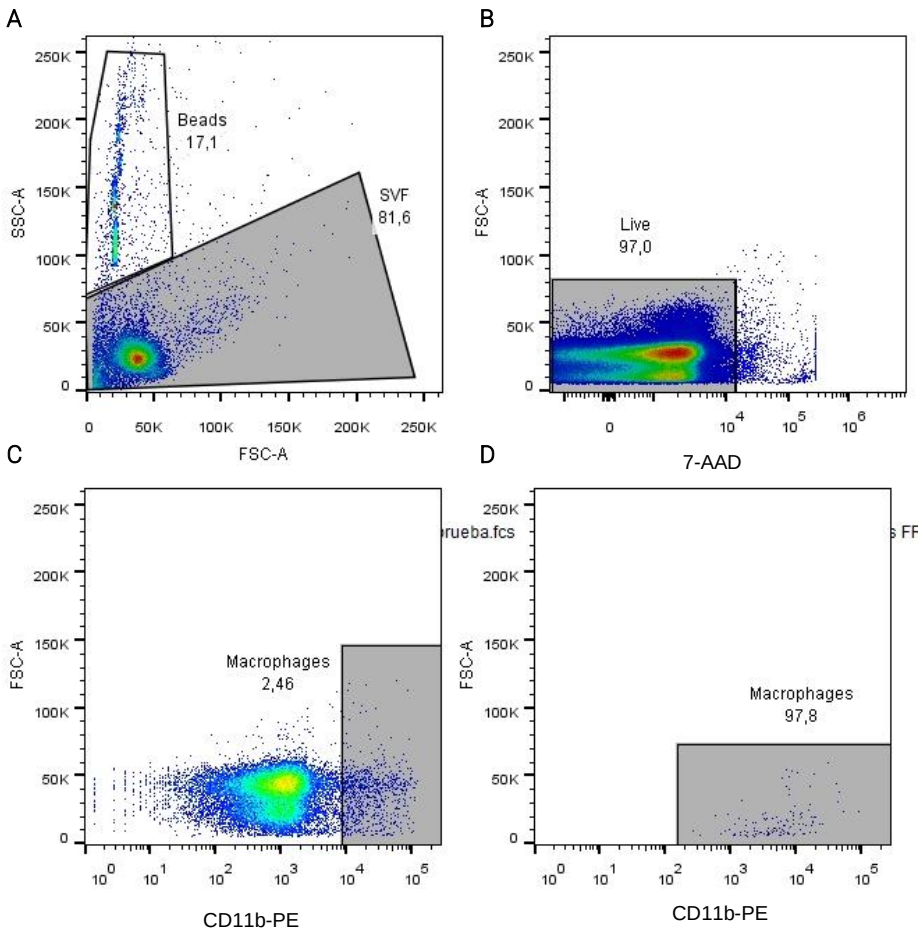

Figure 24. Percentage of CD11b cell enrichment.
CD11b+ cells were isolated from VAT and SAT, and Flow cytometry was performed to evaluate the enrichment of this cell population before RNA isolation. Here is a representative example of one sample. Cell viability was evaluated with 7-AAD dye, and then the CD11b-enrichment was checked in both SVF, before MACs procedure, and in CD11b+ fraction. After MACS enrichment, the CD11b+ population was over 90%.

4.4.2 WAT-resident macrophages showed a different pattern of gene expression in a depot-dependent manner

The raw Clariom D outcome data from SAT- and VAT-macrophages of obese patients were analysed by High Content Genomics and Bioinformatics Unit at IGTP.

First, an exploratory analysis was performed, and sample clustering, dimension reduction, and differential expression analysis were carried out.

A hierarchical clustering analysis was achieved for gene-level analysis sample clustering (Figure 25). It shows that samples do not group by tissue or health status, suggesting that interindividual gene expression differences are more substantial than indicated by the variables of interest.

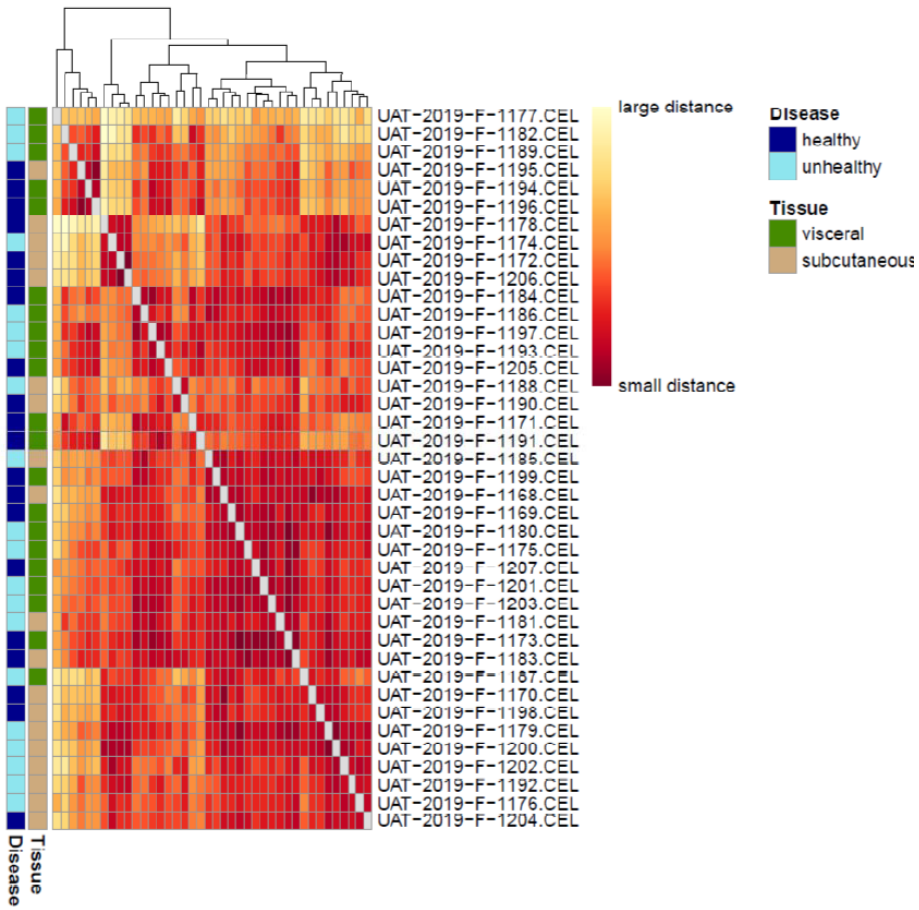

Figure 25. Hierarchical clustering analysis of all samples.

A Principal Component Analysis (PCA) was done for gene-level dimension reduction analysis (Figure 26). It shows that samples tend to group by tissue than by glycemia levels. Therefore, a paired analysis is indicated when assessing differences in gene expression to consider inter-individual variability. However, we did not observe any consistent pattern differentiating treatments among individual samples (no spatial grouping trends can be seen).

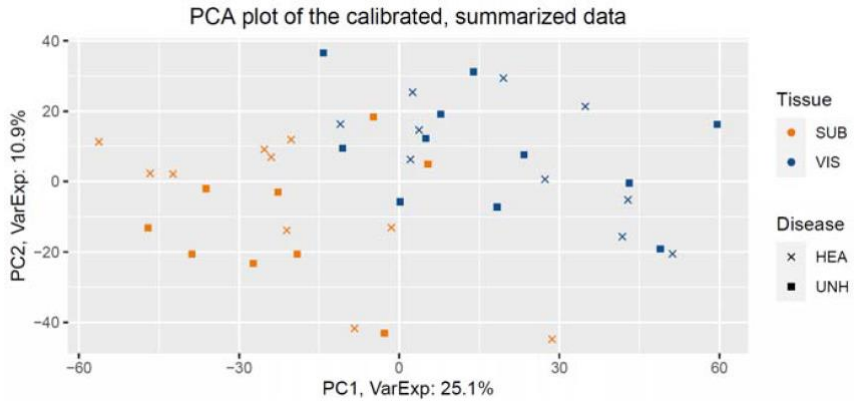

Figure 26. Principal component analysis (PCA) plot of all samples.
Color coded by tissue and sign coded for health status.

Then, a gene-level differential expression was evaluated using a Limma statistical analysis (Table 11). The analysis is represented using a volcano plot for each comparison. When depot differences were evaluated, significance in gene expression between visceral and subcutaneous samples was founded, independently of glycemic levels (Table 11). However, no significant differences were observed in the latter three comparisons (Table 11).

Table 11. Summary of limma differential expression analysis results

	Comparison	VIS vs SUB in HEA	VIS vs SUB in UNH	HEA vs UNH in VIS	HEA vs UNH in SUB	Interaction
	Numerator (1st condition)	VIS.HEA	VIS.UNH	VIS.UNH	SUB.UNH	VIS.HEA - SUB.HEA
	Denominator (2nd condition)	SUB.HEA	SUB.UNH	VIS.HEA	SUB.HEA	VIS.UNH - SUB.UNH
DE Genes |FC|>1.2 Padj<0.05	**TOTAL**	288	156	0	0	0
	UP (over expressed in numerator or under expressed in denominator)	43	25	0	0	0
	DOWN (over expressed in denominator or under expressed in numerator)	245	131	0	0	0

As shown in Figure 27A-B, the omentin gene (ITLN1) is the top visceral biomarker, in agreement with the literature and tissue-specific gene expression databases (https://gtexportal.org/home/gene/ITLN1). In contrast, the neurotrophic tyrosine kinase receptor 2 (NTRK2) is the top subcutaneous biomarker (see https://gtexportal.org/home/gene/NTRK2), independently of the glycemic levels of the patients.

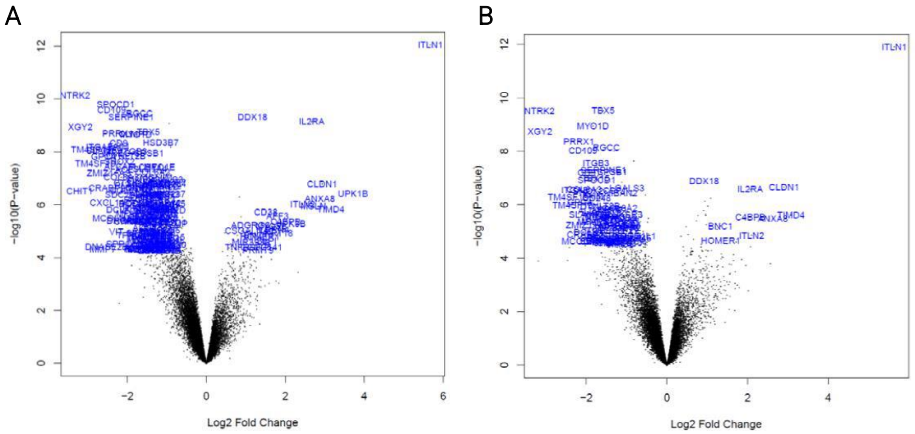

Figure 27. Volcano plot summaries of Limma differential expression analysis results.

Significance using as cutoff criteria padj1.2 is showed as blue highlighted genes. A, comparison between SUB and VIS samples from patients with glycemia ≤100 mg/dL. B, comparison between SUB and VIS samples from patients with glycemia >100 mg/dL.

After all those analyses, a heatmap of the top 100 genes differentially expressed in each of the five comparisons was generated (Data not shown). Moreover, a statistical analysis was performed comparing SAT and VAT gene expression to find the gene that changes between both depots (Data not shown). Among the genes that show a significant difference between SAT and VAT, an Azimuth analysis was performed to identify macrophage-related genes [178] (Table 12).

Table 12. Genes differentially expressed on SAT compared with VAT and associated with macrophages signature.

Term	Overlap (%)	Genes
Classical Monocyte	100	FCN1; VCAN; SELL; FPR1; S100A12; MNDA; S100A9; MYO1F; S100A8; ZFP36L2
Proliferating Macrophage	81.8	ANLN; TPX2; RHEB; UBE2C; CDK1; NUSAP1; BIRC5; KPNA2; TYMS
OLR1+ Classical Monocyte	80	SRGN; CXCL8; CCL20; IL1B; G0S2; CXCL3; CXCL2; EREG
CD14+ Monocyte	75	FCN1; MS4A6A; VCAN; CSF3R; IL1B; G0S2; CD300E; S100A12; CTSD; S100A9; CD99; S100A8
Macrophage	75	C1QB; CYP27A1; C1QA; MARCO; MSR1; APOC1; GPD1; ACP5; OLR1
CD16+ Monocyte	65	FCN1; IFITM3; TCF7L2; IFITM2; LST1; MS4A7; YBX1; RHOC; AIF1; SAT1; FCGR3A; PTPRC; RPS19
Monocyte	60	FCN1; SERPINA1; PSAP; MNDA; AIF1; S100A9
Nonclassical Monocyte	50	SPN; FCGR3A; LST1; NAAA; AIF1
Intermediate Monocyte	20	FCN1; AIF1

Then, a functional enrichment analysis was carried out, taking two approaches. The first one is a gene ontology (GO) enrichment analysis using the GOrilla web tool (using default settings) [163], and the second one, is a Gene Set Enrichment Analysis (GSEA) [164].

Three GO types were performed: Biological process (BP), molecular function (MF), and cellular component (CC). This approach suggests that VAT-resident macrophages show increased complement and humoral immune response activity, whereas SAT-resident macrophages have enhanced cellular response and extracellular matrix functional activities. Furthermore, when glycemia levels are incorporated into the analysis, the exocytic pathway and steroid-related lipid metabolism appear more enriched in genes significantly upregulated on SAT only in the HEA group but not in UNH (Table 13).

Table 13. Up-regulated significant GO terms enriched in subsets of genes. GOrilla Hyper Geometric (HG) statistics with padj <0.05 was used.

Comparison	GO BP	GO MF	GO CC
Genes upregulated in VAT-derived macrophages	• regulation of complement activation, classical pathway • negative regulation of complement activation, classical pathway • negative regulation of serine-type endopeptidase activity • negative regulation of serine-type peptidase activity • regulation of complement activation • regulation of protein activation cascade • negative regulation of humoral immune response mediated by circulating immunoglobulin • regulation of serine-type endopeptidase activity • regulation of serine-type peptidase activity • negative regulation of complement activation • negative regulation of protein activation cascade	-	-
Genes upregulated in SAT-derived macrophages	• extracellular matrix organization • extracellular structure organization • platelet degranulation • movement of cell or subcellular component • developmental process • cellular developmental process • regulation of multicellular organismal process • regulation of developmental process • regulation of multicellular organismal development • response to organic substance • response to amyloid-beta • response to chemical • amyloid fibril formation • regulated exocytosis • regulation of extrinsic apoptotic signaling pathway via death domain receptors • intestinal cholesterol absorption • regulation of cell differentiation • response to organonitrogen compound • intestinal lipid absorption • cell motility • negative regulation of cellular process • mechanoreceptor differentiation • exocytosis • negative regulation of hydrolase activity • cell adhesion • cellular response to chemical stimulus • biological adhesion • response to nitrogen compound • secretion • secretion by cell • locomotion • response to stimulus • cell differentiation • cellular response to oxygen-containing compound • cellular response to organic substance • regulation of extrinsic apoptotic signaling pathway • response to acid chemical • retinoid metabolic process • regulation of localization • negative regulation of endopeptidase activity • regulation of anatomical structure morphogenesis • diterpenoid metabolic process • cell activation • cellular response to organonitrogen compound	• extracellular matrix binding • collagen binding • extracellular matrix structural constituent • growth factor binding • protein-containing complex binding • protease binding	• collagen-containing extracellular matrix • extracellular matrix • platelet alpha granule membrane • extracellular region part • cell surface • extracellular exosome • extracellular space • extracellular vesicle • extracellular organelle • vesicle • plasma membrane • organelle lumen • intracellular organelle lumen • membrane-enclosed lumen • plasma membrane part • growth cone filopodium • collagen type VI trimer • extracellular region • sarcolemma • cytoplasmic vesicle part • endoplasmic reticulum lumen • focal adhesion • cell-substrate adherens junction • cell-substrate junction • membrane • adherens junction
Genes upregulated in SAT-derived macrophages in HEA group	• mitotic nuclear envelope disassembly • membrane disassembly • nuclear envelope disassembly • lipid metabolic process	-	• extracellular exosome • extracellular vesicle • extracellular organelle • extracellular region part • cyclin B1-CDK1 complex • vacuolar part • vesicle

With the information obtained with the help of the High Content Genomics and Bioinformatics Unit and after an exhaustive bibliographic search, we proceeded to select MYO1e (Myosin IE) and NCEH1 (Neutral Cholesterol Ester Hydrolase 1) as genes to study, both upregulated in SAT compared with VAT (Figure 28).

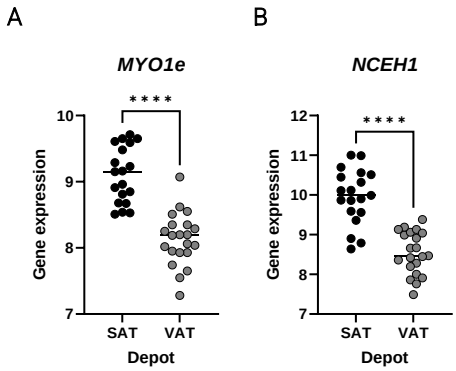

Figure 28. Normalized gene expression of NCEH1 and MYO1e in ATM from VAT and SAT.

A. Gene expression of MYO1e. B, Gene expression of NCEH1. Data are represented as intensities of counts normalized by limma. Individual values are represented. Data were analyzed by paired t-test. SAT, subcutaneous adipose tissue. VAT, visceral adipose tissue. *p<0.05, **p<0.01, ***p<0.001, ****p<0.0001.

4.5 Induction of obesity-related profile on RAW264.7 macrophages using palmitate

WAT-resident macrophages are exposed to adipocytes and are exposed to secretion products from adipocytes. Therefore, in obesity, ATMs are exposed to a higher concentration of FFAs. In this regard, it is broadly described that palmitate treatment promotes a pro-inflammatory response in macrophages like obesity context [179, 180]. As discussed above, palmitate acts on macrophages by activating different pathways that increase the expression of inflammatory cytokines, thus inducing differentiation to M1 and generating a gene expression profile like obese WAT-resident macrophages [181-183].

To standardize the best PA treatment condition, macrophages were treated with concentrations of 0.25mM, 0.5 mM, and 1 mM of PA at 2, 4, and 8 hours, and the expression of the *Tnfa, Il1b,* and *Ccl2* was measured as a parameter of M1 polarization [184], and *Nceh1* and *Myo1e* measured to evaluate if we can see a change in the expression due to the action of palmitate (Figure 29). It can be

observed that 4h promotes the most significant changes at the gene expression level of the markers used (Figure 29A-E).

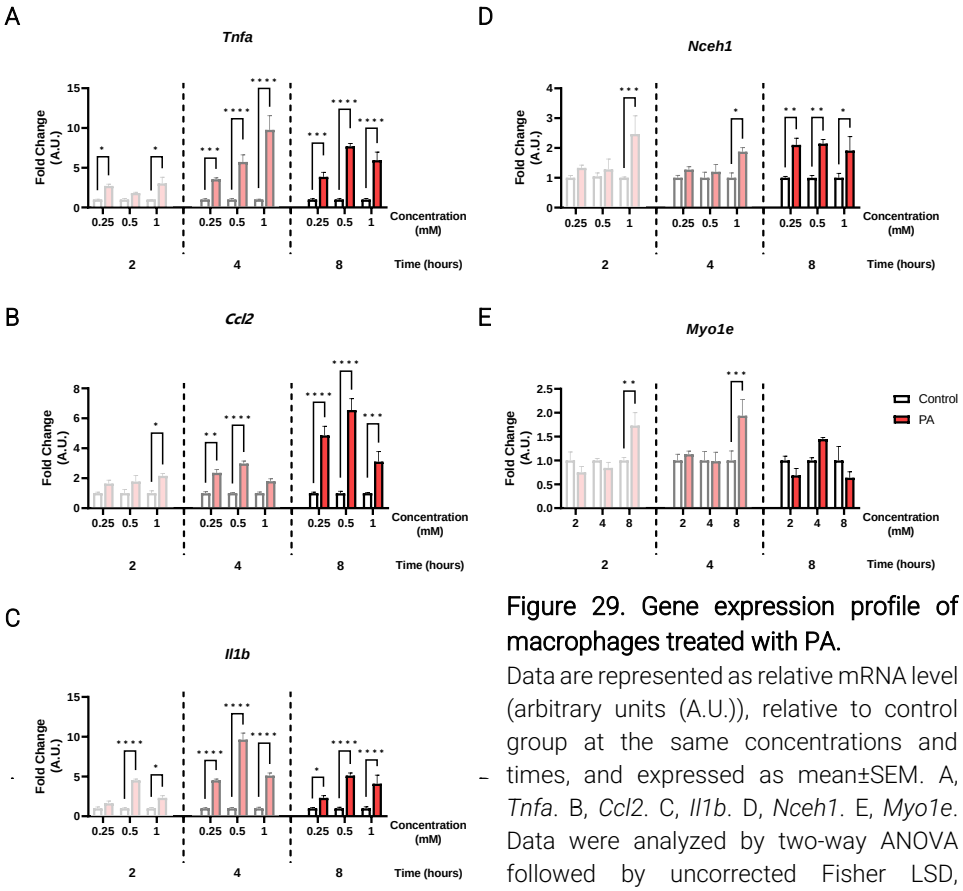

Figure 29. Gene expression profile of macrophages treated with PA.
Data are represented as relative mRNA level (arbitrary units (A.U.)), relative to control group at the same concentrations and times, and expressed as mean±SEM. A, *Tnfa*. B, *Ccl2*. C, *Il1b*. D, *Nceh1*. E, *Myo1e*. Data were analyzed by two-way ANOVA followed by uncorrected Fisher LSD, *p<0.05, **p<0.01, ***p<0.001, ****p<0.0001.

To more accurately determine the optimal conditions of palmitate treatment, a predictive statistical analysis was performed using the FlexPlot tool of the Jamovi 2.3.9 software, to optimize the range of concentrations and time to work (Figure 30). As can be seen, concentrations between 0.5 mM and 1 mM at 4 hours induced the most significant increase in the pro-inflammatory phenotype of the cells (Figure

30A-C). Moreover, *Myo1e* and *Nceh1* are upregulated at the same condition (Figure 30D-E). Therefore, the condition chose to perform the following analysis treatment with 0.75 mM of PA for 4 hours.

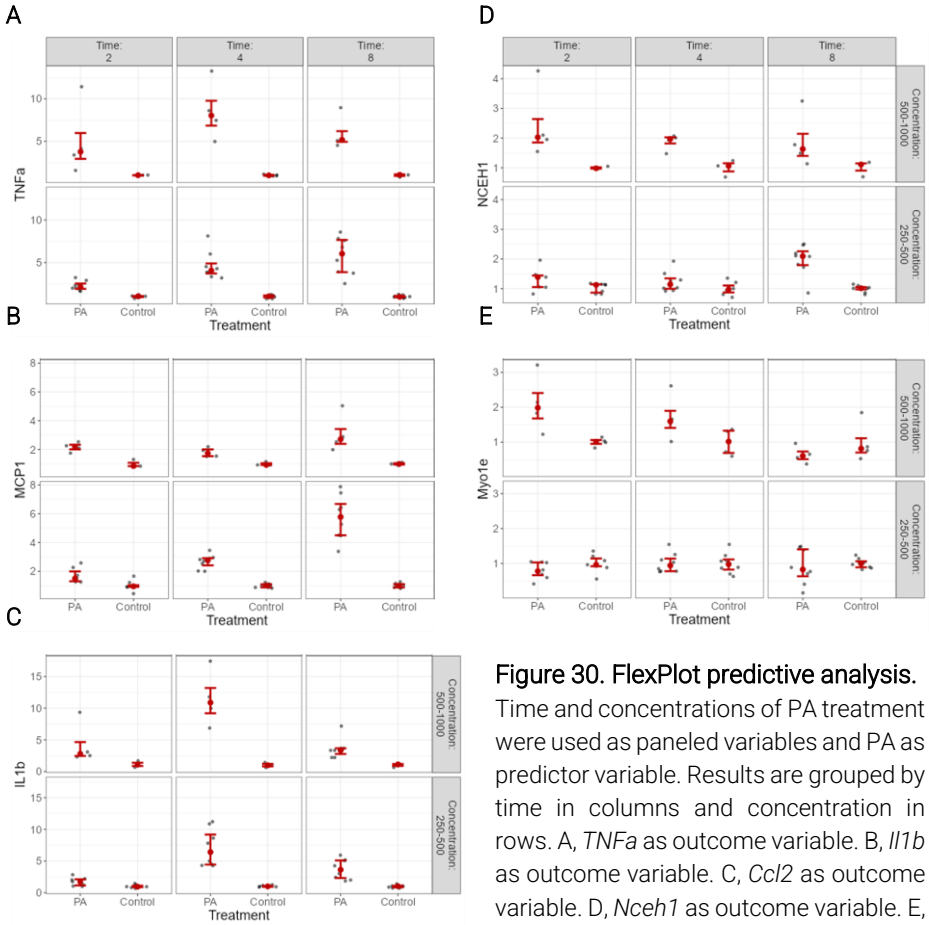

Figure 30. FlexPlot predictive analysis. Time and concentrations of PA treatment were used as paneled variables and PA as predictor variable. Results are grouped by time in columns and concentration in rows. A, *TNFa* as outcome variable. B, *Il1b* as outcome variable. C, *Ccl2* as outcome variable. D, *Nceh1* as outcome variable. E, *Myo1e* as outcome variable. Data is shown as mean±SEM (n=4).

Next, a test was carried out with the selected conditions (0.75mM PA for 4h) to validate the results obtained by the predictive analysis. As observed, 0.75 mM of PA at 4 hours induces a significant increase in the expression of *Ccl2*, *Tnfa*, *Il1b* and *Tlr4* pro-inflammatory genes and on target genes *Nceh1* and *Myo1e* (Figure 31).

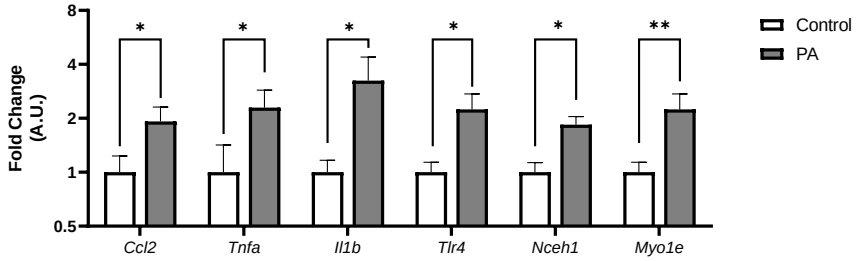

Figure 31. Gene expression profile of macrophages treated with 0.75mM PA for 4h. Data are represented as relative mRNA level (arbitrary units (A.U.)), relative to control group and expressed as mean±SEM. Data were analyzed by unpaired t-test. *p<0.05, **p<0.01.

4.6 Induction of M1 and M2 profile on RAW264.7 macrophages using LPS and IL-4.

To analyze whether the expression of the target genes is associated with the polarization of macrophages towards the M1 or M2 phenotype, it was decided to treat the macrophages with LPS and IL-4 to induce the M1 and M2 phenotype. Briefly, RAW264.7 macrophages were treated with LPS at 60 ng/mL or IL-4 at 40 ng/mL, according to what was described in the literature [185, 186]. In addition, assays were performed at 2, 4, and 8 h to evaluate changes in the expression of *Nceh1* and *Myo1e* and the expression of M1/M2 polarization markers (Figure 32).

As observed, LPS treatment induces the expression of *Tnfa, Il1b,* and *Ccl2*, pro-inflammatory genes linked with the M1 phenotype (Figure 32A-C). However, contrary to what was expected, the expression of *Tlr4* is diminished with the LPS treatment at times studied (Figure 32D).

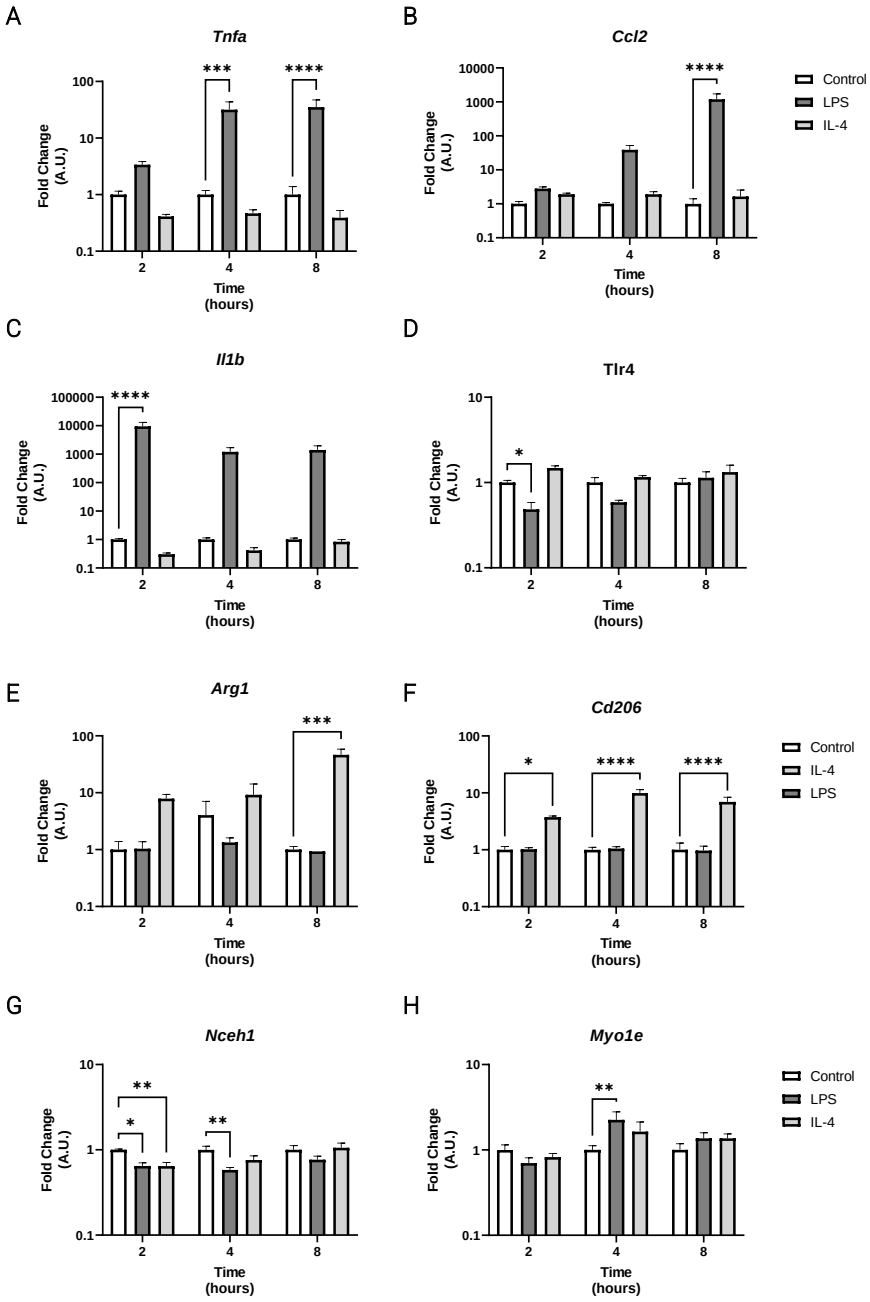

Figure 32. M1 and M2 polarization markers of RAW264.7.

Data are represented as relative mRNA level (arbitrary units (A.U.)), relative to control group. Data represent mean±SEM (n≥3/group in each experiment). Data were analyzed by ordinary one-way ANOVA followed by uncorrected Fisher LSD, *p<0.05, **p<0.01, ***p<0.001, ****p<0.0001.

On the other hand, IL-4 treatment promotes the gene expression of *Arg1* and *Cd206*, two markers of the M2 phenotype (Figure 32E-F). This result indicates that cells can respond to LPS and IL-4 and induce gene expression of M1/M2 polarization markers [187].

Next, to evaluate the best time of treatment to analyze all the gene expressions in RAW264.7, a MANOVA was performed, with a Dunnet post hoc to compare each differentiation time with the control group (Table 14). The results indicate that the differentiation markers are significant 2 hours after stimulation with LPS or IL-4, maintained at 4 and 8 hours. However, when observing the target genes, there are only significant differences after 4 hours of treatment with LPS in *Myo1e* (Figure 32H). Therefore, it was decided to work with that treatment time in the following experiments.

Table 14. MANOVA analysis of polarization markers for the time of treatment with LPS or IL-4.

Time	Contrast	Estimate	Lower	Upper	p-value
2	LPS	24.618	12.226	37.010	0.0036
	IL-4	11.237	2.850	19.624	0.0182
4	LPS	24.618	12.243	36.993	0.0180
	IL-4	11.237	2.862	19.612	0.0040
8	LPS	350.201	98.924	601.478	0.0048
	IL-4	87.797	46.756	128.838	0.0190

4.7 Transfection stability and silencing efficiency on RAW264.7

To determine the role of *Nceh1* and *Myo1e* in macrophage polarization and the pathways involved, it has been decided to silence both genes using siRNAs. Therefore, transfection stability was assessed using TYE563 fluorescent control

(Figure 33). For this, the cells were transfected with 25nM of TYE563 and were photographed at 24h (Figure 33A) and 48h (Figure 33B) post-transfection. Additionally, it was tested to observe the fluorescence at 72h; however, the cells were dead (not shown).

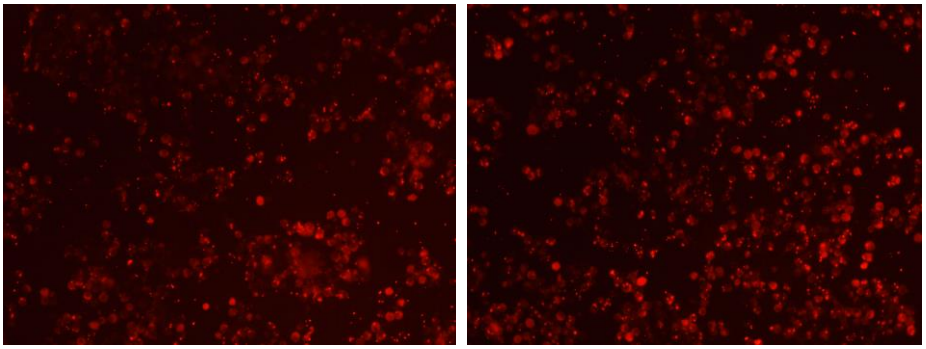

Figure 33. Transfection efficiency and stability in RAW264.7.
Cells were transfected with TYE563 fluorescent dye and fluorecence was observed. A. 24h post transfection. B, 48h post transfection.

As can be seen, there is a fluorescent signal up to 48 hours post-transfection. Therefore, the chosen silencing method allows siRNA incorporation for 48 hours. Once the stability of the transfection was evaluated, the effect of silencing over the Raw264.7 phenotype was tested. The gene markers between vehicle and non-targeting siRNAs (Scramble) were compared for this. Thus, gene expression of *Nceh1*, *Myo1e*, *Ccl2*, *Tnfa* and *Il1b* gene expression was measured to evaluate the Raw264.7 phenotype was performed. Surprisingly, transfection with siRNA Scramble decreases *Il1b* gene expression (Figure 34). Considering this effect, the following tests will be carried out only by comparing the impact between the siRNA target and the scramble siRNA.

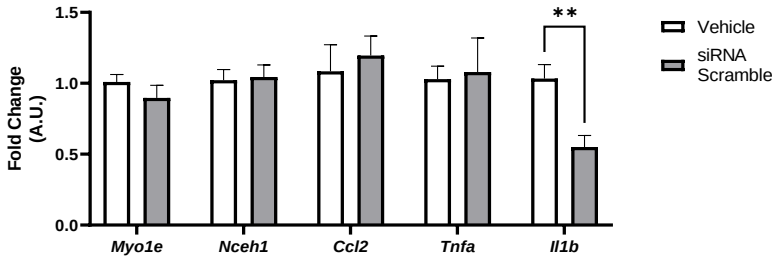

Figure 34. Silencing effect over phenotype.
Raw264.7 cells were transfected or not with scramble siRNA. Data are represented as relative mRNA level (arbitrary units (A.U.)), relative to vehicle. Data is representative of two independent experiments. Data represent mean±SEM (n=4/group in each experiment). Data were analyzed by paired t-test, *p<0.05, **p<0.01.

Finally, the silencing efficiency of *Myo1e* and *Nceh1* was tested after 24h and 48h of transfection (Figure 35). The cells were transfected with a 25nM of siRNA pool for *Nceh1* and *Myo1e*, using a non-targeting pool (Scramble) as a control at the same concentration (Figure 35). As can be seen at 24h post-transfection, a significant silencing of *Myo1e* (~44% silencing, Figure 35A) and *Nceh1* (~76% silencing, Figure 35B) is achieved. However, at 48h, silencing is diminished, losing significance in the case of *Myo1e* (Figure 35A).

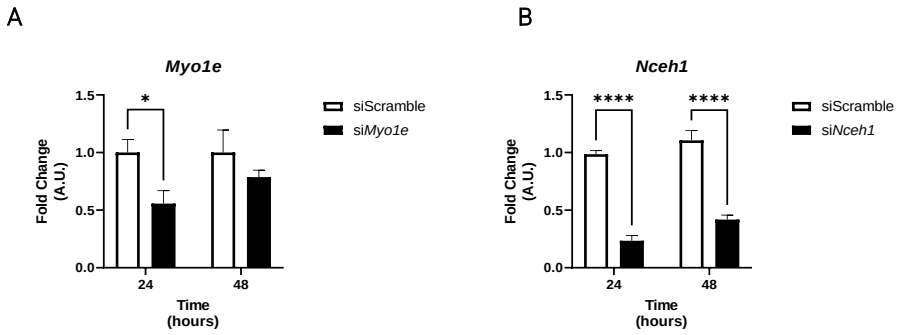

Figure 35. Silencing efficiency of siRNAs.
Raw264.7 cells were transfected with Myo1e or Nceh1 siRNAs and gene expression of these genes were evaluated. A, *Myo1e*. B, *Nceh1*. Data are represented as relative mRNA level (arbitrary units (A.U.)), relative to control group. Data is representative of three independent experiments. Data represent mean±SEM (n=3-4/group in each experiment).

4.7.1 *Myo1e* silencing does not affects the gene expression profile of LPS-treated RAW 264.7 cells

To evaluate the silencing of *Myo1e* in the differentiation process towards M1 or M2 phenotype, RAW264.7 cells were transfected with Scramble siRNA (non-targeting) as a control or with *Myo1e* siRNAs. Then, cells were treated for 4h (according to section 4.6) with 60 ng/mL LPS to differentiate to M1 [188]. DMEM+0.05% BSA was used as a control. First, *Myo1e* silencing was effective in all treatments, with a significant decrease in those transfected with si*Myo1e* compared to those transfected with siScramble (Figure 36A). Silencing of *Myo1e*, reduce the expression of *Cd206* in LPS-treated group (Figure 36E). No other differences were observed. No differences were observed with the addition of IL-4 (Figure S2).

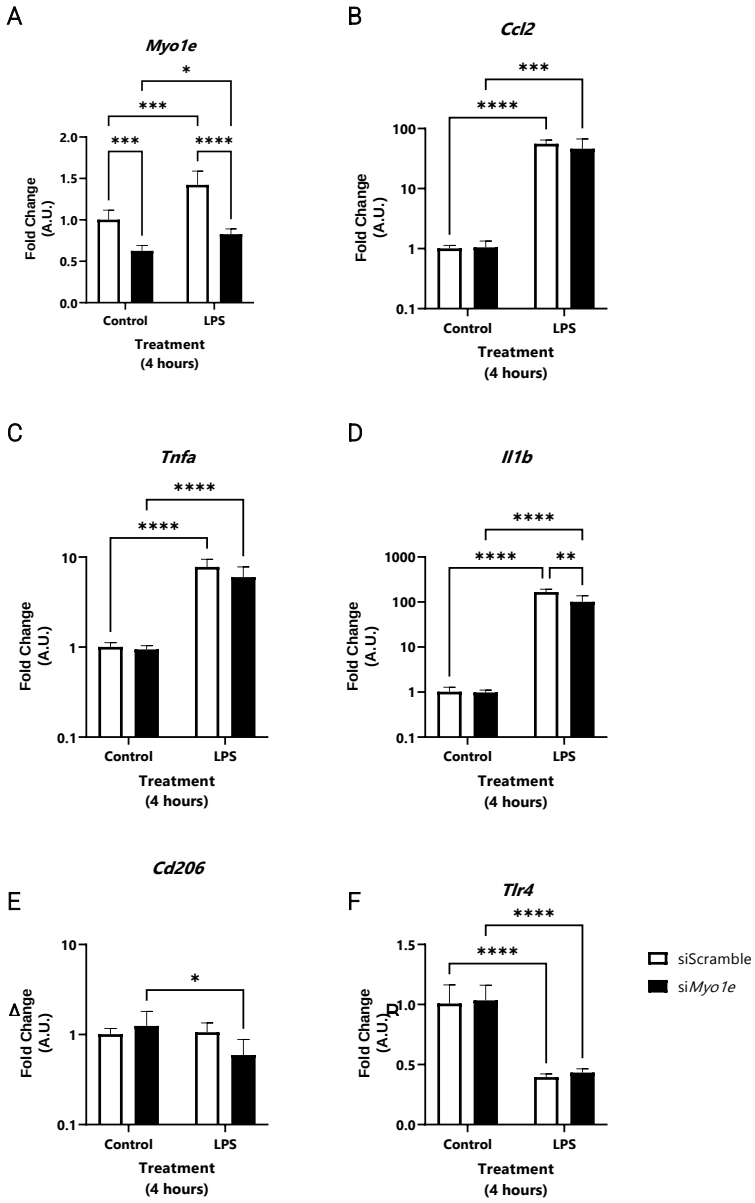

Figure 36. M1 polarization markers of RAW264.7 transfected with Myo1e siRNA.
Cells were transfected and then, treated with medium (control), 60 ng/mL LPS for 4 h. Data are represented as relative mRNA level (arbitrary units (A.U.)), relative to control group. Data represent mean±SEM (n=4). Data were analyzed by ordinary one-way ANOVA followed by uncorrected Fisher LSD, *p<0.05, **p<0.01, ***p<0.001, ****p<0.0001.

4.7.2 *Myo1e* silencing affects the proinflammatory profile of palmitate-treated RAW 264.7 cells

The *Myo1e* gene was silenced in RAW264.7 macrophages, and then cells were treated with PA 0.75 mM for 4h (according to section 4.5.) Because LPS is a pro-inflammatory stimulus that increases obesity and acts synergistically with PA [189, 190], we also decided to stimulate with PA 0.75 mM + 60 ng/mL LPS (PA+LPS).

Myo1e silencing only increases *Il1b* gene expression (Figure 37D). However, *Ccl2* expression substantially increases in silenced cells treated with PA or PA+LPS (Figure 37B). Furthermore, there is a significant increase between the untreated and the silenced groups treated with PA+LPS (Figure 37B). *Myo1e* silencing blunt the PA-LPS-induced expression of *Tnfa* (Figure 37C), and the *Il1b* increases observed control group (Figure 37D). Moreover, *Il1b* expression decreases with PA-BSA and PA+LPS in silenced groups (Figure 37D).

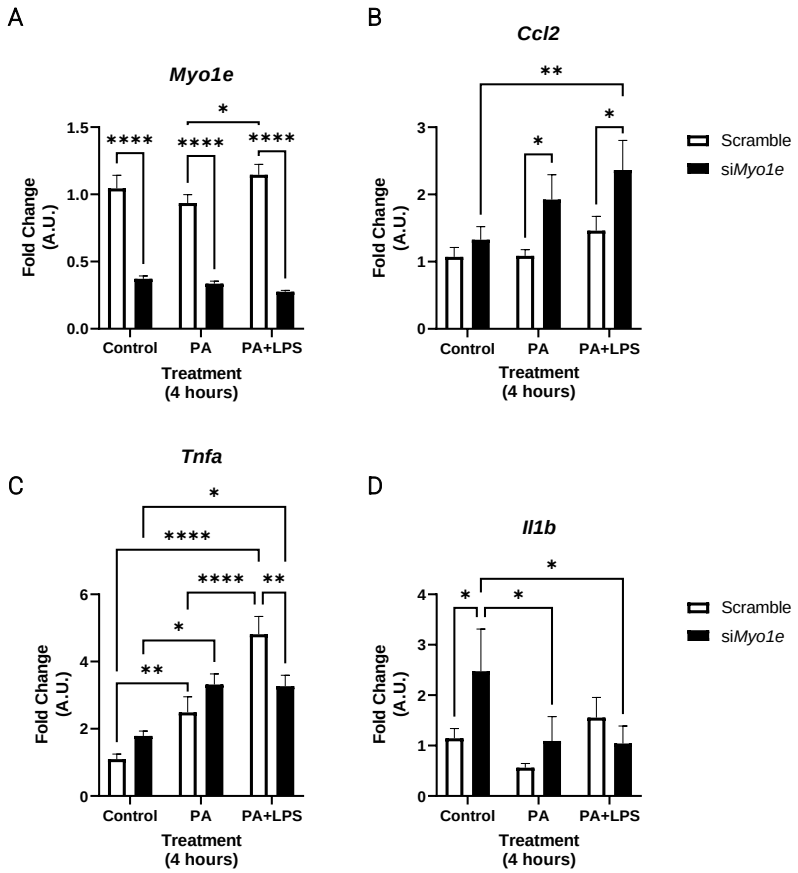

Figure 37. Phenotype of RAW264.7 cells transfected with *Myo1e* siRNA.
Silenced cells were treated with BSA (control), PA-BSA 0.75 μM or PA-BSA 0.75 μM plus 60 ng/mL LPS for 4 h. A, *Myo1e*. B, *Ccl2*. C, *Tnfa*. D, *Il1b*. Data are represented as relative mRNA level (arbitrary units (A.U.)), relative to control group Data is representative of two independent experiments. Data represent mean ± SEM (n ≥ 3/group in each experiment). Data were analyzed by ordinary one-way ANOVA followed by uncorrected Fisher LSD, *p<0.05, **p<0.01, ***p<0.001, ****p<0.0001.

4.7.3 *Myo1e* silencing reduces macrophage migration

Because *Myo1e* is related to immune cell migration and tissue infiltration, a scratch assay was performed in silenced RAW264.7 cells to evaluate the effect of this knockdown on macrophage migration. For this, transfected cells were vertically scratched using a 200µl pipet tip and photographed at time 0. After 24h of incubation in starvation media, cells were photographed to observe cell closure (Figure 38). Images were analyzed using Wound Healing Size Tool (ImageJ/Fiji), and % of cell closure was calculated. After 24h of incubation, the results show that the silencing of *Myo1e* reduces the % of cell closure from 40.5% to 11.3%, which means the migration capacity of macrophages is decreased by ~72%, compared with the scrambled group (Figure 38C).

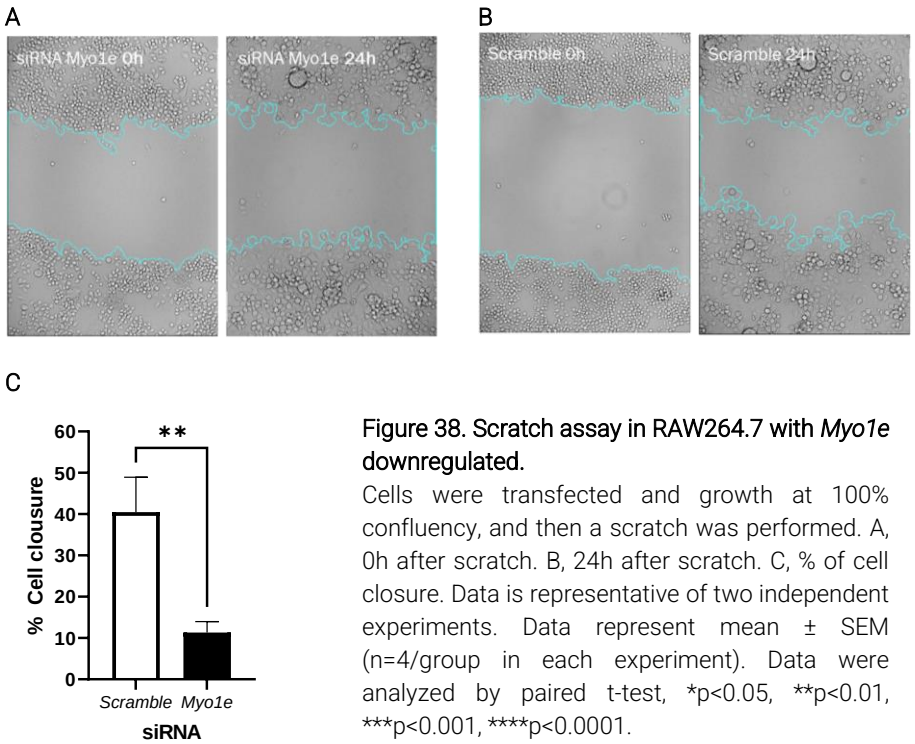

Figure 38. Scratch assay in RAW264.7 with *Myo1e* downregulated.
Cells were transfected and growth at 100% confluency, and then a scratch was performed. A, 0h after scratch. B, 24h after scratch. C, % of cell closure. Data is representative of two independent experiments. Data represent mean ± SEM (n=4/group in each experiment). Data were analyzed by paired t-test, *p<0.05, **p<0.01, ***p<0.001, ****p<0.0001.

4.7.4 *Nceh1* silencing affects the profile of LPS treated RAW 264.7 cells

Similarly, in *Myo1e,* the effect of *Nceh1* silencing was evaluated. For this purpose, the *Nceh1* gene was silenced in the RAW264.7 cell line, and then cells were treated with PA at 0.75 mM and PA at 0.75 mM plus 60 ng/mL LPS, for 4h. First, *Nceh1* silencing increases *Ccl2* and *Il1b* gene expression (Figure 39C-D). However, the addition of LPS itself reduce the expression of Nceh1 like si*Nceh1* treatment (A), promoting an increase in *Tnfa*, *Ccl2* and *Il1b* expression (Figure 39B-D). No differences were observed with the addition of IL-4 (Figure S3).

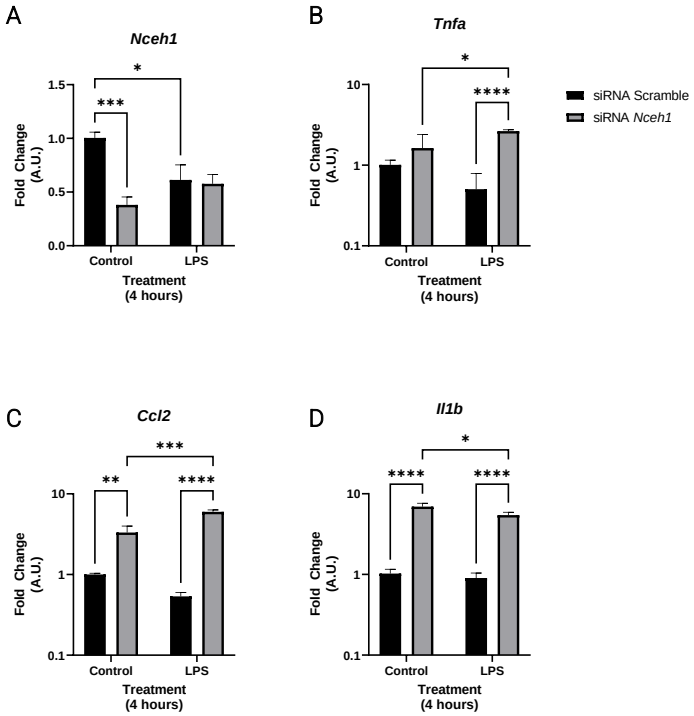

Figure 39. M1 polarization markers of RAW264.7 transfected with *Nceh1* siRNA.
Cells were transfected and then, treated with medium (control), 60 ng/mL for 4 h. Data are represented as relative mRNA level (arbitrary units (A.U.)), relative to control group. Data represent mean±SEM (n=4). Data were analyzed by ordinary one-way ANOVA followed by uncorrected Fisher LSD, *p<0.05, **p<0.01, ***p<0.001, ****p<0.0001.

4.7.5 *Nceh1* silencing affects the proinflammatory profile of palmitate-treated RAW 264.7 cells

To check the effect of *Nceh1* over palmitate-induced gene expression. The *Nceh1* gene was silenced in RAW264.7 macrophages using siRNAs, and then cells were treated with PA 0.75 mM for 4h or PA 0.75 mM + 60 ng/mL LPS (PA+LPS) (According to section 4.5).

In the first place, a *Nceh1* silencing of 75% was achieved (Figure 40A). However, the silencing only promotes the expression of *Il1b* in the control group (Figure 40D) and blunts the PA+LPS-induced *Tnfa* expression (Figure 40C). Furthermore, the downregulation of *Nceh1* can reverse the PA+LPS-induced *Il1b* expression (Figure 40D).

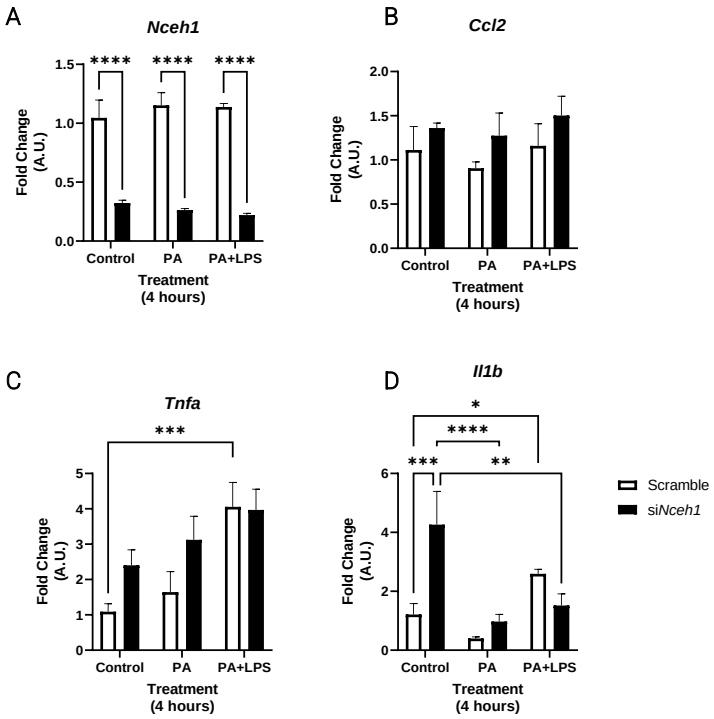

Figure 40. Phenotype of RAW264.7 with *Nceh1* downregulation.
RAW264.7 cells were transfected with si*Nceh1* and treated with BSA (control), PA-BSA 0.75 µM or PA-BSA 0.75 µM plus 60 ng/mL LPS for 4 h. A, *Myo1e*. B, *Ccl2*. C, *Tnfa*. D, *Il1b*. Data are represented as relative mRNA level (arbitrary units (A.U.)), relative to control group. Data represent mean ± SEM (n ≥ 3). Data were analyzed by ordinary one-way ANOVA followed by uncorrected Fisher LSD, *p<0.05, **p<0.01, ***p<0.001, ****p<0.0001.

Because *Nceh1* is a critical enzyme that suppresses lipid droplet formation by removing cholesterol in macrophage foam cells [96, 191]. Genes related to macrophages lipid metabolism were measured (Figure 41). The downregulation of *Nceh1* promotes the expression of *Cd36* in the control group at the same level as the PA stimulus (Figure 41A). Similarly, *Lcn2* expression is increased by *Nceh1* silencing, like the effect of PA+LPS (Figure 41C). Finally, the expression of *Cpt1a* is

increased by silencing in the control group, but the treatments can reverse this effect (Figure 41D).

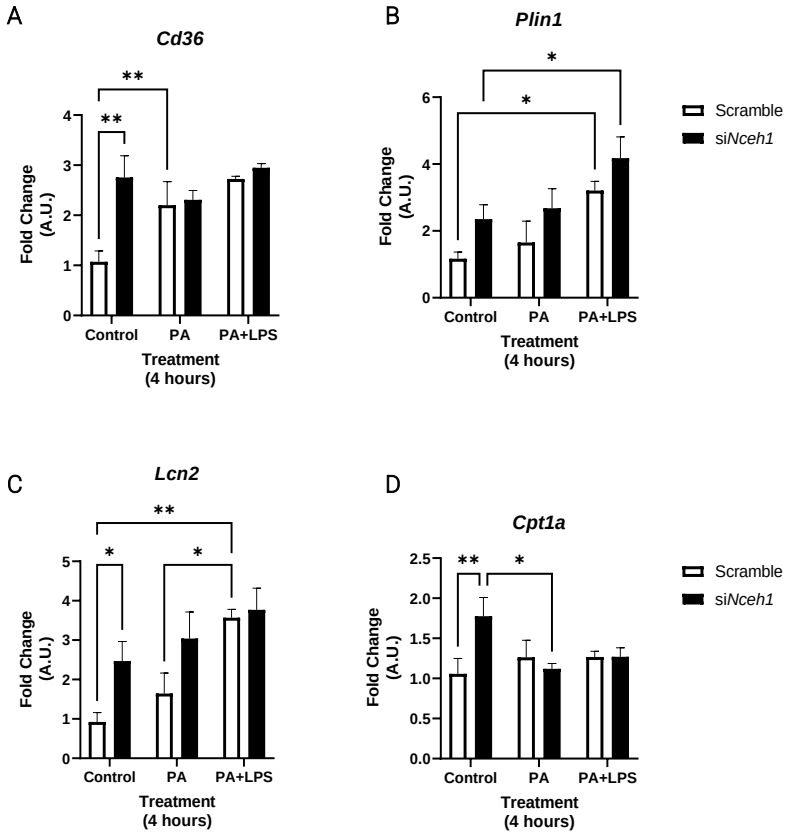

Figure 41. Effect of the downregulation of *Nceh1* over FFA regulated genes in RAW264.7.

Cells were transfected with si*Nceh1* and treated with BSA (control), PA-BSA 0.75 μM or PA-BSA 0.75 μM plus 60 ng/mL LPS for 4 h. A, *Myo1e*. B, *Ccl2*. C, *Tnfa*. D, *Il1b*. Data are represented as relative mRNA level (arbitrary units (A.U.)) relative to the control group. Data represent mean ± SEM (n ≥ 3). Data were analyzed by ordinary one-way ANOVA followed by uncorrected Fisher LSD, *p<0.05, **p<0.01, ***p<0.001, ****p<0.0001.

4.7.6 *Nceh1* downregulation promotes lipid accumulation in RAW264.7 macrophages

Because the silencing of *Nceh1* affects some genes related to lipid metabolism, a functional assay was performed. Briefly, cells were transfected with si*Nceh1* and then were treated with PA for 4h, and lipid accumulation was evaluated using Nile red dye [192]. First, PA treatment promotes lipid accumulation in macrophages (Figure 42C-D, Figure 43). However, *Nceh1* silencing increases the accumulation (Figure 42A) and also decrease the size of lipid vesicles (Figure 42B) in macrophages when treating them with PA.

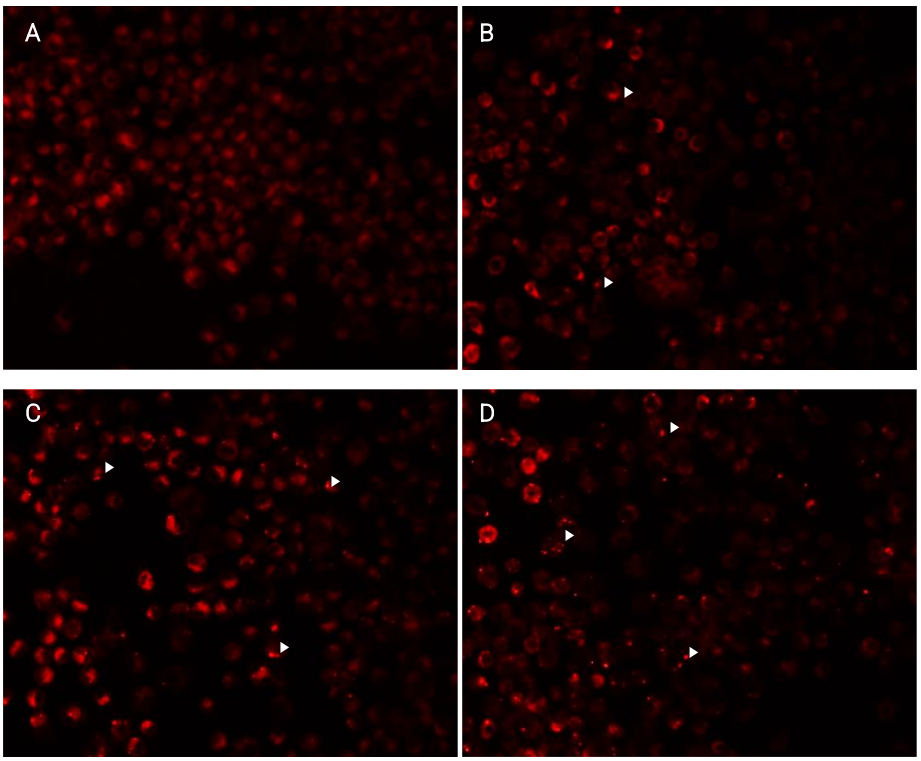

Figure 42. Fluorescent images of lipid accumulation in *Nceh1*-knockdown RAW264.7.

Cells were transfected, and treated with 0.75mM of PA, for 4 hours. A, Scramble+BSA (Control). B, Scramble+PA. C, siNceh1+BSA. D, siNceh1+PA. Data is representative of triplicates.

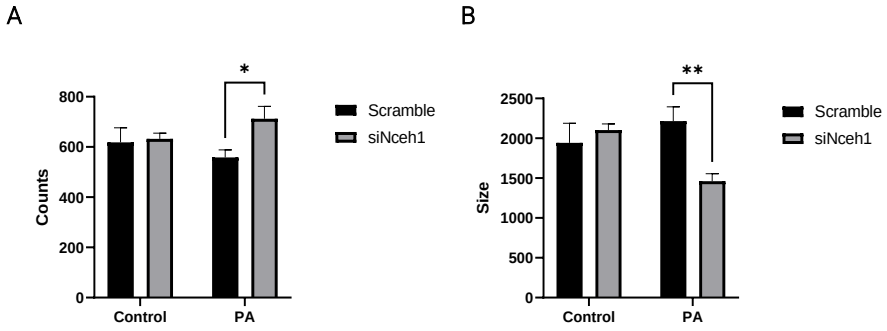

Figure 43. Quantification of lipid droplets from the Nile red assay.
Quantification of lipid accumulation thought Nile red Assay. A total of 9 images per treatment were quantified, with three images of each triplicate. Data represent mean ± SEM. Data were analyzed by ordinary one-way ANOVA followed by uncorrected Fisher LSD, *p<0.05, **p<0.01, ***p<0.001, ****p<0.0001.

5. DISCUSSION

WAT is an organ comprising large adipocytes with a single lipid droplet and few mitochondria content. This morphology confers WAT, the capacity for energy storage and homeostasis in response to nutritional demand [18].

SAT and VAT have been widely studied for their association with the development of IR and cardiometabolic risk [29, 30]. However, each depot has different biochemical features and metabolic functions. It has been demonstrated that an increased VAT mass is an independent factor in metabolic deterioration, and the size of this depot is directly associated with a poor prognosis in metabolic diseases [29-34, 40]. On the other hand, an increase in SAT mass has a protective role, which is inversely associated with glucose intolerance, IR, and risk of T2D diagnosis [33, 35-37, 41, 45, 47]. Therefore, changes in AT distribution are relevant to understanding its role in metabolism.

Obesity is characterized by the excessive accumulation of body fat in WAT, mostly due to an imbalance between energy intake and expenditure. Hence, an increase in VAT and SAT mass leads to a rise in the BMI associated with developing obesity-related co-morbidities [42]. However, the development of co-morbidities is mainly linked to WAT distribution [193].

In this context, the percentage of VAT in obese subjects strongly correlates with IR and poor glycemic control [41, 44, 45], and in animal models, surgical removal of this tissue prevents IR and delays the development of T2D [46]. Furthermore, obese subjects have less SAT, contributing to further deterioration of the insulin response and promoting the establishment of T2D [44, 47]. In addition,

insulin-sensitive obesity is linked to a smaller VAT depot at the same BMI, suggesting increased SAT [48]. All this evidence indicates that both SAT and VAT contribute to the development of IR, but with contrasting roles.

Moreover, the infiltration of immune cells in each depot is associated with different metabolic outcomes [194]. ATMs represent the most abundant immune cell infiltrated in WAT and regulate several physiological processes, such as WAT-remodeling and insulin sensitivity [195]. ATMs can be broadly classified as M1, which has a pro-inflammatory phenotype, and M2, characterized by an immunosuppressive phenotype. Both subpopulations are present in AT in different proportions, being M1-phenotype predominantly found in obese WAT and in high proportions in subjects with metabolic complications [68]. While M2-phenotype is responsible for WAT homeostasis, tissue remodeling, and insulin sensitivity and they are predominantly found in lean WAT [68, 196].

In obesity, there is a similar infiltration of ATMs in VAT and SAT [70, 197]. However, BMI correlates with the number of M1-phenotype cells and inversely with the M2-phenotype on SAT, but not in VAT [198, 199]. Moreover, animal models demonstrated that M2 infiltration if VAT exerts a protective role of HFD and obesity-induced comorbidities [196, 200]

5.1 *IL16* gene is induced in obese VAT and its secretion changes after bariatric surgery

In cohort 1, the expression of IL-16 was increased in VAT from obese patients compared to its standard weight counterpart (Figure 7A).

We also found that bariatric surgery promotes a change in IL-16 plasma levels (Figure 7B). In this regard, obese animal models that underwent caloric restriction show a first increase in IL-16 secretion and a reduction in adipocyte size [153]. Additionally, the authors found that, in obese animals, the levels of IL-16 are higher than their lean counterparts [153].

Taken all together, we could suggest that IL-16 is secreted by enlarged VAT in obese subjects, and its rise after bariatric surgery is due to the remodeling of VAT, which ends in a reduction of VAT adipocyte size and infiltrated immune cell population. However, evaluating, and correlating plasma IL-16 levels with adipocyte size before and after bariatric surgery would be necessary.

5.2 *In vitro* addition of IL-16 modulates adipogenesis and affects the phenotype of mature adipocytes

It has been described that VAT is linked with an increased metabolic risk [201-203]. For this reason, searching for new targets in its pathological role is essential.

In this context, our work shows that *in vitro* addition of IL-16 over 3T3-L1 cells during adipogenesis promotes the expression of fibrosis-related genes, such as *Pref1* and *ColA6*. This effect is accompanied by a reduction in the expression of lipid metabolism genes (*Cd36*, *Fabp4,* and *Plin1*) at the latter stages of differentiation. These results agree with Divoux *et* al., where found that collagen accumulation in WAT is accompanied by a decrease in perilipins [116]. Additionally, fibrotic WAT shows increased lipolysis [204, 205], which plays a crucial role in obesity-associated diseases [206, 207]. Lipolysis is regulated by MAPK/ERK (MEK)1/2 and ERK1/2

pathways [208] and can be activated by Pref-1 [209], leading to a downregulation of Perilipins [210]. Thus, the IL-16-induced *Pref1,* accompanied by a decrease in *Plin1* at the latter stages of adipogenesis, suggests that IL-16 activates lipolysis signaling.

Therefore, our results suggest that IL-16 participates, during the adipogenesis, in the pathological role of VAT on obesity development, promoting fibrosis and mismanagement of lipids of this depot.

In mature adipocytes, the treatment with 1ng/mL and 10 ng/mL, but not 100ng/mL, of IL-16 during 24h decreased the expression of Leptin and Pref1 (Figure 14). Leptin expression is regulated by the nutritional status of an individual, thus, during weight loss, leptin levels decrease [211]. The circulating levels of this adipokine correlate positively with the adipocyte size, and the administration of Leptin promotes lipid mobilization [212]. On the other hand, Pref-1 is a negative regulator of adipogenesis and is related to fibrosis in adipose tissue [104, 116]. Thus a decrease in this gene expression could indicate that IL-16 prevents WAT-fibrosis. Our results suggest that IL-16 at low doses promotes lipid metabolism and WAT-remodeling. Although we expected to see a greater effect with the higher dose, surprisingly, we did not see an impact on gene expression, which can be explained by the fact that this high dose probably produces signaling that internalizes the receptors through which IL-16 exerts its effect, which can be promoting resistance to this cytokine [116].

When pro-inflammatory markers were studied, a significant increase in *Ccl2* expression was observed with 100 ng/mL of IL-16 (Figure 15A). It is broadly known that secretion of CCL2 promotes the infiltration of macrophages into WAT, its levels

are linked with the development of obesity-related diseases [213]. Thus our results indicate that this cytokine promotes pro-inflammatory signaling in mature adipocytes. However, the same dose reduces the *Tnfa* expression (Figure 15B). TNF-α is a pro-inflammatory cytokine whose expression correlates with adiposity in human subjects and promotes WAT-lipolysis [214]. Finally, a reduction of *Il6* was also observed with 10 ng/mL of IL-16. Based on this, it has been described that Il6 expression decreases without changes in macrophage infiltration or CLS during weight loss [215]. Additionally, the expression of this cytokine is regulated by *Tnfa*, and its expression regulates the activity of LPL [216]. Thus the IL-16-induced reduction observed in *Il6* could suggest that IL-16 regulates lipid metabolism through the *Tnfa-Il6* axis.

Then, when lipid metabolism was studied, the highest dose of IL-16 promoted the expression of *Pparg* (Figure 16A). In this context, mice HFD-feed show increased *Pparg* expression in WAT [217], suggesting that IL-16 promotes lipid accumulation *in vitro*. Then, a dose-dependent effect was observed in *Plin1* and *Cd36* gene expression with the addition of IL-16, being significant in the doses of 10 ng/mL and 100 ng/mL (Figure 16B-C). It has been described that a reduced *Plin1* is linked with an increased pro-inflammatory response in lean WAT; thus, this lipid droplet-binding protein help to maintain metabolic homeostasis [218]. Similarly, adipocyte *Cd36* has a metabolically protective role [219]; downregulation of Cd36 helps prevent hyperlipidemia and insulin resistance [220]. Finally, 10 ng/mL decreases the expression of *Glut4* (Figure 16D), suggesting a role of IL-16 in glucose metabolism signaling. Together those results indicate that IL-16 promotes lipid accumulation,

pro-inflammatory, and glucose signaling, which could be the beginning of the development of metabolic diseases in mature adipocytes.

Because pro-inflammatory signaling was altered by IL-16 treatment on mature adipocytes, the next step was evaluating markers of hypoxia fibrosis and WAT-remodeling (Figure 17). Surprisingly, a decrease in the gene expression of *Hif1a* and *Vegf* was observed as dose-dependent (Figure 17A-B). HIF-1α is a transcription factor that contributes to chronic inflammation in obesity [221, 222]; inhibition of HIF-1α in adipocytes leads a reduced WAT-fibrosis and inflammation in cell and animal models [223]. Moreover, the overexpression of *Vegf* protects against diet-induced obesity and insulin resistance [224]. Thus a reduction of *Vegf* could be linked with the establishment of obesity and insulin resistance. Similarly, in a less thoughtful way, *Col4a* expression also decreases with the addition of IL-16, up to a dose of 10 ng/mL, the effect that is reversed when using the dose of 100 ng/mL (Figure 17C). Since changes in genes associated with ECM remodeling are observed, it was decided to evaluate the expression of *Mmp9* and its inhibitor *Timp1*. IL-16 promotes *Mmp9* and decreases *Timp1* expression, significantly increasing the dose-dependent Mmp9/Timp1 ratio (Figure S1). All those results suggest that IL-16 inhibits hypoxia but increases the remodeling and insulin resistance in mature adipocytes, which is linked to *Glut4* expression.

5.3 IL-16 blunts the PA-induced signalling

First, the induction of obesity signaling was studied by adding 1 mM PA (Figure 18). We found that PA promotes the expression of pro-inflammatory genes, according to described previously in the literature [175, 225-227], and promotes lipid

accumulation and glycerol release (such lipolysis parameter) (Figure 20). Those results indicate that PA treatment will be used as an *in vitro* obesity induction in mature adipocytes.

Then, the concomitant effect of adding PA and IL-16 was evaluated. IL-16 at 10 ng/mL dose blunt the PA-induced lipid accumulation and glycerol release (Figure 20). In that sense, it has been described that PA simulates *in vitro* obesity context in adipocytes cell line where treating this lipid promotes adipocyte hypertrophy, insulin resistance, and lipolysis [228, 229]. When gene expression was evaluated, we found that PA-treated mature adipocytes showed a decreased *AdipoQ*, *Leptin,* and *Pref-1*, similar to those described previously by Ceja-Galicia *et* al. [228].

Then the effect of IL-16 was evaluated in this *in vitro* obesity model. The 10 ng/mL dose of IL-16 blunts significatively the PA-induced lipid accumulation and glycerol release (Figure 20). When gene expression was evaluated, similar results were found. IL-16 increases AdipoQ, Leptin, and Pref1 expression in a dose-dependent manner (Figure 21). These results suggest that IL-16 can blunt hypertrophy and lipolysis in an obesity context. Thus, this cytokine may be involved in a metabolic improvement of adipocytes in obesity.

Surprisingly, this cytokine also promotes the expression of *Ccl2* and *Il6* in PA-treated adipocytes (Figure 22). It has been demonstrated that *Ccl2* gene expression is regulated by Leptin [230], so its increment could be related to the changes in *Leptin* gene expression. Moreover, Ccl2 is an important factor that promotes macrophage infiltration and lipid transportation on SAT of animal models [231]. On the other hand, it has been described that in adipocytes, IL-6 induces the release of

FFA and leptin and blunt obesity-associated metabolic complications [39]. Taking all those results together, we could conclude that IL-16 promotes the expression of IL-16 and Leptin, inducing lipolysis and dampening obesity-related signaling.

When the effect of IL-16 on lipid and glucose metabolism was evaluated, we found that IL-16 at 1 ng/mL and 10 ng/ml damp the PA-induced diminution of *Pparg* (Figure 23A). Pparγ is crucial for mature adipocyte supervenience, energy storage, and adiposity [232, 233]. The activation of Pparγ improves insulin sensitivity [233]. Thus IL-16 could be acting in these phenomena through increased *Pparg* expression. In this sense, the effect observed in *Plin1*, *Cd36,* and *Glut4* supports that IL-16 ameliorates the PA-induced changes in lipid and glucose metabolism genes.

All those results suggest that IL-16 is a cytokine responsible for maintaining homeostasis in the adipocytes when these cells are in an obesity context.

5.4 *MYO1e* and *NCEH1* genes are downregulated on VAT-ATMs compared with SAT-ATMs

Clariom D transcriptomic array shows increased *MYO1E* and *NCEH1* gene expression on SAT-ATMs compared with VAT-ATMs from obese subjects (Figure 28).

In macrophages, Myo1E is involved in the phagosome closure cups [94]. Furthermore, in LPS-stimulated macrophages, MYO1E reduces cell spreading, chemokine secretion, and antigen presentation [94], and its deficiency is related to increased secretion of CCL2 [93]. Thus, the increased observation of SAT could be

associated with a less pro-inflammatory phenotype in the SAT- compared with VAT-infiltrated macrophages.

On the other hand, NCEH1 is involved in reducing atherosclerotic lesions [96-98]. Thus, the results could suggest that SAT-macrophages show an increase in the reverse cholesterol transport compared with VAT.

Those results suggest that the protective role of SAT in obesity could be explained partially by the higher expression of *MYO1E* and *NCEH1* on SAT- compared with VAT-macrophages [41, 234, 235]. Our results show the first evidence that the phenotype of macrophages infiltrating adipose tissue is depot dependent. This can be associated with a better prognosis in the metabolic state of the subject. In this sense, it has been described that ATMs activation is related to the metabolic niche [236]. Thus, our results suggest that SAT promotes a less pathogenic activation of WAT-infiltrated macrophages.

5.5 *Myo1e* silencing affects the *in vitro* gene expression profile in M1 macrophages and reduces the migration capacity of macrophages

First, the best condition of *Myo1e* gene expression increase was searched. We found that 60 ng/mL of LPS and 0.75mM of PA at 4 hours increase the expression of *Myo1e* and promote a pro-inflammatory gene expression (Figure 31 andFigure 32). Then, the effect of *Myo1e* silencing through siRNAs was evaluated. We found that si*Myo1e* alone doesn't affect the gene expression and that the treatment with LPS only affected the expression of *Cd206* (Figure 36). In that sense, it has been

described that WAT CD206^{+} cells are mainly anti-inflammatory macrophages (M2 phenotype) and are involved in controlling adiposity and systemic insulin sensitivity due to the secretion of TGF-β1 [237]. Mice with reduced numbers of CD206^{+} cells show an improved insulin sensitivity linked with a higher number of smaller adipocytes [237]. Thus, this result could suggest that silencing of Myo1e might promote the M1 phenotype in macrophages, which could be involved in insulin sensitivity. However, further studies are necessary to evaluate the effect in WAT of *Myo1e* ablation.

When the PA effect was evaluated, we found that *Ccl2* gene expression was significantly increased by PA and PA+LPS treatment in si*Myo1e* groups, compared with Scrambled control (Figure 37B), suggesting that the silencing of *Myo1e* promotes the macrophages recruitment signaling in WAT. In this context, Wenzel *et* al. reported that CCL2 was significantly elevated in the supernatants of LPS-stimulated macrophages from *Myo1e*−/− mice compared to WT controls [93].

Next, si*Myo1e* blunt the PA- and PA+LPS-induced increase of *Tnfa* expression, significantly decreasing the expression in the PA+LPS group treated with si*Myo1e* (Figure 37C). Based on this, animal models with a deficiency of TNF-α expression from ATMs show a decreased WAT amount and enhanced insulin sensitivity [238]. Similarly, *in vitro* studies demonstrated that neutralizing TNF-α inhibits the inflammatory signaling in 3T3-L1 and induces fatty acid lipolysis [239]. Thus, the observed decrease because of *Myo1e* silencing suggests that Myo1e regulates the inflammatory signaling and lipid metabolism in macrophages.

In the *Il1b* expression, we found that both PA and PA+LPS can blunt the increase induced by si*Myo1e* (Figure 37D). According to this, it has been described

that IL-1β is the main cytokine involved in immune cells WAT-infiltration in obesity [240], and its secretion contributes to the development of insulin resistance [87, 240]. The expression and secretion of IL-1 β are regulated by NLRP3-inflammasome activation, an immune cell sensor. Thus, our findings are the first evidence to link *Il1b* with *Myo1e* expression, suggesting that Myo1e might be involved in downregulating the inflammasome in WAT.

Then a functional study was performed to evaluate the effect of *Myo1e* knockdown; a significant reduction in the migration capacity was founded when *Myo1e* was silenced (Figure 38C). Previously it has been reported that ATMs from Myo1e−/− show a reduction in TLR4-driven macrophage spreading [93]. Thus, our finding was supported by this study.

5.6 *Nceh1* silencing affects the *in vitro* gene expression profile in M1 macrophages and promotes lipid accumulation

As previously described (Section 5.4), NCEH1 is responsible for the hydrolysis of intracellular cholesterol ester and contributes to the FC efflux from macrophages [95-98]. Thus, we evaluate the effect of its silencing in macrophages. Knockdown of *Nceh1* promotes the expression of *Ccl2* and *Il1b* (Figure 39). In this regard, it has been described that Nceh1 reduces the ER-stress in macrophages and inflammatory signaling [241, 242]. Thus, the knockdown effect of Nceh1 in Raw264.7 cells is comparable with the previously described [241, 242]. Surprisingly, adding LPS decreases *Nceh1* expression similarly to si*Nceh1* treatment (Figure 39). The treatment with LPS promotes the pro-inflammatory phenotype in macrophages and is the gold standard for obtaining M1 macrophages *in vitro [187, 243]*. However,

this treatment promotes a higher pro-inflammatory response in the *Tnfa* and *Ccl2* gene expression. This suggests that *Nceh1* is a crucial gene to control macrophage polarization through pro-inflammatory phenotype. However, its role and pathway should be studied.

When silenced cells were treated with PA to simulate an obesity context, we found that in silenced cells, the *Tnfa* and *Il1b* expression was dampening in PA and PA+LPS groups, going to reverse the PA+LPS-induced *Il1b* expression (Figure 40).

Accordingly, TNF-α could function through two receptors with opposite signaling pathways; while TNFR1 promotes apoptosis and anti-inflammatory process, TNFR2 activates proliferation and inflammation pathways [244]. Thus, further experiments are necessary to clarify the *Nceh1* role in the Tnf-α signaling. On the other hand, IL1β is secreted in an inflammatory context [245], and its expression is regulated by FFA. Thus, the reduction observed in silenced cells could suggest an alteration in the lipid metabolism of the macrophages.

Next, we decided to measure the expression of *Cd36*, *Plin1*, *Lcn2,* and *Cpt1a* and evaluate the effect of *Nceh1* knockdown (Figure 41Figure 41). Cd36 is a receptor able to bind lipids in ATMs, contributes to WAT inflammation, and is responsible for internalizing lipids into the cells and forming foam cells [242, 246, 247]. Thus, si*Nceh1* cells do not show changes in their expression in response to PA, nor PA+LPS suggesting an effect on lipid handling in macrophages in response to PA. Plin1 promotes a pro-inflammatory phenotype in macrophages and allows a stable accumulation of lipids in these cells [248]. The increment observed in Nceh1 silenced groups and for the PA treatments suggest an increment in lipid

accumulation. Cpt1a has a protective role on macrophages and is responsible for transporting long-chain FA into the mitochondria promoting FAO and inhibiting lipid accumulation in macrophages [249]. Thus, *Nceh1* silencing promotes this expression suggesting a protective role in a control situation. However, when the cells were treated with PA or PA+LPS, this gene expression was reduced, suggesting that the knockdown of *Nceh1* affects the lipid handling in response to PA stimulus. Lcn2 regulates M1-macrophage polarization in obesity because its expression is activated by FFA [250]. Lcn2 contributes to lipid accumulation in foam cells in atherosclerosis [251]. Macrophages Nceh1-silenced show a significant increase in its expression, suggesting an activation in the lipid accumulation pathways, preventing cells from responding to PA or PA+LPS stimulus. Taking all those results together, we could suggest that siNceh1 promotes an increase in pro-inflammatory and lipid accumulation pathways in macrophages. In this regard, si*Nceh1*-treated cells have higher lipid accumulation with smaller vesicles in PA-treated macrophages (Figure 43). Thus, these results validate our gene expression results.

Together we could conclude that *Nceh1* is a crucial gene in ATMs to regulate lipid metabolism and fight against lipotoxicity in an obesity context.

6. CONCLUSSIONS

1. IL-16 mRNA expression is higher in VAT from obese patients and its plasmatic levels changes after bariatric surgery. Moreover, its expression correlates with markers of inflammation and immune cell activation.

2. *In vitro* assays demonstrate that addition of IL-16 significantly decrease gene expression related with inflammation, lipid metabolism and adipose tissue remodeling, in mature adipocytes. During adipogenesis IL-16 affects *Pref1* expression and genes related with lipid metabolism.

3. IL-16 blunts PA-induced lipid accumulation and changes in gene expression controlling the homeostasis in an obesity context.

4. Our results show the first evidence that the phenotype of human ATMs have a different gene expression profile according to the depot.

5. SAT-ATMs express more *MYO1E* and *NCEH1* compared with VAT-ATMs, suggesting a protective role in SAT.

6. Silencing of *Myo1e* and *Nceh1* alters LPS- and PA-induced gene expression.

7. *Myo1e* seems to be an essential gene in ATMs migration during obesity.

8. *Nceh1* downregulation promotes lipid accumulation in macrophages treated with PA.

7. PUBLICATIONS

Reyes-Farias M, Fos-Domenech J, Serra D, Herrero L, Sánchez-Infantes D. White adipose tissue dysfunction in obesity and aging. Biochem Pharmacol. 2021 Oct;192:114723. doi: 10.1016/j.bcp.2021.114723. Epub 2021 Aug 5. PMID: 34364887.

Reyes M, González L, Ibeas K, Cereijo R, Taxerås SD, Pellitero S, Martínez E, Tarascó J, Moreno P, Malagón P, Higueras C, Soria A, Puig-Domingo M, Villarroya F, Serra D, Herrero L, Sánchez-Infantes D. White adipose tissue-infiltrated CD11b+ myeloid cells are a source of S100A4, a new potential marker of hepatic damage. Eur J Endocrinol. 2021 Apr;184(4):533-541. doi: 10.1530/EJE-20-1130. PMID: 33524007.

Cereijo R, Quesada-López T, Gavaldà-Navarro A, Tarascó J, Pellitero S, **Reyes M**, Puig-Domingo M, Giralt M, Sánchez-Infantes D, Villarroya F. The chemokine CXCL14 is negatively associated with obesity and concomitant type-2 diabetes in humans. Int J Obes (Lond). 2021 Mar;45(3):706-710. doi: 10.1038/s41366-020-00732-y. Epub 2021 Jan 7. PMID: 33414488.

Piquer-Garcia I, Campderros L, Taxerås SD, Gavaldà-Navarro A, Pardo R, Vila M, Pellitero S, Martínez E, Tarascó J, Moreno P, Villarroya J, Cereijo R, González L, **Reyes M**, Rodriguez-Fernández S, Vives-Pi M, Lerin C, Elks CM, Stephens JM, Puig-Domingo M, Villarroya F, Villena JA, Sánchez-Infantes D. A Role for Oncostatin M in the Impairment of Glucose Homeostasis in Obesity. J Clin Endocrinol Metab. 2020 Mar 1;105(3):e337–48. doi: 10.1210/clinem/dgz090. PMID: 31606738; PMCID: PMC7112982.

Reyes-Farias M, Carrasco-Pozo C. The Anti-Cancer Effect of Quercetin: Molecular Implications in Cancer Metabolism. Int J Mol Sci. 2019 Jun 28;20(13):3177. doi: 10.3390/ijms20133177. PMID: 31261749; PMCID: PMC6651418.

8. BIBLIOGRAPHY

1. Bray, G.A., et al., *Obesity: a chronic relapsing progressive disease process. A position statement of the World Obesity Federation.* Obes Rev, 2017. **18**(7): p. 715-723.
2. Federation, W.O. *Obesity is a disease*. 2021; Available from: www.worldobesityday.org/assets/downloads/Obesity_Is_a_Disease.pdf.
3. Haththotuwa, R.N., C.N. Wijeyaratne, and U. Senarath, *Worldwide Epidemic of Obesity*, in *Obesity*, T. Mahmood and S. Arulkumaran, Editors. 2013, Elsevier: Oxford. p. 3-11.
4. WHO. *Obesity and overweight*. 2021; Available from: https://www.who.int/news-room/fact-sheets/detail/obesity-and-overweight.
5. OECD, *Health at a Glance 2021*. Health at a Glance. 2021.
6. Social, M.d.S.y.B., *Encuesta Europea de Salud en España (EESE)*. 2020: Instituto Nacional de Estadística.
7. Panuganti, K.K., M. Nguyen, and R.K. Kshirsagar, *Obesity*, in *StatPearls*. 2023, StatPearls Publishing

Copyright © 2022, StatPearls Publishing LLC.: Treasure Island (FL).

8. Solomon, C.G. and J.E. Manson, *Obesity and mortality: a review of the epidemiologic data.* Am J Clin Nutr, 1997. **66**(4 Suppl): p. 1044S-1050S.
9. WHO, *Surveillance of chronic disease: risk factors: country-level data and comparable estimates. (SuRF reports; 2)*. 2005, World Health Organization.
10. Rahman, I., M.T. Athar, and M. Islam, *Type 2 Diabetes, Obesity, and Cancer Share Some Common and Critical Pathways.* Front Oncol, 2020. **10**: p. 600824.
11. Khaodhiar, L., K.C. McCowen, and G.L. Blackburn, *Obesity and its comorbid conditions.* Clin Cornerstone, 1999. **2**(3): p. 17-31.
12. Semenkovich, C.F., *Insulin resistance and atherosclerosis.* J Clin Invest, 2006. **116**(7): p. 1813-22.
13. Prospective Studies, C., et al., *Body-mass index and cause-specific mortality in 900 000 adults: collaborative analyses of 57 prospective studies.* Lancet, 2009. **373**(9669): p. 1083-96.
14. Finkelstein, E.A., et al., *Individual and aggregate years-of-life-lost associated with overweight and obesity.* Obesity (Silver Spring), 2010. **18**(2): p. 333-9.
15. Anderson, J.W. and E.C. Konz, *Obesity and disease management: effects of weight loss on comorbid conditions.* Obes Res, 2001. **9 Suppl 4**: p. 326S-334S.
16. Preston, S.H. and A. Stokes, *Contribution of obesity to international differences in life expectancy.* Am J Public Health, 2011. **101**(11): p. 2137-43.
17. Peeters, A., et al., *Obesity in adulthood and its consequences for life expectancy: a life-table analysis.* Ann Intern Med, 2003. **138**(1): p. 24-32.
18. Szablewski, L., *Introductory Chapter: Adipose Tissue*, in *Adipose Tissue-An Update*. 2019, IntechOpen.
19. Cinti, S., *White, brown, beige and pink: A rainbow in the adipose organ.* Current Opinion in Endocrine and Metabolic Research, 2019. **4**: p. 29-36.

20. Zinngrebe, J., K.M. Debatin, and P. Fischer-Posovszky, *Adipocytes in hematopoiesis and acute leukemia: friends, enemies, or innocent bystanders?* Leukemia, 2020. **34**(9): p. 2305-2316.

21. van Marken Lichtenbelt, W., *Brown adipose tissue and the regulation of nonshivering thermogenesis.* Curr Opin Clin Nutr Metab Care, 2012. **15**(6): p. 547-52.

22. Pfeifer, A. and L.S. Hoffmann, *Brown, beige, and white: the new color code of fat and its pharmacological implications.* Annu Rev Pharmacol Toxicol, 2015. **55**: p. 207-27.

23. Cinti, S., *Pink Adipocytes.* Trends Endocrinol Metab, 2018. **29**(9): p. 651-666.

24. Giordano, A., et al., *White, brown and pink adipocytes: the extraordinary plasticity of the adipose organ.* Eur J Endocrinol, 2014. **170**(5): p. R159-71.

25. Rosell, M., et al., *Brown and white adipose tissues: intrinsic differences in gene expression and response to cold exposure in mice.* Am J Physiol Endocrinol Metab, 2014. **306**(8): p. E945-64.

26. Reyes-Farias, M., et al., *White adipose tissue dysfunction in obesity and aging.* Biochem Pharmacol, 2021. **192**: p. 114723.

27. Scherer, P.E., *Adipose tissue: from lipid storage compartment to endocrine organ.* Diabetes, 2006. **55**(6): p. 1537-45.

28. Frayn, K.N., et al., *Integrative physiology of human adipose tissue.* Int J Obes Relat Metab Disord, 2003. **27**(8): p. 875-88.

29. Fruhbeck, G., *Overview of adipose tissue and its role in obesity and metabolic disorders.* Methods Mol Biol, 2008. **456**: p. 1-22.

30. Salvador, J., et al., *Abdominal obesity: an indicator of cardiometabolic risk.* Endocrinol Nutr, 2008. **55**(9): p. 420-32.

31. Booth, A., A. Magnuson, and M. Foster, *Detrimental and protective fat: body fat distribution and its relation to metabolic disease.* Horm Mol Biol Clin Investig, 2014. **17**(1): p. 13-27.

32. Zwick, R.K., et al., *Anatomical, Physiological, and Functional Diversity of Adipose Tissue.* Cell Metab, 2018. **27**(1): p. 68-83.

33. Schlecht, I., et al., *Visceral adipose tissue but not subcutaneous adipose tissue is associated with urine and serum metabolites.* PLoS One, 2017. **12**(4): p. e0175133.

34. Shuster, A., et al., *The clinical importance of visceral adiposity: a critical review of methods for visceral adipose tissue analysis.* Br J Radiol, 2012. **85**(1009): p. 1-10.

35. Philipsen, A., et al., *Associations between ultrasound measures of abdominal fat distribution and indices of glucose metabolism in a population at high risk of type 2 diabetes: the ADDITION-PRO study.* PLoS One, 2015. **10**(4): p. e0123062.

36. Wajchenberg, B.L., *Subcutaneous and visceral adipose tissue: their relation to the metabolic syndrome.* Endocr Rev, 2000. **21**(6): p. 697-738.

37. Lee, M.J., Y. Wu, and S.K. Fried, *Adipose tissue heterogeneity: implication of depot differences in adipose tissue for obesity complications.* Mol Aspects Med, 2013. **34**(1): p. 1-11.

38. Item, F. and D. Konrad, *Visceral fat and metabolic inflammation: the portal theory revisited.* Obes Rev, 2012. **13 Suppl 2**: p. 30-9.

39. Wueest, S., et al., *Mesenteric Fat Lipolysis Mediates Obesity-Associated Hepatic Steatosis and Insulin Resistance.* Diabetes, 2016. **65**(1): p. 140-8.

40. Ritchie, S.A. and J.M. Connell, *The link between abdominal obesity, metabolic syndrome and cardiovascular disease.* Nutr Metab Cardiovasc Dis, 2007. **17**(4): p. 319-26.

41. McLaughlin, T., et al., *Preferential fat deposition in subcutaneous versus visceral depots is associated with insulin sensitivity.* J Clin Endocrinol Metab, 2011. **96**(11): p. E1756-60.

42. Virtue, S. and A. Vidal-Puig, *Adipose tissue expandability, lipotoxicity and the Metabolic Syndrome--an allostatic perspective.* Biochim Biophys Acta, 2010. **1801**(3): p. 338-49.

43. Shulman, G.I., *Ectopic fat in insulin resistance, dyslipidemia, and cardiometabolic disease.* N Engl J Med, 2014. **371**(23): p. 2237-8.

44. Indulekha, K., et al., *Association of visceral and subcutaneous fat with glucose intolerance, insulin resistance, adipocytokines and inflammatory markers in Asian Indians (CURES-113).* Clin Biochem, 2011. **44**(4): p. 281-7.

45. Preis, S.R., et al., *Abdominal subcutaneous and visceral adipose tissue and insulin resistance in the Framingham heart study.* Obesity (Silver Spring), 2010. **18**(11): p. 2191-8.

46. Gabriely, I., et al., *Removal of visceral fat prevents insulin resistance and glucose intolerance of aging: an adipokine-mediated process?* Diabetes, 2002. **51**(10): p. 2951-8.

47. Chen, P., et al., *Abdominal subcutaneous adipose tissue: a favorable adipose depot for diabetes?* Cardiovasc Diabetol, 2018. **17**(1): p. 93.

48. Kloting, N., et al., *Insulin-sensitive obesity.* Am J Physiol Endocrinol Metab, 2010. **299**(3): p. E506-15.

49. Kershaw, E.E. and J.S. Flier, *Adipose tissue as an endocrine organ.* J Clin Endocrinol Metab, 2004. **89**(6): p. 2548-56.

50. Grant, R.W. and V.D. Dixit, *Adipose tissue as an immunological organ.* Obesity (Silver Spring), 2015. **23**(3): p. 512-8.

51. Hotamisligil, G.S., *Inflammation and metabolic disorders.* Nature, 2006. **444**(7121): p. 860-7.

52. Leon-Pedroza, J.I., et al., *[Low-grade systemic inflammation and the development of metabolic diseases: from the molecular evidence to the clinical practice].* Cir Cir, 2015. **83**(6): p. 543-51.

53. Unamuno, X., et al., *Adipokine dysregulation and adipose tissue inflammation in human obesity.* Eur J Clin Invest, 2018. **48**(9): p. e12997.

54. Ding, S. and P.K. Lund, *Role of intestinal inflammation as an early event in obesity and insulin resistance.* Curr Opin Clin Nutr Metab Care, 2011. **14**(4): p. 328-33.

55. Kwon, H. and J.E. Pessin, *Adipokines mediate inflammation and insulin resistance.* Front Endocrinol (Lausanne), 2013. **4**: p. 71.

56. Spalding, K.L., et al., *Dynamics of fat cell turnover in humans.* Nature, 2008. **453**(7196): p. 783-7.

57. Ito, A., et al., *Role of MAPK phosphatase-1 in the induction of monocyte chemoattractant protein-1 during the course of adipocyte hypertrophy.* J Biol Chem, 2007. **282**(35): p. 25445-52.

58. Shoelson, S.E., J. Lee, and M. Yuan, *Inflammation and the IKK beta/I kappa B/NF-kappa B axis in obesity- and diet-induced insulin resistance.* Int J Obes Relat Metab Disord, 2003. **27 Suppl 3**: p. S49-52.

59. Nieto-Vazquez, I., et al., *Insulin resistance associated to obesity: the link TNF-alpha.* Arch Physiol Biochem, 2008. **114**(3): p. 183-94.

60. Longo, M., et al., *Adipose Tissue Dysfunction as Determinant of Obesity-Associated Metabolic Complications.* Int J Mol Sci, 2019. **20**(9).

61. Verboven, K., et al., *Abdominal subcutaneous and visceral adipocyte size, lipolysis and inflammation relate to insulin resistance in male obese humans.* Sci Rep, 2018. **8**(1): p. 4677.

62. Greenberg, A.S. and M.S. Obin, *Obesity and the role of adipose tissue in inflammation and metabolism.* Am J Clin Nutr, 2006. **83**(2): p. 461S-465S.

63. Shoelson, S.E., J. Lee, and A.B. Goldfine, *Inflammation and insulin resistance.* J Clin Invest, 2006. **116**(7): p. 1793-801.

64. Corona-Meraz, F.-I., et al., *Adipose Tissue in Health and Disease*, in *Obesity*, H. Çakmur, Editor. 2020.

65. Louwen, F., et al., *Insight into the development of obesity: functional alterations of adipose-derived mesenchymal stem cells.* Obes Rev, 2018. **19**(7): p. 888-904.

66. Ferrante, A.W., Jr., *The immune cells in adipose tissue.* Diabetes Obes Metab, 2013. **15 Suppl 3**(0 3): p. 34-8.

67. Hill, A.A., W. Reid Bolus, and A.H. Hasty, *A decade of progress in adipose tissue macrophage biology.* Immunol Rev, 2014. **262**(1): p. 134-52.

68. Orliaguet, L., et al., *Mechanisms of Macrophage Polarization in Insulin Signaling and Sensitivity.* Front Endocrinol (Lausanne), 2020. **11**: p. 62.

69. Tourniaire, F., et al., *Chemokine Expression in Inflamed Adipose Tissue Is Mainly Mediated by NF-kappaB.* PLoS One, 2013. **8**(6): p. e66515.

70. Weisberg, S.P., et al., *Obesity is associated with macrophage accumulation in adipose tissue.* J Clin Invest, 2003. **112**(12): p. 1796-808.

71. Kosteli, A., et al., *Weight loss and lipolysis promote a dynamic immune response in murine adipose tissue.* J Clin Invest, 2010. **120**(10): p. 3466-79.

72. Frikke-Schmidt, H., et al., *Weight loss independent changes in adipose tissue macrophage and T cell populations after sleeve gastrectomy in mice.* Mol Metab, 2017. **6**(4): p. 317-326.

73. Zamarron, B., et al., *Impact of weight loss on obese adipose tissue immune cell function (CAM1P.154).* J Immunol, 2015. **194**(1).

74. Auerbach, P., et al., *Differential effects of endurance training and weight loss on plasma adiponectin multimers and adipose tissue macrophages in younger, moderately overweight men.* Am J Physiol Regul Integr Comp Physiol, 2013. **305**(5): p. R490-8.

75. Aron-Wisnewsky, J., et al., *Human adipose tissue macrophages: m1 and m2 cell surface markers in subcutaneous and omental depots and after weight loss.* J Clin Endocrinol Metab, 2009. **94**(11): p. 4619-23.

76. Aleman, J.O., et al., *Effects of Rapid Weight Loss on Systemic and Adipose Tissue Inflammation and Metabolism in Obese Postmenopausal Women.* J Endocr Soc, 2017. **1**(6): p. 625-637.

77. Flaherty, S.E., 3rd, et al., *A lipase-independent pathway of lipid release and immune modulation by adipocytes.* Science, 2019. **363**(6430): p. 989-993.

78. Shapiro, H., et al., *Adipose tissue foam cells are present in human obesity.* J Clin Endocrinol Metab, 2013. **98**(3): p. 1173-81.

79. Vatarescu, M., et al., *Adipose tissue supports normalization of macrophage and liver lipid handling in obesity reversal.* J Endocrinol, 2017. **233**(3): p. 293-305.

80. Nguyen, M.T., et al., *A subpopulation of macrophages infiltrates hypertrophic adipose tissue and is activated by free fatty acids via Toll-like receptors 2 and 4 and JNK-dependent pathways.* J Biol Chem, 2007. **282**(48): p. 35279-92.

81. Chen, Y., et al., *CD36, a signaling receptor and fatty acid transporter that regulates immune cell metabolism and fate.* J Exp Med, 2022. **219**(6): p. e20211314.

82. Johnson, A.R., et al., *Metabolic reprogramming through fatty acid transport protein 1 (FATP1) regulates macrophage inflammatory potential and adipose inflammation.* Mol Metab, 2016. **5**(7): p. 506-526.

83. Hsieh, W.Y., et al., *Toll-Like Receptors Induce Signal-Specific Reprogramming of the Macrophage Lipidome.* Cell Metab, 2020. **32**(1): p. 128-143 e5.

84. Almeida, L. and B. Everts, *Fa(c)t checking: How fatty acids shape metabolism and function of macrophages and dendritic cells.* Eur J Immunol, 2021. **51**(7): p. 1628-1640.

85. Sukhorukov, V.N., et al., *Endoplasmic Reticulum Stress in Macrophages: The Vicious Circle of Lipid Accumulation and Pro-Inflammatory Response.* Biomedicines, 2020. **8**(7).

86. Batista-Gonzalez, A., et al., *New Insights on the Role of Lipid Metabolism in the Metabolic Reprogramming of Macrophages.* Front Immunol, 2019. **10**: p. 2993.

87. Wani, K., et al., *Role of NLRP3 Inflammasome Activation in Obesity-Mediated Metabolic Disorders.* Int J Environ Res Public Health, 2021. **18**(2).

88. Vogel, A., et al., *Lipid scavenging macrophages and inflammation.* Biochim Biophys Acta Mol Cell Biol Lipids, 2022. **1867**(1): p. 159066.

89. Ertunc, M.E. and G.S. Hotamisligil, *Lipid signaling and lipotoxicity in metaflammation: indications for metabolic disease pathogenesis and treatment.* J Lipid Res, 2016. **57**(12): p. 2099-2114.

90. Diaz-Valencia, J.D., et al., *Class I Myosins, molecular motors involved in cell migration and cancer.* Cell Adh Migr, 2022. **16**(1): p. 1-12.

91. Maravillas-Montero, J.L. and L. Santos-Argumedo, *The myosin family: unconventional roles of actin-dependent molecular motors in immune cells.* J Leukoc Biol, 2012. **91**(1): p. 35-46.

92. Feeser, E.A., et al., *Myo1e binds anionic phospholipids with high affinity.* Biochemistry, 2010. **49**(43): p. 9353-60.

93. Wenzel, J., et al., *Class I myosin Myo1e regulates TLR4-triggered macrophage spreading, chemokine release, and antigen presentation via MHC class II.* Eur J Immunol, 2015. **45**(1): p. 225-37.

94. Giron-Perez, D.A., Z.L. Piedra-Quintero, and L. Santos-Argumedo, *Class I myosins: Highly versatile proteins with specific functions in the immune system.* J Leukoc Biol, 2019. **105**(5): p. 973-981.

95. Igarashi, M., et al., *The critical role of neutral cholesterol ester hydrolase 1 in cholesterol removal from human macrophages.* Circ Res, 2010. **107**(11): p. 1387-95.

96. Sekiya, M., et al., *The role of neutral cholesterol ester hydrolysis in macrophage foam cells.* J Atheroscler Thromb, 2011. **18**(5): p. 359-64.

97. Sekiya, M., et al., *Ablation of neutral cholesterol ester hydrolase 1 accelerates atherosclerosis.* Cell Metab, 2009. **10**(3): p. 219-28.

98. Matsuoka, H., et al., *Retinoic acid receptor-related orphan receptor α reduces lipid droplets by upregulating neutral cholesterol ester hydrolase 1 in macrophages.* BMC Molecular and Cell Biology, 2020. **21**(1): p. 32.

99. Lee, M.J., Y. Wu, and S.K. Fried, *Adipose tissue remodeling in pathophysiology of obesity.* Curr Opin Clin Nutr Metab Care, 2010. **13**(4): p. 371-6.

100. Suganami, T. and Y. Ogawa, *Adipose tissue macrophages: their role in adipose tissue remodeling.* J Leukoc Biol, 2010. **88**(1): p. 33-9.

101. Sun, K., C.M. Kusminski, and P.E. Scherer, *Adipose tissue remodeling and obesity.* J Clin Invest, 2011. **121**(6): p. 2094-101.

102. Sun, K., et al., *Fibrosis and adipose tissue dysfunction.* Cell Metab, 2013. **18**(4): p. 470-7.

103. Han, J., et al., *The spatiotemporal development of adipose tissue.* Development, 2011. **138**(22): p. 5027-37.

104. de Sousa Neto, I.V., et al., *Adipose Tissue Extracellular Matrix Remodeling in Response to Dietary Patterns and Exercise: Molecular Landscape, Mechanistic Insights, and Therapeutic Approaches.* Biology (Basel), 2022. **11**(5).

105. Arner, E., et al., *Adipocyte turnover: relevance to human adipose tissue morphology.* Diabetes, 2010. **59**(1): p. 105-9.

106. Gustafson, B., et al., *Restricted adipogenesis in hypertrophic obesity: the role of WISP2, WNT, and BMP4.* Diabetes, 2013. **62**(9): p. 2997-3004.

107. Gustafson, B., et al., *Inflammation and impaired adipogenesis in hypertrophic obesity in man.* Am J Physiol Endocrinol Metab, 2009. **297**(5): p. E999-E1003.

108. Ahima, R.S., *Connecting obesity, aging and diabetes.* Nat Med, 2009. **15**(9): p. 996-7.

109. Barzilai, N. and G. Gupta, *Revisiting the role of fat mass in the life extension induced by caloric restriction.* J Gerontol A Biol Sci Med Sci, 1999. **54**(3): p. B89-96; discussion B97-8.

110. Masoro, E.J., *Caloric restriction and aging: controversial issues.* J Gerontol A Biol Sci Med Sci, 2006. **61**(1): p. 14-9.

111. Picard, F. and L. Guarente, *Molecular links between aging and adipose tissue.* Int J Obes (Lond), 2005. **29 Suppl 1**: p. S36-9.

112. Chang, G.R., et al., *Rapamycin protects against high fat diet-induced obesity in C57BL/6J mice.* J Pharmacol Sci, 2009. **109**(4): p. 496-503.

113. Selman, C., et al., *Ribosomal protein S6 kinase 1 signaling regulates mammalian life span.* Science, 2009. **326**(5949): p. 140-4.

114. Selman, C., et al., *Evidence for lifespan extension and delayed age-related biomarkers in insulin receptor substrate 1 null mice.* FASEB J, 2008. **22**(3): p. 807-18.

115. Berryman, D.E., et al., *Role of the GH/IGF-1 axis in lifespan and healthspan: lessons from animal models.* Growth Horm IGF Res, 2008. **18**(6): p. 455-71.

116. Divoux, A., et al., *Fibrosis in human adipose tissue: composition, distribution, and link with lipid metabolism and fat mass loss.* Diabetes, 2010. **59**(11): p. 2817-25.

117. Datta, R., M.J. Podolsky, and K. Atabai, *Fat fibrosis: friend or foe?* JCI Insight, 2018. **3**(19).

118. O'Hara, A., et al., *Microarray analysis identifies matrix metalloproteinases (MMPs) as key genes whose expression is up-regulated in human adipocytes by macrophage-conditioned medium.* Pflugers Arch, 2009. **458**(6): p. 1103-14.

119. Henegar, C., et al., *Adipose tissue transcriptomic signature highlights the pathological relevance of extracellular matrix in human obesity.* Genome Biol, 2008. **9**(1): p. R14.

120. Catalan, V., et al., *Increased tenascin C and Toll-like receptor 4 levels in visceral adipose tissue as a link between inflammation and extracellular matrix remodeling in obesity.* J Clin Endocrinol Metab, 2012. **97**(10): p. E1880-9.

121. Reggio, S., et al., *Increased Basement Membrane Components in Adipose Tissue During Obesity: Links With TGFbeta and Metabolic Phenotypes.* J Clin Endocrinol Metab, 2016. **101**(6): p. 2578-87.

122. Pasarica, M., et al., *Adipose tissue collagen VI in obesity.* J Clin Endocrinol Metab, 2009. **94**(12): p. 5155-62.

123. Dankel, S.N., et al., *COL6A3 expression in adipocytes associates with insulin resistance and depends on PPARgamma and adipocyte size.* Obesity (Silver Spring), 2014. **22**(8): p. 1807-13.

124. Spencer, M., et al., *Adipose tissue macrophages in insulin-resistant subjects are associated with collagen VI and fibrosis and demonstrate alternative activation.* Am J Physiol Endocrinol Metab, 2010. **299**(6): p. E1016-27.

125. Khan, T., et al., *Metabolic dysregulation and adipose tissue fibrosis: role of collagen VI.* Mol Cell Biol, 2009. **29**(6): p. 1575-91.

126. Sorisky, A., R. Magun, and A.M. Gagnon, *Adipose cell apoptosis: death in the energy depot.* Int J Obes Relat Metab Disord, 2000. **24 Suppl 4**: p. S3-7.

127. Alkhouri, N., et al., *Adipocyte apoptosis, a link between obesity, insulin resistance, and hepatic steatosis.* J Biol Chem, 2010. **285**(5): p. 3428-38.

128. Cinti, S., et al., *Adipocyte death defines macrophage localization and function in adipose tissue of obese mice and humans.* J Lipid Res, 2005. **46**(11): p. 2347-55.

129. Murano, I., et al., *Dead adipocytes, detected as crown-like structures, are prevalent in visceral fat depots of genetically obese mice.* J Lipid Res, 2008. **49**(7): p. 1562-8.

130. Lumeng, C.N., J.L. Bodzin, and A.R. Saltiel, *Obesity induces a phenotypic switch in adipose tissue macrophage polarization.* J Clin Invest, 2007. **117**(1): p. 175-84.

131. Lumeng, C.N., et al., *Phenotypic switching of adipose tissue macrophages with obesity is generated by spatiotemporal differences in macrophage subtypes.* Diabetes, 2008. **57**(12): p. 3239-46.

132. Fischer-Posovszky, P., et al., *Targeted deletion of adipocytes by apoptosis leads to adipose tissue recruitment of alternatively activated M2 macrophages.* Endocrinology, 2011. **152**(8): p. 3074-81.

133. Brand, M.D., et al., *The role of mitochondrial function and cellular bioenergetics in ageing and disease.* Br J Dermatol, 2013. **169 Suppl 2**(0 2): p. 1-8.

134. Lee, J.H., et al., *The Role of Adipose Tissue Mitochondria: Regulation of Mitochondrial Function for the Treatment of Metabolic Diseases.* Int J Mol Sci, 2019. **20**(19).

135. Forner, F., et al., *Proteome differences between brown and white fat mitochondria reveal specialized metabolic functions.* Cell Metab, 2009. **10**(4): p. 324-35.

136. Schottl, T., et al., *Limited OXPHOS capacity in white adipocytes is a hallmark of obesity in laboratory mice irrespective of the glucose tolerance status.* Mol Metab, 2015. **4**(9): p. 631-42.

137. Kim, J.A., Y. Wei, and J.R. Sowers, *Role of mitochondrial dysfunction in insulin resistance.* Circ Res, 2008. **102**(4): p. 401-14.

138. Choi, S., et al., *Comparative proteome analysis using amine-reactive isobaric tagging reagents coupled with 2D LC/MS/MS in 3T3-L1 adipocytes following hypoxia or normoxia.* Biochem Biophys Res Commun, 2009. **383**(1): p. 135-40.

139. Perez de Heredia, F., I.S. Wood, and P. Trayhurn, *Hypoxia stimulates lactate release and modulates monocarboxylate transporter (MCT1, MCT2, and MCT4) expression in human adipocytes.* Pflugers Arch, 2010. **459**(3): p. 509-18.

140. Wood, I.S., et al., *Hypoxia increases expression of selective facilitative glucose transporters (GLUT) and 2-deoxy-D-glucose uptake in human adipocytes.* Biochem Biophys Res Commun, 2007. **361**(2): p. 468-73.

141. Geiger, K., et al., *Identification of hypoxia-induced genes in human SGBS adipocytes by microarray analysis.* PLoS One, 2011. **6**(10): p. e26465.

142. Ortega, F.J., et al., *The gene expression of the main lipogenic enzymes is downregulated in visceral adipose tissue of obese subjects.* Obesity (Silver Spring), 2010. **18**(1): p. 13-20.

143. Diraison, F., et al., *Increased hepatic lipogenesis but decreased expression of lipogenic gene in adipose tissue in human obesity.* American Journal of Physiology-Endocrinology And Metabolism, 2002. **282**(1): p. E46-E51.

144. Cruikshank, W.W., H. Kornfeld, and D.M. Center, *Interleukin-16.* J Leukoc Biol, 2000. **67**(6): p. 757-66.

145. Zhang, Y., et al., *Processing and activation of pro-interleukin-16 by caspase-3.* J Biol Chem, 1998. **273**(2): p. 1144-9.

146. Distler, O., *CD4 as a receptor for IL-16: To be or not to be?* Arthritis Research & Therapy, 2000. **3**(1): p. 66813.

147. Mathy, N.L., et al., *Interleukin-16 stimulates the expression and production of pro-inflammatory cytokines by human monocytes.* Immunology, 2000. **100**(1): p. 63-9.

148. Lynch, E.A., et al., *Cutting edge: IL-16/CD4 preferentially induces Th1 cell migration: requirement of CCR5.* J Immunol, 2003. **171**(10): p. 4965-8.

149. Elssner, A., et al., *IL-16 is constitutively present in peripheral blood monocytes and spontaneously released during apoptosis.* J Immunol, 2004. **172**(12): p. 7721-5.

150. Lichtenauer, M., et al., *Elevated plasma levels of interleukin-12p40 and interleukin-16 in overweight adolescents.* Biomed Res Int, 2015. **2015**: p. 940910.

151. Popova, V.V., *[Level of circulating interleukin-16 during preclinical stage of type I diabetes mellitus development in children].* Lik Sprava, 2007(8): p. 45-7.

152. Meagher, C., et al., *Neutralization of interleukin-16 protects nonobese diabetic mice from autoimmune type 1 diabetes by a CCL4-dependent mechanism.* Diabetes, 2010. **59**(11): p. 2862-71.

153. Kurki, E., et al., *Distinct effects of calorie restriction on adipose tissue cytokine and angiogenesis profiles in obese and lean mice.* Nutr Metab (Lond), 2012. **9**(1): p. 64.

154. Quesada-Lopez, T., et al., *The lipid sensor GPR120 promotes brown fat activation and FGF21 release from adipocytes.* Nat Commun, 2016. **7**: p. 13479.

155. Cnop, M., et al., *RNA sequencing identifies dysregulation of the human pancreatic islet transcriptome by the saturated fatty acid palmitate.* Diabetes, 2014. **63**(6): p. 1978-93.

156. Eizirik, D.L., et al., *The human pancreatic islet transcriptome: expression of candidate genes for type 1 diabetes and the impact of pro-inflammatory cytokines.* PLoS Genet, 2012. **8**(3): p. e1002552.

157. Spector, A.A., *Fatty acid binding to plasma albumin.* J Lipid Res, 1975. **16**(3): p. 165-79.

158. Bäcker, V., *ImageJ Macro Tool Sets for Biological Image Analysis*. 2012.

159. Livak, K.J. and T.D. Schmittgen, *Analysis of relative gene expression data using real-time quantitative PCR and the 2(-Delta Delta C(T)) Method.* Methods, 2001. **25**(4): p. 402-8.

160. Patro, R., et al., *Salmon provides fast and bias-aware quantification of transcript expression.* Nat Methods, 2017. **14**(4): p. 417-419.

161. Harrow, J., et al., *GENCODE: the reference human genome annotation for The ENCODE Project.* Genome Res, 2012. **22**(9): p. 1760-74.

162. Love, M.I., W. Huber, and S. Anders, *Moderated estimation of fold change and dispersion for RNA-seq data with DESeq2.* Genome Biol, 2014. **15**(12): p. 550.

163. Eden, E., et al., *GOrilla: a tool for discovery and visualization of enriched GO terms in ranked gene lists.* BMC Bioinformatics, 2009. **10**: p. 48.

164. Subramanian, A., et al., *Gene set enrichment analysis: a knowledge-based approach for interpreting genome-wide expression profiles.* Proc Natl Acad Sci U S A, 2005. **102**(43): p. 15545-50.

165. Lun, K.B.a.A., *PCAtools: Everything Principal Components Analysis*. 2022.

166. Petrova, D., et al., *[Obesity as a risk factor in COVID-19: Possible mechanisms and implications].* Aten Primaria, 2020. **52**(7): p. 496-500.

167. Singh, R., et al., *Association of Obesity With COVID-19 Severity and Mortality: An Updated Systemic Review, Meta-Analysis, and Meta-Regression.* Front Endocrinol (Lausanne), 2022. **13**: p. 780872.

168. Wendemi, S., et al., *Overweight and obesity as risk factors for COVID-19-associated hospitalisations and death: systematic review and meta-analysis.* BMJ Nutrition, Prevention & Health, 2022: p. e000375.

169. Abdisa, T., et al., *Cytokine and chemokine profile in patients hospitalized with COVID-19: A comparative study.* bioRxiv, 2022: p. 2022.03.17.484837.

170. Wilson, J.G., et al., *Cytokine profile in plasma of severe COVID-19 does not differ from ARDS and sepsis.* JCI Insight, 2020. **5**(17).

171. Bonny, T.S., et al., *Cytokine and Chemokine Levels in Coronavirus Disease 2019 Convalescent Plasma.* Open Forum Infectious Diseases, 2020. **8**(2).

172. Manickam, E., A.J. Sinclair, and D. Cameron-Smith, *Suppressive actions of eicosapentaenoic acid on lipid droplet formation in 3T3-L1 adipocytes.* Lipids Health Dis, 2010. **9**: p. 57.

173. den Besten, G., et al., *Short-Chain Fatty Acids Protect Against High-Fat Diet-Induced Obesity via a PPARgamma-Dependent Switch From Lipogenesis to Fat Oxidation.* Diabetes, 2015. **64**(7): p. 2398-408.

174. Guo, W., et al., *Palmitate modulates intracellular signaling, induces endoplasmic reticulum stress, and causes apoptosis in mouse 3T3-L1 and rat primary preadipocytes.* Am J Physiol Endocrinol Metab, 2007. **293**(2): p. E576-86.

175. Morita, N., et al., *Novel Mechanisms Modulating Palmitate-Induced Inflammatory Factors in Hypertrophied 3T3-L1 Adipocytes by AMPK.* J Diabetes Res, 2018. **2018**: p. 9256482.

176. Malandrino, M.I., et al., *Enhanced fatty acid oxidation in adipocytes and macrophages reduces lipid-induced triglyceride accumulation and inflammation.* Am J Physiol Endocrinol Metab, 2015. **308**(9): p. E756-69.

177. Aprile, M., et al., *In-Vitro-Generated Hypertrophic-Like Adipocytes Displaying PPARG Isoforms Unbalance Recapitulate Adipocyte Dysfunctions In Vivo.* Cells, 2020. **9**(5).

178. Hao, Y., et al., *Integrated analysis of multimodal single-cell data.* Cell, 2021. **184**(13): p. 3573-3587 e29.

179. Chen, Q., et al., *Resident macrophages restrain pathological adipose tissue remodeling and protect vascular integrity in obese mice.* EMBO Rep, 2021. **22**(8): p. e52835.

180. Hidalgo, M.A., M.D. Carretta, and R.A. Burgos, *Long Chain Fatty Acids as Modulators of Immune Cells Function: Contribution of FFA1 and FFA4 Receptors.* Front Physiol, 2021. **12**: p. 668330.

181. Cullberg, K.B., et al., *Effects of LPS and dietary free fatty acids on MCP-1 in 3T3-L1 adipocytes and macrophages in vitro.* Nutr Diabetes, 2014. **4**(3): p. e113.

182. Ishiyama, J., et al., *Palmitic acid enhances lectin-like oxidized LDL receptor (LOX-1) expression and promotes uptake of oxidized LDL in macrophage cells.* Atherosclerosis, 2010. **209**(1): p. 118-24.

183. Korbecki, J. and K. Bajdak-Rusinek, *The effect of palmitic acid on inflammatory response in macrophages: an overview of molecular mechanisms.* Inflamm Res, 2019. **68**(11): p. 915-932.

184. Yunna, C., et al., *Macrophage M1/M2 polarization.* Eur J Pharmacol, 2020. **877**: p. 173090.

185. Xu, J., et al., *The Regulating Effect of CII-3 and Its Active Components from Periplaneta americana on M1/M2 Macrophage Polarization.* Molecules, 2022. **27**(14).

186. Cereijo, R., et al., *CXCL14, a Brown Adipokine that Mediates Brown-Fat-to-Macrophage Communication in Thermogenic Adaptation.* Cell Metab, 2018. **28**(5): p. 750-763 e6.

187. Orecchioni, M., et al., *Macrophage Polarization: Different Gene Signatures in M1(LPS+) vs. Classically and M2(LPS-) vs. Alternatively Activated Macrophages.* Front Immunol, 2019. **10**: p. 1084.

188. He, Z., et al., *The interaction between different types of activated RAW 264.7 cells and macrophage inflammatory protein-1 alpha.* Radiat Oncol, 2011. **6**: p. 86.

189. Jin, J., et al., *LPS and palmitate synergistically stimulate sphingosine kinase 1 and increase sphingosine 1 phosphate in RAW264.7 macrophages.* J Leukoc Biol, 2018. **104**(4): p. 843-853.

190. Schilling, J.D., et al., *TLR4 activation under lipotoxic conditions leads to synergistic macrophage cell death through a TRIF-dependent pathway.* J Immunol, 2013. **190**(3): p. 1285-96.

191. Okazaki, H., et al., *Identification of neutral cholesterol ester hydrolase, a key enzyme removing cholesterol from macrophages.* J Biol Chem, 2008. **283**(48): p. 33357-64.

192. Greenspan, P., E.P. Mayer, and S.D. Fowler, *Nile red: a selective fluorescent stain for intracellular lipid droplets.* J Cell Biol, 1985. **100**(3): p. 965-73.

193. Chait, A. and L.J. den Hartigh, *Adipose Tissue Distribution, Inflammation and Its Metabolic Consequences, Including Diabetes and Cardiovascular Disease.* Front Cardiovasc Med, 2020. **7**: p. 22.

194. Michailidou, Z., M. Gomez-Salazar, and V.I. Alexaki, *Innate Immune Cells in the Adipose Tissue in Health and Metabolic Disease.* J Innate Immun, 2022. **14**(1): p. 4-30.

195. Russo, L. and C.N. Lumeng, *Properties and functions of adipose tissue macrophages in obesity.* Immunology, 2018. **155**(4): p. 407-417.

196. Khan, S., et al., *The Immune Landscape of Visceral Adipose Tissue During Obesity and Aging.* Front Endocrinol (Lausanne), 2020. **11**: p. 267.

197. Amano, S.U., et al., *Local proliferation of macrophages contributes to obesity-associated adipose tissue inflammation.* Cell Metab, 2014. **19**(1): p. 162-171.

198. Lesna, I.K., et al., *Human adipose tissue accumulation is associated with pro-inflammatory changes in subcutaneous rather than visceral adipose tissue.* Nutrition & diabetes, 2017. **7**(4): p. e264-e264.

199. Wentworth, J.M., et al., *Pro-inflammatory CD11c+CD206+ adipose tissue macrophages are associated with insulin resistance in human obesity.* Diabetes, 2010. **59**(7): p. 1648-56.

200. Liu, L., et al., *TACI-Deficient Macrophages Protect Mice Against Metaflammation and Obesity-Induced Dysregulation of Glucose Homeostasis.* Diabetes, 2018. **67**(8): p. 1589-1603.

201. Fox, C.S., et al., *Abdominal visceral and subcutaneous adipose tissue compartments: association with metabolic risk factors in the Framingham Heart Study.* Circulation, 2007. **116**(1): p. 39-48.

202. Liu, J., et al., *Impact of abdominal visceral and subcutaneous adipose tissue on cardiometabolic risk factors: the Jackson Heart Study.* J Clin Endocrinol Metab, 2010. **95**(12): p. 5419-26.

203. Smith, J.D., et al., *Visceral adipose tissue indicates the severity of cardiometabolic risk in patients with and without type 2 diabetes: results from the INSPIRE ME IAA study.* J Clin Endocrinol Metab, 2012. **97**(5): p. 1517-25.

204. Jaworski, K., et al., *Regulation of triglyceride metabolism. IV. Hormonal regulation of lipolysis in adipose tissue.* Am J Physiol Gastrointest Liver Physiol, 2007. **293**(1): p. G1-4.

205. Suganami, T., M. Tanaka, and Y. Ogawa, *Adipose tissue inflammation and ectopic lipid accumulation.* Endocr J, 2012. **59**(10): p. 849-57.

206. Arner, P., et al., *Weight Gain and Impaired Glucose Metabolism in Women Are Predicted by Inefficient Subcutaneous Fat Cell Lipolysis.* Cell Metab, 2018. **28**(1): p. 45-54 e3.

207. Arner, P. and D. Langin, *Lipolysis in lipid turnover, cancer cachexia, and obesity-induced insulin resistance.* Trends Endocrinol Metab, 2014. **25**(5): p. 255-62.

208. Kassouf, T. and G. Sumara, *Impact of Conventional and Atypical MAPKs on the Development of Metabolic Diseases.* Biomolecules, 2020. **10**(9).

209. Kim, K.A., et al., *Pref-1 (preadipocyte factor 1) activates the MEK/extracellular signal-regulated kinase pathway to inhibit adipocyte differentiation.* Mol Cell Biol, 2007. **27**(6): p. 2294-308.

210. Ryden, M., et al., *Targets for TNF-alpha-induced lipolysis in human adipocytes.* Biochem Biophys Res Commun, 2004. **318**(1): p. 168-75.

211. Maffei, M., et al., *Leptin levels in human and rodent: measurement of plasma leptin and ob RNA in obese and weight-reduced subjects.* Nat Med, 1995. **1**(11): p. 1155-61.

212. Harris, R.B., *Direct and indirect effects of leptin on adipocyte metabolism.* Biochim Biophys Acta, 2014. **1842**(3): p. 414-23.

213. Dommel, S. and M. Blüher, *Does C-C Motif Chemokine Ligand 2 (CCL2) Link Obesity to a Pro-Inflammatory State?* Int J Mol Sci, 2021. **22**(3).

214. Gasic, S., B. Tian, and A. Green, *Tumor necrosis factor alpha stimulates lipolysis in adipocytes by decreasing Gi protein concentrations.* J Biol Chem, 1999. **274**(10): p. 6770-5.

215. Casimiro, I., et al., *Reduction of IL-6 gene expression in human adipose tissue after sleeve gastrectomy surgery.* Obes Sci Pract, 2020. **6**(2): p. 215-224.

216. Greenberg, A.S., et al., *Interleukin 6 reduces lipoprotein lipase activity in adipose tissue of mice in vivo and in 3T3-L1 adipocytes: a possible role for interleukin 6 in cancer cachexia.* Cancer Res, 1992. **52**(15): p. 4113-6.

217. Vidal-Puig, A., et al., *Regulation of PPAR gamma gene expression by nutrition and obesity in rodents.* J Clin Invest, 1996. **97**(11): p. 2553-61.

218. Sohn, J.H., et al., *Perilipin 1 (Plin1) deficiency promotes inflammatory responses in lean adipose tissue through lipid dysregulation.* Journal of Biological Chemistry, 2018. **293**(36): p. 13974-13988.

219. Pietka, T.A., et al., *Adipose and muscle tissue profile of CD36 transcripts in obese subjects highlights the role of CD36 in fatty acid homeostasis and insulin resistance.* Diabetes Care, 2014. **37**(7): p. 1990-7.

220. Glatz, J.F., et al., *CD36 as a target to prevent cardiac lipotoxicity and insulin resistance.* Prostaglandins Leukot Essent Fatty Acids, 2013. **88**(1): p. 71-7.

221. He, Q., et al., *Regulation of HIF-1{alpha} activity in adipose tissue by obesity-associated factors: adipogenesis, insulin, and hypoxia.* Am J Physiol Endocrinol Metab, 2011. **300**(5): p. E877-85.

222. Kihira, Y., et al., *Deletion of Hypoxia-Inducible Factor-1α in Adipocytes Enhances Glucagon-Like Peptide-1 Secretion and Reduces Adipose Tissue Inflammation.* PLOS ONE, 2014. **9**(4): p. e93856.

223. Sun, K., et al., *Selective inhibition of hypoxia-inducible factor 1α ameliorates adipose tissue dysfunction.* Mol Cell Biol, 2013. **33**(5): p. 904-17.

224. Elias, I., S. Franckhauser, and F. Bosch, *New insights into adipose tissue VEGF-A actions in the control of obesity and insulin resistance.* Adipocyte, 2013. **2**(2): p. 109-12.

225. Ajuwon, K.M. and M.E. Spurlock, *Palmitate activates the NF-kappaB transcription factor and induces IL-6 and TNFalpha expression in 3T3-L1 adipocytes.* J Nutr, 2005. **135**(8): p. 1841-6.

226. Hancock, D., et al., *The Expression of Inflammatory Genes in 3T3-L1 Adipocytes Exhibits a Memory to Stimulation by Macrophage Secretions.* bioRxiv, 2018: p. 336610.

227. Sustar, U., D. Lainscek, and S. Horvat, *Effect of palmitate and TST gene on inflammation and insulin resistance in adipocytes.* Atherosclerosis, 2018. **275**: p. e71.

228. Ceja-Galicia, Z., et al., *Leptin and adiponectin synthesis and secretion in mature 3T3-L1 adipocytes are differentially down-regulated by arsenic and palmitic acid exposure throughout different stages of adipogenesis.* Life Sciences, 2022. **291**: p. 120262.

229. Yin, J., et al., *Palmitate induces endoplasmic reticulum stress and autophagy in mature adipocytes: implications for apoptosis and inflammation.* Int J Mol Med, 2015. **35**(4): p. 932-40.

230. Pereira, S. and J. Alvarez-Leite, *Adipokines: Biological functions and metabolically healthy obese profile.* Journal of Receptor, Ligand and Channel Research, 2014. **2014**: p. 15-25.

231. Zhao, H., et al., *RNA-seq Based Transcriptome Analysis Reveals The Cross-Talk of Macrophage and Adipocyte of Chicken Subcutaneous Adipose Tissue during The Embryonic and Post-Hatch Period.* Front Immunol, 2022. **13**: p. 889439.

232. Imai, T., et al., *Peroxisome proliferator-activated receptor gamma is required in mature white and brown adipocytes for their survival in the mouse.* Proc Natl Acad Sci U S A, 2004. **101**(13): p. 4543-7.

233. Yamauchi, T., et al., *The mechanisms by which both heterozygous peroxisome proliferator-activated receptor gamma (PPARgamma) deficiency and PPARgamma agonist improve insulin resistance.* J Biol Chem, 2001. **276**(44): p. 41245-54.

234. Porter, S.A., et al., *Abdominal subcutaneous adipose tissue: a protective fat depot?* Diabetes Care, 2009. **32**(6): p. 1068-75.

235. Booth, A.D., et al., *Subcutaneous adipose tissue accumulation protects systemic glucose tolerance and muscle metabolism.* Adipocyte, 2018. **7**(4): p. 261-272.

236. Daemen, S. and J.D. Schilling, *The Interplay Between Tissue Niche and Macrophage Cellular Metabolism in Obesity.* Frontiers in Immunology, 2020. **10**.

237. Nawaz, A., et al., *CD206(+) M2-like macrophages regulate systemic glucose metabolism by inhibiting proliferation of adipocyte progenitors.* Nat Commun, 2017. **8**(1): p. 286.

238. De Taeye, B.M., et al., *Macrophage TNF-alpha contributes to insulin resistance and hepatic steatosis in diet-induced obesity.* Am J Physiol Endocrinol Metab, 2007. **293**(3): p. E713-25.

239. Suganami, T., J. Nishida, and Y. Ogawa, *A paracrine loop between adipocytes and macrophages aggravates inflammatory changes: role of free fatty acids and tumor necrosis factor alpha.* Arterioscler Thromb Vasc Biol, 2005. **25**(10): p. 2062-8.

240. Nagareddy, P.R., et al., *Adipose tissue macrophages promote myelopoiesis and monocytosis in obesity.* Cell Metab, 2014. **19**(5): p. 821-35.

241. Sekiya, M., et al., *Absence of Nceh1 augments 25-hydroxycholesterol-induced ER stress and apoptosis in macrophages.* J Lipid Res, 2014. **55**(10): p. 2082-92.

242. Feng, X., et al., *Metformin, Macrophage Dysfunction and Atherosclerosis.* Frontiers in Immunology, 2021. **12**: p. 682853.

243. Zhang, W., et al., *Lipopolysaccharide mediates time-dependent macrophage M1/M2 polarization through the Tim-3/Galectin-9 signalling pathway.* Exp Cell Res, 2019. **376**(2): p. 124-132.

244. Parameswaran, N. and S. Patial, *Tumor necrosis factor-α signaling in macrophages.* Crit Rev Eukaryot Gene Expr, 2010. **20**(2): p. 87-103.

245. Ipseiz, N., et al., *Tissue-resident macrophages actively suppress IL-1beta release via a reactive prostanoid/IL-10 pathway.* EMBO J, 2020. **39**(14): p. e103454.

246. Cai, L., et al., *Scavenger receptor CD36 expression contributes to adipose tissue inflammation and cell death in diet-induced obesity.* PLoS One, 2012. **7**(5): p. e36785.

247. Rahaman, S.O., et al., *A CD36-dependent signaling cascade is necessary for macrophage foam cell formation.* Cell Metab, 2006. **4**(3): p. 211-21.

248. Cho, K.Y., et al., *Lipid Droplet Protein PLIN1 Regulates Inflammatory Polarity in Human Macrophages and is Involved in Atherosclerotic Plaque Development by Promoting Stable Lipid Storage.* J Atheroscler Thromb, 2023. **30**(2): p. 170-181.

249. Nomura, M., et al., *Macrophage fatty acid oxidation inhibits atherosclerosis progression.* J Mol Cell Cardiol, 2019. **127**: p. 270-276.

250. Zhang, J., et al., *The role of lipocalin 2 in the regulation of inflammation in adipocytes and macrophages.* Mol Endocrinol, 2008. **22**(6): p. 1416-26.

251. Oberoi, R., et al., *Lipocalin (LCN) 2 Mediates Pro-Atherosclerotic Processes and Is Elevated in Patients with Coronary Artery Disease.* PLOS ONE, 2015. **10**(9): p. e0137924.

9. SUPPLEMENTARY INFORMATION

Table S1. Used primers in this work.

GENE	FOR (3' –> 5')	REV (3' –> 5')
Adipoq	GCAGAGATGGCACTCCTGGA	CCCTTCAGCTCCTGTCATTCC
Arg1	CTCCAAGCCAAAGTCCTTAGAG	AGGAGCTGTCATTAGGGACATC
Ccl2	GCAGGTGTCCCAAAGAAGCT	CAGCACAGACCTCTCTCTTGA
Cd206	5'GTGGGGACCTGGCAAGTATC	5'CACTGGGGTTCCATCACTCC
Cd36	TTGTACCTATACTGTGGCTAAATGAGA	CTTGTGTTTTGAACATTTCTGCTT
Col4a1	TTAAAGGACTCCAGGGACCAC	CCCACTGAGCCTGTCACAC
Col6a1	GTCCACGTGCTCTTGCATC	GCAAGGATGAGCTGGTCAA
Cpt1a	GACTCCGCTCGCTCATTC	AAGGCCACAGCTTGGTGA
Fabp4	GGATGGAAAGTCGACCACAA	TGGAAGTCACGCCTTTCATA
Glut4	GATGACCGTGGCTCTGCT	GCTCTGCCACAATGAACCA
Hif1a	GCACTAGACAAAGTTCACCTGAGA	CGCTATCCACATCAAAGCAA
Il1b	GCCCATCCTCTGTGACTCAT	AGGCCACAGGTATTTTGTCG
Il6	GATGGATGCTACCAAACTG	CCAGGTAGCTATGGTACTCCAGAA
Lcn2	CCATCTATGAGCTACAAGAGAACAAT	TCTGATCCAGTAGCGACAGC
Lep	AGAAGATCCCAGGGAGGAAA	TGATGAGGGTTTTGGTGTCA
Mmp9	ACGACATAGACGGCATCCA	GCTGTGGTTCAGTTGTGGTG
Nceh1	GCCCTGGCTAGTGCAAAGAT	GGCACGGATGACATCATGGA
Pgc1a	GAAAGGGCCAAACAGAGAGA	GTAAATCACACGGCGCTCTT
Plin1	AACGTGGTAGACACTGTGGTACA	TCTCGGAATTCGCTCTCG
Pparg	CGCTGATGCACTGCCTATGA	AGAGGTCCACAGAGCTGATTCC
Ppia	TGCCAAGACTGAATGGCTGG	ATTCCTGGACCCAAAACGCT
Pref1	CGGGAAATTCTGCGAAATAG	TGTGCAGGAGCATTCGTACT
Timp1	GCAAAGAGCTTTCTCAAAGACC	AGGGATAGATAAACAGGGAAACACT
Tlr4	GGACTCTGATCATGGCACTG	CTGATCCATGCATTGGTAGGT
Tnfa	CTGTAGCCCACGTCGTAGC	TTTGAGATCCATGCCGTTG
Vegf	AAGACAGAACAAAGCCAGAAAA	AGAGGTCTGGTTCCCGAAA

Table S2. Correlation of *IL16* gene expression with inflammation markers.

GENE	COEFF.	p-VALUE
AARS2	0.7982	4.58E-19
ABAT	0.6819	2.41E-12
ABCA7	0.7762	1.72E-17
ABCB1	0.6750	4.82E-12
ABCC10	0.7608	1.71E-16
ABCC4	0.7344	6.12E-15
ABHD16A	0.7011	3.16E-13
ABHD17AP5	0.6093	1.57E-09
ABHD17C	0.6008	3.03E-09
ABI3	0.7436	1.84E-15
ABRACL	0.8207	6.76E-21
ACAP1	0.7793	1.05E-17
ACD	0.7909	1.59E-18
ACHE	0.8025	2.12E-19
ACIN1	0.7003	3.45E-13
ACRBP	0.6919	8.54E-13
ACSL6	0.8105	4.92E-20
ACSM1	0.6041	2.36E-09
ACSM3	0.6447	8.29E-11
ACSS1	0.8603	7.99E-25
ACTB	0.6336	2.18E-10
ACTL10	0.7692	4.97E-17
ACTL6A	0.7015	3.03E-13
ACTR5	0.8213	6.03E-21
ACY3	0.8075	8.56E-20
ACYP1	0.6198	6.87E-10
ADAM19	0.8242	3.31E-21
ADAM1A	0.7789	1.11E-17
ADAM28	0.7405	2.76E-15
ADAM8	0.6757	4.51E-12
ADAMDEC1	0.7027	2.64E-13
ADAMTS7P4	0.7967	5.88E-19
ADAT2	0.7118	9.45E-14
ADCY7	0.7166	5.39E-14
ADCY9	0.6458	0.00E+00

ADD3	0.6009	5.15E-09
ADGRA3	0.6091	2.20E-09
ADGRB1	0.6622	1.67E-11
ADGRG5	0.7648	9.60E-17
ADGRL4	-0.6363	0.00E+00
ADIRF	-0.6504	0.00E+00
ADM2	0.8128	3.14E-20
ADNP	0.6994	0.00E+00
ADORA2A	0.8060	1.12E-19
ADPGK	0.6896	1.08E-12
ADTRP	0.7985	4.33E-19
AEBP2	0.7175	0.00E+00
AFTPH	0.7190	4.03E-14
AGAP2	0.7584	2.42E-16
AGAP7P	0.6364	1.71E-10
AGBL2	0.8676	1.10E-25
AGGF1P2	0.6425	1.01E-10
AGKP1	0.6827	2.23E-12
AGMAT	0.8961	1.33E-29
AICDA	0.7280	1.36E-14
AIM2	0.7628	1.28E-16
AIP	0.7325	7.71E-15
AIRE	0.7766	1.60E-17
AKAP17A	0.8129	3.11E-20
AKAP5	0.6800	2.93E-12
AKNA	0.7820	6.79E-18
ALDH7A1P3	0.7477	1.07E-15
ALG1L8P	0.6187	7.48E-10
ALKBH6	0.7191	3.99E-14
ALOX15P1	0.8570	1.85E-24
ALOX5	0.7856	3.80E-18
ALPK2	0.6009	3.01E-09
AMPD2	0.7297	1.11E-14
ANAPC1P1	0.7442	1.70E-15
ANGPTL6	0.7959	6.80E-19
ANKFY1	0.6589	0.00E+00
ANKHD1	0.6574	2.62E-11

ANKK1	0.7257	1.81E-14
ANKLE1	0.6293	3.14E-10
ANKMY1	0.7109	1.05E-13
ANKRD11	0.6012	2.94E-09
ANKRD13A	0.7452	1.49E-15
ANKRD13D	0.8298	1.04E-21
ANKRD22	0.6481	6.14E-11
ANKRD23	0.6272	3.72E-10
ANKRD36BP2	0.6834	2.08E-12
ANKRD44	0.8226	4.63E-21
ANKRD49	0.8214	5.84E-21
ANKRD55	0.7834	5.46E-18
ANKZF1	0.7362	4.82E-15
ANO9	0.8240	3.47E-21
ANP32E	0.6687	9.01E-12
ANTXRLP1	0.7658	8.30E-17
ANXA2R	0.7436	1.83E-15
AOC1	0.7713	3.61E-17
AP1G2	0.9268	2.45E-35
AP1S2P1	0.7789	1.11E-17
AP4B1	0.6466	7.02E-11
APBA2	0.6073	1.84E-09
APBA3	0.7137	7.58E-14
APBB1	0.8248	2.98E-21
APEH	0.6068	1.91E-09
APELA	0.7695	4.77E-17
APOBEC3B	0.6072	1.87E-09
APOBEC3C	0.7101	1.15E-13
APOBEC3D	0.8463	2.60E-23
APOBEC3F	0.8821	1.52E-27
APOBEC3G	0.8924	5.07E-29
APOBEC3H	0.8643	2.73E-25
APOM	0.6154	9.75E-10
APRT	0.6502	5.09E-11
AQP3	0.7073	1.58E-13
AQR	0.6397	1.29E-10
ARFGAP1	0.7030	2.55E-13

ARG1	0.6342	2.06E-10
ARHGAP15	0.6240	4.87E-10
ARHGAP22	0.8493	1.27E-23
ARHGAP25	0.8156	1.86E-20
ARHGAP30	0.8358	2.84E-22
ARHGAP4	0.7935	1.03E-18
ARHGAP45	0.8363	2.59E-22
ARHGAP9	0.8191	9.25E-21
ARHGDIB	0.8075	8.48E-20
ARHGEF1	0.8307	8.60E-22
ARHGEF18	0.8657	1.86E-25
ARID3B	0.6341	2.08E-10
ARID4B	0.6829	2.17E-12
ARL4C	0.6603	2.00E-11
ARMH1	0.8014	2.57E-19
ARRB2	0.6206	6.43E-10
ARRDC1	0.6110	1.38E-09
ARRDC5	0.8097	5.63E-20
ARSK	0.6014	4.93E-09
ASB2	0.7796	1.00E-17
ASB6	0.6225	5.47E-10
ASCL2	0.7009	3.21E-13
ASCL4	0.6996	3.72E-13
ASF1B	0.6810	2.65E-12
ASH2LP3	0.6498	5.25E-11
ASIC3	0.6385	1.44E-10
ASNS	0.8151	2.04E-20
ASPHD2	0.8695	6.55E-26
ASPM	0.7085	1.37E-13
ASS1	-0.6041	3.81E-09
ASS1P1	0.7900	1.83E-18
ATAD2	0.7727	2.91E-17
ATAD2B	0.6397	1.29E-10
ATAD5	0.7657	8.43E-17
ATF4P1	0.7588	2.29E-16
ATF7IP2	0.7020	2.83E-13
ATG16L1	0.7715	3.50E-17

ATG16L2	0.7198	3.67E-14
ATG4D	0.6737	5.50E-12
ATG9B	0.7964	6.21E-19
ATM	0.8801	2.78E-27
ATP10D	0.6256	0.00E+00
ATP13A1	0.7990	3.94E-19
ATP1A3	0.6795	3.06E-12
ATP2A3	0.8015	2.54E-19
ATP2B1	0.6163	9.11E-10
ATP5MC2	0.6084	1.69E-09
ATP5PDP4	0.6582	2.44E-11
ATP6V1G1	0.7198	3.69E-14
ATP6V1G2	0.7246	2.06E-14
ATP8A1	0.6985	4.16E-13
ATP8B2	0.8445	3.94E-23
ATP8B3	0.7000	3.56E-13
ATXN1	0.6090	2.20E-09
ATXN2L	0.7460	1.34E-15
ATXN7L2	0.8121	3.60E-20
AUP1	0.7158	5.93E-14
AURKB	0.7674	6.50E-17
B3GAT1	0.6782	3.53E-12
B3GAT3	0.6420	1.05E-10
B3GNTL1	0.6304	2.86E-10
B4GALNT3	0.8356	3.01E-22
BACH2	0.9273	1.88E-35
BAHD1	0.6284	3.38E-10
BANF1	0.6000	5.59E-09
BATF	0.7343	6.18E-15
BAX	0.7448	1.57E-15
BCL11A	0.8189	9.63E-21
BCL11B	0.8053	1.28E-19
BCL2L12	0.6467	6.93E-11
BCL2L14	0.7999	3.39E-19
BCOR	0.7031	2.53E-13
BCORP1	0.7731	2.75E-17
BCRP5	0.6684	9.21E-12

BEND4	0.7026	2.65E-13
BEST4	0.7044	2.17E-13
BEX2	0.6910	9.32E-13
BFSP2	0.7550	3.90E-16
BGLAP	0.7663	7.72E-17
BICD1	0.6231	5.22E-10
BICRA	0.6399	1.27E-10
BICRAL	0.7476	0.00E+00
BIK	0.7733	2.69E-17
BIN2	0.8461	2.70E-23
BIRC3	0.7060	1.81E-13
BLK	0.6420	1.05E-10
BLM	0.8204	7.14E-21
BLNK	0.8772	6.88E-27
BLOC1S4	0.6248	4.55E-10
BMP10	0.6636	1.46E-11
BNIP3P23	0.6216	5.90E-10
BNIP3P41	0.7817	7.18E-18
BNIP5	0.6727	6.05E-12
BRD8	0.6212	3.85E-11
BRI3BP	0.6436	9.11E-11
BRICD5	0.6142	1.08E-09
BRIP1	0.7159	5.87E-14
BRPF1	0.6529	3.97E-11
BRWD1P2	0.7789	1.11E-17
BTAF1	0.8195	8.54E-21
BTBD6P1	0.6787	3.35E-12
BTBD9	0.6491	0.00E+00
BTG1P1	0.6537	3.70E-11
BTK	0.7256	1.83E-14
BTLA	0.7375	4.11E-15
BTN1A1	0.7243	2.15E-14
BTN2A1	0.7206	3.35E-14
BTN2A2	0.8892	1.49E-28
BTN3A1	0.7927	1.17E-18
BTN3A2	0.7431	1.97E-15
BTN3A3	0.7177	4.70E-14

BUB1	0.7037	2.37E-13
BUB1B	0.6537	3.67E-11
BUB3	0.7359	5.02E-15
C11orf21	0.8395	1.25E-22
C11orf49	0.7784	0.00E+00
C11orf80	0.7908	1.62E-18
C11orf98	0.6274	3.68E-10
C12orf42	0.6974	4.71E-13
C12orf65	0.8032	1.86E-19
C16orf54	0.8651	2.19E-25
C16orf58	0.6011	5.06E-09
C17orf67	0.7475	1.10E-15
C17orf99	0.6835	2.06E-12
C18orf25	0.6009	3.01E-09
C19orf48	0.6431	9.54E-11
C19orf71	0.7332	7.06E-15
C1orf131	0.6396	1.30E-10
C1orf162	0.6638	1.44E-11
C1orf61	0.7376	4.06E-15
C1QL2	0.7358	5.09E-15
C1QTNF6	0.6762	4.28E-12
C20orf204	0.7367	4.54E-15
C22orf15	0.6093	1.57E-09
C2CD2L	0.6270	3.79E-10
C2CD5	0.6327	0.00E+00
C2orf68	0.6138	1.11E-09
C2orf81	0.6520	4.31E-11
C4orf50	0.6426	1.00E-10
C6orf62	0.6999	3.58E-13
C9orf135	0.6873	1.38E-12
CABIN1	0.8047	1.42E-19
CABLES2	0.7481	1.01E-15
CACNA1F	0.7167	5.34E-14
CACNA1I	0.7965	6.06E-19
CACNA2D2	0.6596	2.14E-11
CAD	0.6212	6.12E-10
CALHM6	0.8065	1.03E-19

CALY	0.7144	6.94E-14
CAMK1	-0.6080	1.74E-09
CAMK1G	0.6365	1.70E-10
CAMK4	0.7710	3.78E-17
CAPN1	0.6700	0.00E+00
CAPN10	0.7550	3.88E-16
CAPN12	0.8554	2.81E-24
CAPN14	0.7133	7.90E-14
CAPN15	0.6522	4.23E-11
CAPRIN2	0.7202	3.51E-14
CAPS	0.7002	3.48E-13
CAPZA1	0.6722	6.39E-12
CARD11	0.8398	1.17E-22
CARD16	0.6852	1.73E-12
CARD17	0.7903	1.76E-18
CARMIL2	0.8098	5.60E-20
CASC4	0.7133	0.00E+00
CASP1	0.6734	5.69E-12
CASP1P2	0.7685	5.52E-17
CASP2	0.7239	2.25E-14
CASP8	0.8559	2.44E-24
CATSPER2	0.6371	1.62E-10
CBFA2T2	0.6696	8.18E-12
CBFB	0.6906	9.82E-13
CBLN3	0.6749	4.90E-12
CBX4	0.7265	1.63E-14
CBX5	0.7269	1.55E-14
CBX7	0.6371	0.00E+00
CCDC12	0.6570	2.71E-11
CCDC130	0.6413	1.12E-10
CCDC137	0.7943	8.96E-19
CCDC154	0.6928	7.78E-13
CCDC159	0.7201	3.57E-14
CCDC163	0.6420	1.05E-10
CCDC186	0.6445	0.00E+00
CCDC189	0.7251	1.93E-14
CCDC28B	0.7453	1.47E-15

CCDC57	0.7895	2.01E-18
CCDC65	0.7881	2.52E-18
CCDC78	0.8520	6.55E-24
CCDC84	0.7083	1.40E-13
CCDC88B	0.8155	1.89E-20
CCDC88C	0.7158	5.91E-14
CCDC97	0.6781	0.00E+00
CCL17	0.7935	1.02E-18
CCL19	0.7394	3.20E-15
CCL21	0.7904	1.73E-18
CCL5	0.7646	9.82E-17
CCNA1	0.6755	4.61E-12
CCNB1	0.6825	2.28E-12
CCNB2	0.6898	1.06E-12
CCND3	0.7363	4.78E-15
CCNI2	0.8827	1.24E-27
CCR12P	0.7661	7.85E-17
CCR2	0.6455	7.72E-11
CCR4	0.8122	3.52E-20
CCR6	0.7145	6.89E-14
CCR7	0.7175	4.82E-14
CCR8	0.6991	3.90E-13
CCR9	0.7860	3.57E-18
CD101	0.8551	3.00E-24
CD160	0.6022	2.72E-09
CD180	0.8297	1.06E-21
CD19	0.6429	9.76E-11
CD1A	0.7301	1.05E-14
CD1C	0.7034	2.45E-13
CD1D	0.7114	9.89E-14
CD1E	0.7649	9.41E-17
CD2	0.8250	2.86E-21
CD207	0.6161	9.26E-10
CD22	0.7965	6.13E-19
CD226	0.7855	3.90E-18
CD24	0.7285	1.28E-14
CD247	0.7970	5.61E-19

CD27	0.8096	5.79E-20
CD28	0.7487	9.33E-16
CD37	0.8299	1.03E-21
CD38	0.6265	3.96E-10
CD3D	0.7984	4.38E-19
CD3E	0.8136	2.71E-20
CD3G	0.8257	2.48E-21
CD4	0.7025	2.70E-13
CD40	0.6696	8.20E-12
CD40LG	0.8041	1.58E-19
CD47	0.7431	1.97E-15
CD48	0.8359	2.77E-22
CD5	0.8272	1.81E-21
CD52	0.6011	2.97E-09
CD53	0.8663	1.58E-25
CD5L	0.7862	3.45E-18
CD6	0.8098	5.57E-20
CD69	0.6561	2.95E-11
CD7	0.8330	5.21E-22
CD72	0.6970	4.92E-13
CD74	0.6931	7.51E-13
CD79A	0.6854	1.68E-12
CD79B	0.8045	1.47E-19
CD80	0.8579	1.47E-24
CD8A	0.8336	4.59E-22
CD8B	0.8290	1.24E-21
CD8B2	0.7900	1.85E-18
CD96	0.7527	5.34E-16
CDC14A	0.8321	6.34E-22
CDC25B	0.7586	2.36E-16
CDC25C	0.6271	3.76E-10
CDC40	0.6424	0.00E+00
CDC42BPG	0.9118	2.90E-32
CDC42SE1	0.7859	3.64E-18
CDC42SE2	0.8045	1.49E-19
CDC45	0.6079	1.76E-09
CDCA3	0.7422	2.23E-15

CDCA4	0.6710	7.19E-12
CDCA7	0.7825	6.28E-18
CDCA8	0.6099	1.50E-09
CDH1	0.6100	1.49E-09
CDH10	0.6653	1.25E-11
CDH17	0.6490	5.67E-11
CDH2	0.6182	7.81E-10
CDHR1	0.7897	1.96E-18
CDHR2	0.6918	8.60E-13
CDK10	0.6686	9.10E-12
CDK11A	0.6119	1.29E-09
CDK13	0.6572	2.66E-11
CDK5R1	0.6780	3.58E-12
CDK5RAP2	0.6160	9.32E-10
CDK5RAP3	0.8804	2.59E-27
CDRT15	0.7220	2.84E-14
CDT1	0.6440	8.80E-11
CDX1	0.7336	6.76E-15
CEACAM21	0.8091	6.33E-20
CEBPE	0.6943	6.62E-13
CELA1	0.7911	1.52E-18
CELSR1	0.7324	7.84E-15
CELSR3	0.7556	3.57E-16
CEMIP	0.6078	1.77E-09
CEND1	0.7167	5.31E-14
CENPF	0.6627	1.59E-11
CENPK	0.7588	2.29E-16
CENPVL2	0.7630	1.24E-16
CEP135	0.8731	2.33E-26
CEP85	0.6691	8.60E-12
CEP85L	0.7737	2.50E-17
CEP95	0.6329	2.32E-10
CERK	0.7626	1.31E-16
CERKL	0.6815	2.50E-12
CERS2	0.6529	0.00E+00
CERS5	0.7720	3.28E-17
CFAP73	0.7197	3.73E-14

CFAP97D2	0.7477	1.06E-15
CFP	0.7746	2.19E-17
CGAS	0.6404	1.21E-10
CHD1L	0.7702	4.25E-17
CHD2	0.8077	8.29E-20
CHD3	0.8851	5.74E-28
CHD4	0.6716	6.75E-12
CHD6	0.7108	0.00E+00
CHD8	0.8193	8.92E-21
CHEK2	0.6099	1.50E-09
CHERP	0.7035	2.42E-13
CHFR	0.6767	4.06E-12
CHIAP1	0.7789	1.11E-17
CHKB	0.6350	1.92E-10
CHKB-CPT1B	0.6731	5.81E-12
CHMP7	0.7303	1.02E-14
CHRNA3	0.6963	5.33E-13
CHRNA6	0.7743	2.29E-17
CHTF18	0.6648	1.31E-11
CHTOP	0.6817	2.46E-12
CIDEB	0.6294	3.10E-10
CIITA	0.6133	1.15E-09
CLASRP	0.7376	4.02E-15
CLDN3	0.7607	1.73E-16
CLEC17A	0.7953	7.45E-19
CLEC18B	0.6932	7.45E-13
CLEC2D	0.8101	5.26E-20
CLEC4C	0.7390	3.39E-15
CLEC4M	0.8139	2.56E-20
CLEC9A	0.7824	6.39E-18
CLECL1	0.6572	2.68E-11
CLIP4	0.6136	1.15E-09
CLK2	0.8009	2.81E-19
CLNK	0.7973	5.36E-19
CLSTN1	0.6236	5.04E-10
CLSTN3	0.6906	9.80E-13
CLUHP3	0.9378	4.88E-38

CMTM7	0.7563	3.25E-16
CMTR1	0.7054	1.95E-13
CNKSR1	0.6721	6.42E-12
CNNM3	0.7680	0.00E+00
CNNM4	0.6666	1.09E-11
CNOT1	0.6996	3.73E-13
CNOT10	0.7347	5.90E-15
CNOT4	0.6461	0.00E+00
CNOT6	0.6472	0.00E+00
CNOT9	0.6913	9.10E-13
CNPY3	0.8306	8.85E-22
CNR2	0.7939	9.55E-19
CNTRL	0.8246	3.10E-21
COASY	0.6015	2.88E-09
COIL	0.6654	0.00E+00
COL19A1	0.8144	2.31E-20
COL6A5	0.6368	1.65E-10
COL9A2	0.8774	6.37E-27
COQ8B	0.6054	3.31E-09
CORO1A	0.8385	1.56E-22
CORO7	0.7834	5.48E-18
COX5A	-0.6252	0.00E+00
CPA5	0.7715	3.54E-17
CPLX3	0.6764	4.22E-12
CPNE5	0.8255	2.57E-21
CPNE7	0.6743	5.20E-12
CPSF1P1	0.6008	3.04E-09
CPSF6	0.6625	1.63E-11
CPT1B	0.6077	1.79E-09
CR1	0.6143	1.06E-09
CR1L	0.6490	5.64E-11
CR2	0.7944	8.74E-19
CRACR2A	0.7806	8.58E-18
CRB3	0.6048	2.23E-09
CRIP3	0.8126	3.29E-20
CRKL	0.7010	0.00E+00
CRLF3	0.7924	1.24E-18

CRNKL1	0.6566	0.00E+00
CRTAM	0.6580	2.49E-11
CRTC2	0.7643	1.03E-16
CRYBG2	0.6923	8.13E-13
CSAG1	0.7918	1.36E-18
CSAG2	0.7784	1.21E-17
CSF2RB	0.6782	3.52E-12
CSK	0.8505	9.51E-24
CSKMT	0.6575	2.59E-11
CST7	0.6336	2.17E-10
CSTF3	0.6324	2.41E-10
CTBP1	0.6012	2.95E-09
CTC1	0.8428	5.88E-23
CTLA4	0.7973	5.28E-19
CTRL	0.6374	1.57E-10
CTSW	0.7844	4.62E-18
CTXND1	0.6907	9.71E-13
CUL9	0.7396	3.12E-15
CUTA	0.6073	1.84E-09
CUTALP	0.6510	4.71E-11
CUX2	0.6082	1.72E-09
CUZD1	0.7536	4.75E-16
CWF19L1	0.6989	4.01E-13
CXCL13	0.7773	1.43E-17
CXCL5	0.7511	6.69E-16
CXCR2P1	0.7907	1.64E-18
CXCR3	0.8512	7.99E-24
CXCR5	0.8182	1.11E-20
CXorf65	0.7999	3.37E-19
CXXC1	0.7063	1.76E-13
CYB561D1	0.6292	3.15E-10
CYB5A	-0.6401	0.00E+00
CYBA	0.7208	3.28E-14
CYBC1	0.8188	9.96E-21
CYCSP34	0.6261	4.09E-10
CYFIP2	0.7751	2.03E-17
CYLD	0.8603	7.93E-25

CYP2R1	0.7221	2.80E-14
CYTH1	0.6182	7.76E-10
CYTH4	0.7618	1.49E-16
CYTIP	0.7805	8.70E-18
DAPP1	0.6355	1.86E-10
DAZL	0.7871	2.97E-18
DBF4	0.7328	7.43E-15
DCAF15	0.6658	1.19E-11
DCANP1	0.7372	4.28E-15
DCK	0.6903	1.01E-12
DCLRE1C	0.6680	9.57E-12
DCP1B	0.6612	0.00E+00
DCP2	0.7859	3.61E-18
DCPS	0.6462	7.29E-11
DDB2	0.6276	3.62E-10
DDIAS	0.6049	2.23E-09
DDX17	0.6302	2.91E-10
DDX23	0.6365	1.70E-10
DDX27	0.6676	9.94E-12
DDX31	0.6595	2.15E-11
DDX39A	0.7326	7.66E-15
DDX54	0.6090	1.61E-09
DDX56	0.6796	3.06E-12
DEAF1	0.6451	0.00E+00
DEDD2	0.8481	1.69E-23
DEF6	0.8273	1.76E-21
DEK	0.6893	0.00E+00
DENND1C	0.8275	1.70E-21
DENND2D	0.7752	1.99E-17
DENND4B	0.7264	1.65E-14
DEPDC1	0.6288	3.27E-10
DEPDC1B	0.6322	2.45E-10
DEPDC5	0.7067	1.69E-13
DERL3	0.6643	1.37E-11
DFFB	0.6957	5.68E-13
DGKA	0.8094	6.01E-20
DGKQ	0.6187	7.49E-10

DGUOK	0.7279	1.37E-14
DHPS	0.7621	1.41E-16
DHRS13	0.7123	8.89E-14
DHX30	0.7469	1.18E-15
DHX34	0.8363	2.56E-22
DHX37	0.7147	6.75E-14
DHX38	0.6497	5.30E-11
DHX58	0.7243	2.13E-14
DHX9	0.6383	0.00E+00
DIABLO	0.6102	1.89E-09
DIAPH1	0.8636	3.25E-25
DIP2A	0.7446	1.62E-15
DIS3L2	0.6438	8.97E-11
DISP3	0.6105	1.43E-09
DLGAP5	0.6092	1.59E-09
DMRTC1	0.6542	3.52E-11
DMRTC1B	0.8098	5.55E-20
DNAH8	0.6784	3.43E-12
DNAI2	0.7547	4.09E-16
DNAJC4	0.8008	2.89E-19
DNAJC8P1	0.6506	4.89E-11
DNASE1	0.6105	1.43E-09
DND1	0.6309	2.73E-10
DNMT1	0.7624	1.36E-16
DNMT3A	0.8080	7.81E-20
DNTT	0.7706	4.05E-17
DOC2GP	0.6508	4.80E-11
DOCK10	0.8165	1.54E-20
DOCK2	0.8788	4.16E-27
DOCK8	0.7443	1.69E-15
DOK3	0.8000	3.29E-19
DPEP2	0.6294	3.11E-10
DPF2	0.6323	0.00E+00
DPH7	0.7260	1.75E-14
DPP9	0.6248	4.54E-10
DPY19L2P2	0.6436	9.17E-11
DPY19L3	0.7829	0.00E+00

DRICH1	0.6231	5.24E-10
DTHD1	0.6554	3.15E-11
DTNB	0.6662	1.14E-11
DTX3	0.6066	1.95E-09
DUX4L50	0.6398	1.27E-10
DXO	0.6508	4.78E-11
DYRK2	0.7352	5.52E-15
DYRK4	0.7353	5.43E-15
E2F2	0.7328	7.49E-15
E2F5	0.8796	3.29E-27
E2F8	0.7607	1.73E-16
EAF2	0.7317	8.52E-15
EBI3	0.7997	3.51E-19
EDAR	0.8670	1.30E-25
EDC4	0.7022	2.78E-13
EDEM1	0.7938	9.65E-19
EED	0.6747	4.99E-12
EEF1A1P14	0.7775	1.39E-17
EEF1B2	0.7294	1.14E-14
EEF1D	0.7160	5.78E-14
EEF1G	0.6569	2.74E-11
EFNA4	0.6770	3.96E-12
EHBP1L1	0.6033	2.52E-09
EIF3CL	0.7431	1.97E-15
EIF3D	0.6681	9.54E-12
EIF3EP1	0.7179	4.60E-14
EIF3H	0.6248	0.00E+00
EIF3L	0.6090	1.62E-09
EIF4EBP2P2	0.6399	1.27E-10
ELF4	0.6155	9.64E-10
ELK4	0.7238	2.29E-14
ELL3	0.7914	1.47E-18
ELMO3	0.7626	1.32E-16
ELOF1	0.6890	0.00E+00
ELP1	0.6062	3.06E-09
EMB	0.6591	2.25E-11
EMID1	0.7428	2.06E-15

EML2	0.8507	8.94E-24
EML4	0.8056	1.21E-19
EML5	0.6178	8.07E-10
EML6	0.6656	1.21E-11
ENGASE	0.6595	2.15E-11
ENO2	0.8556	2.63E-24
ENO3	0.7326	7.65E-15
ENPP6	0.7915	1.44E-18
ENPP7P8	0.6718	6.62E-12
ENTHD1	0.7627	1.29E-16
ENTR1	0.8113	4.23E-20
EOMES	0.8352	3.22E-22
EP400	0.6581	2.45E-11
EPHA1	0.7904	1.72E-18
EPHB6	0.6855	1.67E-12
EPM2AIP1	0.7430	2.00E-15
EPSTI1	0.7064	1.74E-13
EPX	0.7612	1.61E-16
ERBIN	0.7406	2.74E-15
ERCC5	0.6206	6.41E-10
ERFL	0.7829	5.88E-18
ERICH3	0.6779	3.63E-12
ERMN	0.7954	7.33E-19
ERP27	0.7890	2.19E-18
ERP29	0.7156	6.02E-14
ETNK1	0.6648	1.31E-11
EVI2A	0.6991	3.91E-13
EVI2B	0.7864	3.33E-18
EVI5	0.6189	3.05E-10
EVL	0.7968	5.81E-19
EWSR1	0.6038	2.42E-09
EXOC3L4	0.6928	7.76E-13
EXOC8	0.6062	2.01E-09
EXOSC2	0.7022	2.77E-13
EXOSC8	0.6855	1.66E-12
EXOSC9	0.6240	4.86E-10
EZH2	0.7261	1.71E-14

EZHIP	0.7709	3.84E-17
F5	0.6554	3.15E-11
F8	-0.6059	3.14E-09
FA2H	0.8175	1.27E-20
FAAH2	0.8002	3.18E-19
FAAP100	0.6225	5.47E-10
FABP4	-0.6693	8.46E-12
FAM102A	0.9370	7.94E-38
FAM110A	0.8047	1.44E-19
FAM111A	0.6206	6.43E-10
FAM111B	0.6039	2.40E-09
FAM117A	0.7600	1.91E-16
FAM117B	0.7550	3.90E-16
FAM122B	0.7327	7.57E-15
FAM133DP	0.6278	3.56E-10
FAM136A	0.6509	4.74E-11
FAM153A	0.8304	9.26E-22
FAM163B	0.7883	2.43E-18
FAM169A	0.7451	1.52E-15
FAM172BP	0.7245	2.10E-14
FAM177B	0.7861	3.54E-18
FAM192A	0.7917	1.39E-18
FAM193B	0.6564	2.87E-11
FAM209A	0.6794	3.10E-12
FAM216A	0.7796	1.00E-17
FAM227B	0.7602	1.85E-16
FAM24B	0.7619	1.46E-16
FAM78A	0.8559	2.50E-24
FAM81A	0.6103	1.46E-09
FAM98C	0.6392	1.35E-10
FANCA	0.7355	5.27E-15
FANCD2	0.8545	3.47E-24
FANCF	0.8254	2.64E-21
FANCG	0.6564	2.88E-11
FANCI	0.6202	6.64E-10
FASLG	0.6394	1.33E-10
FAU	0.6679	9.71E-12

FBF1	0.7223	2.74E-14
FBL	0.7829	5.91E-18
FBRS	0.7921	1.30E-18
FBRSL1	0.6601	2.04E-11
FBXL16	0.8414	8.05E-23
FBXO34	0.6963	0.00E+00
FBXO41	0.9575	2.01E-44
FBXO44	0.8432	5.40E-23
FBXO46	0.7816	7.24E-18
FBXO5	0.6751	4.79E-12
FCAMR	0.7903	1.76E-18
FCER2	0.7311	9.24E-15
FCHO1	0.9045	5.74E-31
FCHSD1	0.8920	5.75E-29
FCMR	0.7944	8.83E-19
FCRL1	0.7752	2.01E-17
FCRL2	0.7821	6.73E-18
FCRL3	0.6830	2.15E-12
FCRL4	0.7154	6.21E-14
FCRLA	0.7252	1.92E-14
FCSK	0.6683	9.28E-12
FDCSP	0.8016	2.47E-19
FERMT2	-0.6058	2.07E-09
FERMT3	0.6749	4.88E-12
FFAR1	0.6065	1.96E-09
FGD1	0.6221	0.00E+00
FGD2	0.7975	5.11E-19
FGD3	0.8579	1.49E-24
FGFR1OP	0.6876	1.33E-12
FIP1L1	0.6899	1.06E-12
FITM1	0.6331	2.27E-10
FLT3	0.8085	7.09E-20
FLT3LG	0.7942	9.12E-19
FMNL1	0.7865	3.31E-18
FMR1	0.7510	6.78E-16
FNBP1	0.9251	5.84E-35
FOXB1	0.6094	1.56E-09

FOXD4L1	0.7028	2.62E-13
FOXD4L3	0.7781	1.27E-17
FOXD4L4	0.6790	3.25E-12
FOXD4L6	0.7402	2.88E-15
FOXG1	0.6665	1.11E-11
FOXP1	0.6718	6.62E-12
FOXP3	0.7827	6.07E-18
FSCN2	0.6116	1.32E-09
FSD1	0.7064	1.74E-13
FTH1P1	0.7005	3.34E-13
FTH1P22	0.7780	1.28E-17
FUBP1	0.7392	3.28E-15
FUNDC2P4	0.7637	1.12E-16
FUS	0.8004	3.08E-19
FUT7	0.7887	2.29E-18
FXYD5	0.7656	8.54E-17
FXYD7	0.7913	1.49E-18
FYB1	0.8598	9.15E-25
FYN	0.6516	4.48E-11
GAK	0.6395	1.31E-10
GAL3ST4	0.6665	1.10E-11
GALNS	0.6386	1.42E-10
GALNT7	0.6851	1.73E-12
GALT	0.6588	2.31E-11
GAPDHP1	0.6421	1.04E-10
GAPDHP67	0.6205	6.44E-10
GAPT	0.7931	1.10E-18
GBA3	0.7381	3.77E-15
GBP5	0.8413	8.27E-23
GCNT3	0.7025	2.70E-13
GCNT4	0.6842	1.90E-12
GCSAM	0.8345	3.80E-22
GDI1	0.6750	4.83E-12
GFI1	0.7962	6.46E-19
GGA1	0.7306	9.79E-15
GGA2	0.7865	3.29E-18
GGA3	0.7899	1.88E-18

GGT4P	0.6709	7.24E-12
GGT7	0.7716	3.48E-17
GHDC	0.6999	3.57E-13
GHRL	0.7934	1.04E-18
GID8	0.7117	0.00E+00
GIGYF1	0.6057	2.09E-09
GIMAP2	0.7183	4.40E-14
GIMAP3P	0.7727	2.93E-17
GINS2	0.6980	4.42E-13
GJA3	0.6603	2.01E-11
GJB6	0.7518	6.07E-16
GLB1L3	0.7179	4.64E-14
GLS2	0.8250	2.84E-21
GLYATL1B	0.6790	3.25E-12
GMEB2	0.6550	3.26E-11
GMIP	0.8101	5.24E-20
GNB5	0.7398	3.05E-15
GNG7	0.7751	2.04E-17
GNG8	0.7898	1.92E-18
GNGT2	0.7344	6.13E-15
GOLGA2P5	0.8431	5.53E-23
GOLGA8B	0.8406	9.79E-23
GOLPH3L	0.6041	3.80E-09
GORAB	0.6744	5.15E-12
GOT2	0.6824	2.29E-12
GP1BA	0.8049	1.38E-19
GPA33	0.8411	8.70E-23
GPBP1	0.7531	5.07E-16
GPC2	0.7133	7.94E-14
GPHA2	0.6425	1.01E-10
GPR132	0.8137	2.67E-20
GPR15	0.6986	4.15E-13
GPR171	0.6237	4.98E-10
GPR174	0.8309	8.20E-22
GPR18	0.8453	3.32E-23
GPR19	0.7461	1.32E-15
GPR25	0.7798	9.75E-18

GPR31	0.7387	3.52E-15
GPR35	0.7960	6.62E-19
GPR55	0.7436	1.84E-15
GPR65	0.7016	2.98E-13
GPRASP1	0.7284	1.29E-14
GPX4	-0.6332	0.00E+00
GRAMD1B	0.7153	6.25E-14
GRAP	0.7612	1.63E-16
GRAP2	0.7996	3.56E-19
GRAPL	0.6587	2.32E-11
GRIA4	0.7339	6.52E-15
GRIN1	0.8193	9.03E-21
GRK2	0.8057	1.19E-19
GRK6	0.8614	6.00E-25
GSAP	0.7260	1.75E-14
GSDMD	0.7731	2.77E-17
GTF3C2	0.7287	1.25E-14
GTF3C4	0.6354	0.00E+00
GTF3C5	0.7420	2.28E-15
GTPBP3	0.6569	2.74E-11
GTSF1L	0.7660	8.00E-17
GUCY2C	0.7809	8.21E-18
GVINP1	0.8101	5.23E-20
GZMA	0.6268	3.85E-10
GZMK	0.8516	7.21E-24
GZMM	0.8227	4.49E-21
H2AFJ	-0.6175	4.96E-10
H2AFY2	0.7330	7.25E-15
H3F3A	0.7676	6.30E-17
HACD4	0.6363	1.72E-10
HADHB	-0.6044	2.31E-09
HAGHL	0.8052	1.30E-19
HAPLN3	0.6086	1.67E-09
HAUS5	0.8373	2.05E-22
HCFC1	0.7493	8.52E-16
HCLS1	0.8098	5.57E-20
HCN2	0.8936	3.24E-29

HCST	0.6465	7.06E-11
HDAC1	0.9130	1.73E-32
HDAC10	0.6741	5.30E-12
HDAC3	0.6117	1.30E-09
HDGFL2	0.6459	0.00E+00
HEATR6	0.7320	0.00E+00
HELB	0.6495	5.39E-11
HELLS	0.8337	4.54E-22
HERPUD2	0.7379	0.00E+00
HEXD	0.7710	3.78E-17
HGS	0.6897	1.07E-12
HIST1H2BH	0.6569	2.74E-11
HIST1H4E	0.7024	2.72E-13
HIST2H2BC	0.7533	4.95E-16
HIST2H2BD	0.6827	2.22E-12
HJURP	0.6240	4.85E-10
HKDC1	0.7148	6.65E-14
HLA-DMB	0.6845	1.85E-12
HLA-DOB	0.7936	1.00E-18
HLA-DPB2	0.8224	4.80E-21
HLA-F	0.6286	3.31E-10
HLA-T	0.7109	1.04E-13
HMG20A	0.6231	0.00E+00
HMGB1P17	0.7481	1.00E-15
HMGB2P1	0.8018	2.39E-19
HMGN1	0.8732	2.21E-26
HMGN2	0.6661	1.15E-11
HMGN2P31	0.7345	6.04E-15
HMGN4	0.6600	0.00E+00
HMMR	0.6143	1.06E-09
HMSD	0.6940	6.84E-13
HNRNPA1	0.7089	1.31E-13
HNRNPA1L2	0.7974	5.20E-19
HNRNPA1P16	0.6949	6.16E-13
HNRNPA1P21	0.7704	4.17E-17
HNRNPA1P70	0.7895	2.00E-18
HNRNPCP1	0.6080	1.75E-09

HNRNPD	0.7832	5.61E-18
HNRNPH1	0.6813	2.55E-12
HNRNPL	0.7316	8.65E-15
HNRNPM	0.6043	2.33E-09
HOOK1	0.6397	1.29E-10
HOPX	0.6130	1.18E-09
HPCAL4	0.8255	2.58E-21
HPS3	0.7103	1.12E-13
HS3ST3A1	0.7826	6.22E-18
HS3ST3B1	0.8014	2.59E-19
HSF5	0.6651	1.27E-11
HSH2D	0.7338	6.57E-15
HTR3A	0.8090	6.51E-20
HVCN1	0.8877	2.50E-28
ICAM3	0.6343	2.05E-10
ICAM5	0.6076	1.80E-09
ICOS	0.8187	1.01E-20
ICOSLG	0.7351	5.55E-15
IDO2	0.7892	2.12E-18
IFFO1	0.6016	2.86E-09
IFIH1	0.6179	7.99E-10
IFNE	0.7134	7.87E-14
IFNL1	0.7276	1.43E-14
IFNL3P1	0.7712	3.71E-17
IFT80	0.7784	1.22E-17
IGF1R	0.7113	0.00E+00
IGFLR1	0.8109	4.52E-20
IGHA2	0.7877	2.70E-18
IGHD	0.6793	3.13E-12
IGHG2	0.6548	3.33E-11
IGHJ4	0.6870	1.43E-12
IGHM	0.8281	1.50E-21
IGHMBP2	0.6143	1.06E-09
IGHV1-17	0.6115	1.32E-09
IGHV1OR15-1	0.8019	2.38E-19
IGHV2-70	0.6052	2.17E-09
IGHV3-16	0.6134	1.15E-09

IGHV3-20	0.6223	5.60E-10
IGHV3-38	0.6664	1.12E-11
IGHV4-39	0.6703	7.71E-12
IGHV5-10-1	0.6516	4.48E-11
IGHV5-78	0.8082	7.57E-20
IGHV7-40	0.7789	1.11E-17
IGHVII-53-1	0.7789	1.11E-17
IGHVIII-11-1	0.7789	1.11E-17
IGHVIII-38-1	0.7681	5.87E-17
IGKV1-27	0.6550	3.29E-11
IGKV1D-33	0.7079	1.48E-13
IGKV1D-43	0.7819	6.96E-18
IGKV2-10	0.7037	2.36E-13
IGKV2D-26	0.6613	1.83E-11
IGKV7-3	0.7678	6.11E-17
IGLC4	0.7150	6.48E-14
IGLJ1	0.7852	4.05E-18
IGLJ2	0.7120	9.15E-14
IGLV11-55	0.6871	1.41E-12
IGLV1-51	0.6204	6.52E-10
IGLV2-5	0.6711	7.07E-12
IGLV2-8	0.6106	1.43E-09
IGLV3-12	0.6827	2.23E-12
IGLV3-13	0.6750	4.85E-12
IGLV3-2	0.7789	1.11E-17
IGLV3-21	0.6609	1.89E-11
IGLV3-6	0.7724	3.04E-17
IGLV4-60	0.7809	8.14E-18
IGLV4-69	0.7003	3.45E-13
IGLV9-49	0.6153	9.82E-10
IKBKB	0.6944	6.55E-13
IKBKE	0.8068	9.67E-20
IKZF1	0.8600	8.68E-25
IKZF2	0.7641	1.06E-16
IKZF3	0.8204	7.23E-21
IL10RA	0.7762	1.72E-17
IL12B	0.6045	2.29E-09

IL12RB1	0.8757	1.06E-26
IL17F	0.7285	1.27E-14
IL17REL	0.8108	4.62E-20
IL2	0.7313	9.00E-15
IL21	0.7723	3.10E-17
IL21R	0.8537	4.28E-24
IL22RA2	0.7760	1.75E-17
IL23A	0.7532	5.03E-16
IL27RA	0.7682	5.81E-17
IL2RB	0.8404	1.03E-22
IL2RG	0.8387	1.51E-22
IL32	0.7337	6.62E-15
IL36A	0.7769	1.54E-17
IL36G	0.8000	3.34E-19
IL4I1	0.7528	5.27E-16
IL4R	0.6115	1.33E-09
IL7	0.7077	1.50E-13
IL7R	0.7536	4.72E-16
IL9R	0.6970	4.90E-13
IL9RP3	0.7777	1.36E-17
ILDR1	0.8100	5.33E-20
ILF3	0.8493	1.27E-23
IMP3	0.6190	7.29E-10
INPP4A	0.7332	7.08E-15
INPP5D	0.8338	4.44E-22
INPP5F	0.8245	3.12E-21
INSL3	0.7585	2.38E-16
INSM1	0.7128	8.41E-14
INTS1	0.6098	1.51E-09
INTS11	0.6519	4.34E-11
INTS13	0.6595	2.16E-11
INTS4	0.7003	3.44E-13
INTS6L	0.8849	6.23E-28
IPCEF1	0.7724	3.09E-17
IQCB1	0.6840	1.95E-12
IRAK4	0.6983	4.27E-13
IRF2	0.7099	1.16E-13

IRF3	0.7150	6.52E-14
IRF4	0.7419	2.30E-15
IRF5	0.7093	1.26E-13
IRF7	0.6680	9.62E-12
IRF9	0.7895	2.00E-18
ISG20	0.6176	8.15E-10
ITFG2	0.7263	1.68E-14
ITGA4	0.7941	9.21E-19
ITGAL	0.8284	1.40E-21
ITGB1BP2	0.6197	6.90E-10
ITGB7	0.8039	1.66E-19
ITIH1	0.6307	2.78E-10
ITIH4	0.6023	2.71E-09
ITK	0.7954	7.43E-19
ITPA	0.6327	2.34E-10
ITPR3	0.7615	1.56E-16
ITSN2	0.6154	9.73E-10
IZUMO1R	0.7272	1.50E-14
JADE2	0.6331	2.27E-10
JAK3	0.8011	2.72E-19
JAKMIP1	0.6270	3.79E-10
JAML	0.6870	1.42E-12
JPT1	0.6363	1.72E-10
KANSL2	0.7062	1.78E-13
KAT5	0.6257	4.22E-10
KAT7	0.6327	0.00E+00
KAT8	0.6790	3.25E-12
KBTBD8	0.7241	2.18E-14
KCNA3	0.8025	2.13E-19
KCNAB2	0.6982	4.34E-13
KCNAB3	0.7028	2.60E-13
KCNC3	0.7721	3.21E-17
KCNF1	0.6905	9.84E-13
KCNG1	0.7552	3.79E-16
KCNH3	0.8948	2.11E-29
KCNH8	0.7909	1.59E-18
KCNJ10	0.8238	3.59E-21

KCNK12	0.7489	9.10E-16
KCNN4	0.8109	4.53E-20
KCNQ2	0.7569	2.98E-16
KCTD13	0.6930	7.55E-13
KCTD17	0.7961	6.55E-19
KDF1	0.8314	7.37E-22
KDM1A	0.6422	0.00E+00
KDM2A	0.7389	3.42E-15
KDM2B	0.9170	2.86E-33
KDM4C	0.7516	6.26E-16
KDM8	0.7649	9.47E-17
KIAA0556	0.7551	0.00E+00
KIAA0753	0.6310	0.00E+00
KIAA1191	0.6575	0.00E+00
KIAA1324	0.7654	8.78E-17
KIF11	0.6268	3.87E-10
KIF14	0.7106	1.08E-13
KIF18A	0.6399	1.26E-10
KIF18B	0.6823	2.31E-12
KIF21B	0.8128	3.15E-20
KIF22	0.7504	7.32E-16
KIF26B	0.6999	3.60E-13
KIF2C	0.6955	5.79E-13
KIFC2	0.6774	3.80E-12
KISS1R	0.6476	6.41E-11
KITLG	0.6364	0.00E+00
KLF12	0.8387	1.51E-22
KLF3	0.6135	1.18E-09
KLHDC4	0.7913	1.50E-18
KLHDC7B	0.7950	7.87E-19
KLHL11	0.6034	4.09E-09
KLHL17	0.7433	1.92E-15
KLHL28	0.6895	1.10E-12
KLHL42	0.6031	2.54E-09
KLHL6	0.7681	5.86E-17
KLHL9	0.6272	0.00E+00
KLRB1	0.7903	1.75E-18

KLRC4	0.6109	1.39E-09
KLRC4-KLRK1	0.6898	1.07E-12
KLRK1	0.8155	1.89E-20
KMT2A	0.6095	1.56E-09
KMT2B	0.6912	9.16E-13
KNL1	0.7548	4.00E-16
KNTC1	0.6675	1.01E-11
KRBA1	0.6404	1.22E-10
KREMEN2	0.7316	8.66E-15
KRI1	0.8372	2.08E-22
KRT17P1	0.7360	4.94E-15
KRT72	0.7622	1.40E-16
KRT73	0.7621	1.41E-16
KRT8P5	0.6328	2.34E-10
KRTCAP3	0.6475	6.46E-11
KSR2	0.6801	2.90E-12
L3MBTL3	0.8993	4.12E-30
LAD1	0.8198	8.11E-21
LAG3	0.8832	1.05E-27
LAMP3	0.7982	4.56E-19
LAMP5	0.7808	8.23E-18
LARGE2	0.7992	3.80E-19
LARS	0.6120	1.47E-09
LAT	0.8026	2.07E-19
LAT2	0.7542	4.34E-16
LAX1	0.8684	8.79E-26
LBH	0.8999	3.32E-30
LCK	0.8071	9.22E-20
LCN8	0.7786	1.17E-17
LCP2	0.7835	5.41E-18
LDB1	0.7011	3.13E-13
LDLRAP1	0.7734	2.64E-17
LEAP2	0.6085	1.68E-09
LEF1	0.8128	3.18E-20
LEMD2	0.6086	1.67E-09
LEO1	0.6311	0.00E+00
LGALS2	0.7507	7.11E-16

LIG1	0.8749	1.36E-26
LILRB1	0.6430	9.63E-11
LIMD2	0.8240	3.50E-21
LIME1	0.8187	1.00E-20
LINC00869	0.7736	2.55E-17
LINGO3	0.6198	6.82E-10
LINGO4	0.6301	2.92E-10
LINS1	0.7443	1.69E-15
LLGL2	0.7312	9.12E-15
LMAN1L	0.6254	4.32E-10
LMNB1	0.7918	1.36E-18
LMNTD2	0.6213	6.07E-10
LMO7	0.6741	5.31E-12
LMTK3	0.8366	2.42E-22
LPAR2	0.7400	2.97E-15
LPAR3	0.7150	6.52E-14
LPAR5	0.6966	5.13E-13
LPXN	0.7595	2.07E-16
LRCH4	0.8731	2.28E-26
LRFN1	0.7995	3.62E-19
LRMP	0.6933	7.36E-13
LRP8	0.7129	8.32E-14
LRRC14	0.6405	1.20E-10
LRRC26	0.7349	5.75E-15
LRRC37A15P	0.7463	1.28E-15
LRRC37A2	0.7350	5.65E-15
LRRC37A4P	0.7880	2.56E-18
LRRC37B	0.7775	1.41E-17
LRRC55	0.6880	1.29E-12
LRRC61	0.6178	8.05E-10
LRRC8D	0.7858	3.71E-18
LRRK1	0.6159	9.40E-10
LRSAM1	0.6378	0.00E+00
LRWD1	0.6564	2.86E-11
LSM14B	0.6890	0.00E+00
LSR	0.6005	3.11E-09
LTA	0.8160	1.70E-20

LTB	0.7843	4.72E-18
LTBP3	0.6084	2.37E-09
LTK	0.6514	4.54E-11
LUC7L	0.6989	4.02E-13
LY75	0.8860	4.26E-28
LY86	0.6798	2.98E-12
LY9	0.7843	4.73E-18
LYG1	0.6943	6.56E-13
LYL1	0.6350	1.92E-10
LYPLA2	0.6490	5.65E-11
LYSMD2	0.7667	7.20E-17
LZTFL1	0.6237	0.00E+00
M6PR	0.6546	3.40E-11
MAD1L1	0.7027	2.63E-13
MADCAM1	0.7266	1.61E-14
MADD	0.6483	6.02E-11
MAGEE1	0.6940	6.82E-13
MAL	0.7725	3.03E-17
MALT1	0.8069	9.54E-20
MAN1C1	0.6441	8.76E-11
MANBA	0.6406	0.00E+00
MANSC4	0.6816	2.49E-12
MAP11	0.8316	7.15E-22
MAP3K1	0.8626	4.26E-25
MAP3K14	0.7924	1.23E-18
MAP3K7	0.6340	2.10E-10
MAP3K9	0.7163	5.56E-14
MAP4K1	0.8238	3.65E-21
MAP4K2	0.7613	1.60E-16
MAPK11	-0.6158	7.57E-10
MAPK8IP3	0.6411	1.14E-10
MARCH1	0.6035	2.48E-09
MARCH9	0.7748	2.12E-17
MARCKSL1	0.8552	2.98E-24
MARK2	0.6276	0.00E+00
MARK3	0.6530	3.92E-11
MARS	0.6113	1.35E-09

MAT2B	0.7511	6.71E-16
MATR3	0.6429	0.00E+00
MAX	0.6880	1.29E-12
MAZ	0.6029	2.59E-09
MBD4	0.6515	4.49E-11
MBLAC2	0.6295	0.00E+00
MC1R	0.7787	1.15E-17
MCF2	0.7882	2.49E-18
MCFD2	0.6061	3.08E-09
MCM2	0.7308	9.60E-15
MCM3	0.6217	0.00E+00
MCM5	0.7444	1.67E-15
MCM7	0.6282	3.44E-10
MCM9	0.6334	2.21E-10
MCOLN2	0.8196	8.47E-21
MCUB	0.6545	3.44E-11
MDM1	0.6082	1.71E-09
MDM4	0.6329	2.31E-10
MDN1	0.6998	3.64E-13
MECP2	0.6687	8.97E-12
MED14	0.6194	7.07E-10
MED16	0.6744	5.14E-12
MED23	0.8090	6.45E-20
MED25	0.6876	0.00E+00
MED29	0.7015	0.00E+00
MEF2B	0.6811	2.62E-12
MEI1	0.7955	7.29E-19
MEN1	0.7519	6.02E-16
METAP1	0.7303	1.02E-14
METTL16	0.6022	2.72E-09
METTL17	0.6253	4.36E-10
METTL18	0.6700	7.89E-12
METTL23	0.6451	8.04E-11
METTL3	0.6944	6.50E-13
MFAP1	0.6083	2.40E-09
MFSD8	0.6687	9.00E-12
MGST3	-0.6564	0.00E+00

MIA-RAB4B	0.6510	4.70E-11
MIB1	0.6749	0.00E+00
MICAL1	0.7463	1.28E-15
MIGA2	0.6223	5.57E-10
MIIP	0.8019	2.35E-19
MINK1	0.6061	2.02E-09
MIOS	0.6111	1.37E-09
MITD1	0.7149	6.57E-14
MMS19	0.7643	1.03E-16
MND1	0.6651	1.27E-11
MOB3A	0.6475	6.49E-11
MORN3	0.7727	2.91E-17
MOV10	0.6781	3.56E-12
MPC1	-0.6273	0.00E+00
MPHOSPH9	0.7250	1.96E-14
MPZL1	0.6185	3.64E-10
MRFAP1L1	0.6373	1.59E-10
MRNIP	0.7773	1.45E-17
MRPL38	0.6850	1.75E-12
MRPS21P2	0.7248	2.02E-14
MRPS31	0.7344	6.10E-15
MRPS31P4	0.6118	1.52E-09
MS4A1	0.6209	6.26E-10
MS4A18	0.7152	6.35E-14
MSI2	0.6469	6.82E-11
MSL2	0.7682	5.74E-17
MSL3	0.7850	4.23E-18
MST02P	0.7074	1.56E-13
MTCH1	0.6002	5.53E-09
MTCO2P33	0.6757	4.50E-12
MTERF4	0.6326	2.38E-10
MTF2	0.6688	8.87E-12
MTFP1	0.7183	4.41E-14
MTMR1	0.8577	1.57E-24
MTMR14	0.6486	5.87E-11
MTMR4	0.6653	1.24E-11
MTND4LP14	0.7789	1.11E-17

MTO1	0.8125	3.33E-20
MTRF1	0.6775	3.75E-12
MUS81	0.7917	1.40E-18
MUSK	0.7561	3.36E-16
MUTYH	0.7494	8.51E-16
MVP	0.6974	4.72E-13
MYB	0.8068	9.75E-20
MYBBP1A	0.6051	2.18E-09
MYBL1	0.6284	3.37E-10
MYBL2	0.7129	8.33E-14
MYBPC2	0.7795	1.02E-17
MYCL	0.8001	3.24E-19
MYD88	0.6696	8.23E-12
MYH3	0.6140	1.09E-09
MYL12BP2	0.7450	1.54E-15
MYL5	-0.6013	4.98E-09
MYO18A	0.7251	1.95E-14
MYO1G	0.8202	7.45E-21
MYO7B	0.6460	7.38E-11
MYO9B	0.6810	2.63E-12
N4BP2L1	0.6217	5.88E-10
NAA16	0.7536	4.72E-16
NAA40	0.6279	3.53E-10
NAALADL1	0.6123	1.25E-09
NADSYN1	0.8257	2.43E-21
NAGS	0.6242	4.77E-10
NAP1L1	0.6475	6.48E-11
NAP1L2	0.6016	2.86E-09
NAP1L3	0.7234	2.38E-14
NAPSA	0.6691	8.63E-12
NAPSB	0.7830	5.79E-18
NAT10	0.7070	1.64E-13
NBEAL2	0.7033	2.48E-13
NBL1	0.6353	0.00E+00
NBPF15	0.6494	5.47E-11
NBPF8	0.7755	1.91E-17
NBR1	0.6279	0.00E+00

NCAPD2	0.7206	3.35E-14
NCAPG	0.6310	2.71E-10
NCAPH2	0.6073	1.84E-09
NCCRP1	0.7871	2.98E-18
NCF1	0.7792	1.06E-17
NCF1B	0.7758	1.81E-17
NCF1C	0.8130	3.06E-20
NCKAP1L	0.7412	2.54E-15
NCOA3	0.6134	1.14E-09
NDC80	0.7310	9.36E-15
NDOR1	0.7273	1.48E-14
NDUFA3P3	0.7789	1.11E-17
NDUFB4P11	0.6753	4.71E-12
NDUFS4	-0.6031	2.55E-09
NECAP2	0.6580	2.49E-11
NECTIN3	0.6255	0.00E+00
NEIL3	0.7051	2.02E-13
NEK8	0.9108	4.32E-32
NELL2	0.6906	9.72E-13
NEMP1	0.6841	1.93E-12
NEURL3	0.6077	1.79E-09
NFATC2IP	0.8454	3.24E-23
NFKBIE	0.6672	1.03E-11
NFYC	0.6130	1.18E-09
NGLY1	0.7566	3.13E-16
NIBAN3	0.7889	2.23E-18
NIN	0.6127	1.20E-09
NIPBL	0.7317	8.58E-15
NKRF	0.8293	1.16E-21
NKX2-2	0.6442	8.64E-11
NKX6-3	0.7880	2.59E-18
NLRC3	0.8102	5.13E-20
NLRC5	0.7550	3.90E-16
NLRP1	0.6428	9.86E-11
NLRP4	0.7826	6.22E-18
NLRP6	0.6891	1.14E-12
NOD2	0.7444	1.66E-15

NOG	0.7536	4.76E-16
NOL4	0.6670	1.06E-11
NOL8	0.7737	2.50E-17
NONO	0.6974	4.72E-13
NOP2	0.6126	1.22E-09
NOP53	0.7675	6.42E-17
NOSIP	0.6787	3.34E-12
NOXO1	0.7761	1.73E-17
NPAT	0.8295	1.12E-21
NPM1P25	0.8330	5.25E-22
NPPC	0.6242	4.78E-10
NPRL2	0.6990	3.94E-13
NPTX1	0.7658	8.28E-17
NR1H4	0.6474	6.53E-11
NR1I2	0.7267	1.60E-14
NR2C2AP	0.6557	3.08E-11
NSUN5	0.8045	1.48E-19
NSUN5P1	0.6581	2.46E-11
NSUN5P2	0.6872	1.39E-12
NT5C	0.7968	5.81E-19
NTNG2	0.6672	1.04E-11
NUAK2	0.7962	6.42E-19
NUDT16L1	0.6802	2.87E-12
NUDT21	0.6040	3.86E-09
NUDT22	0.6546	3.38E-11
NUF2	0.7152	6.31E-14
NUGGC	0.6781	3.56E-12
NUP205	0.7748	2.13E-17
NUP210	0.8206	6.85E-21
NUP42	0.7202	3.50E-14
NUP62	0.6382	1.47E-10
NUP88	0.6299	2.98E-10
NUP93	0.6258	4.19E-10
NUS1P1	0.6326	2.37E-10
NUSAP1	0.7400	2.95E-15
NVL	0.7413	2.51E-15
NXF1	0.7255	1.86E-14

NYAP2	0.6921	8.37E-13
OAS2	0.6162	9.18E-10
OBSCN	0.7704	4.13E-17
OCIAD2	0.7451	1.51E-15
OCM	0.8021	2.29E-19
ODF2	0.6389	1.38E-10
OFD1	0.8752	1.24E-26
OGFR	0.8215	5.81E-21
OGG1	0.6039	3.86E-09
OGT	0.7919	1.33E-18
OR13A1	0.7756	1.89E-17
OR1D2	0.6961	5.44E-13
OR2I1P	0.6720	6.48E-12
OR4D1	0.8035	1.78E-19
OR4E1	0.7698	4.56E-17
OR52N2	0.6581	2.46E-11
OR7E12P	0.7300	1.06E-14
OR7E22P	0.6803	2.84E-12
OR7E24	0.7415	2.45E-15
OSBPL3	0.8024	2.17E-19
OSBPL7	0.7517	6.17E-16
OSGEP	0.7028	2.61E-13
OTOF	0.6839	1.96E-12
OTUB1	0.7272	1.50E-14
OTUD5	0.7443	1.69E-15
OXNAD1	0.7261	1.72E-14
P2RX5	0.8183	1.09E-20
P2RX5-TAX1BP3	0.7803	9.04E-18
P2RX7	0.6650	1.28E-11
P2RY10	0.8154	1.90E-20
P2RY10BP	0.6776	3.71E-12
P2RY11	0.8001	3.27E-19
P2RY8	0.6985	4.17E-13
P4HTM	0.6414	1.11E-10
PABPC1	0.7380	3.84E-15
PABPC1L	0.9245	7.75E-35
PACSIN1	0.7030	2.56E-13

PAFAH1B3	0.7502	7.57E-16
PAG1	0.7125	8.66E-14
PAGE5	0.7865	3.31E-18
PAGR1	0.6455	0.00E+00
PAICSP3	0.6233	5.14E-10
PAK1	0.6487	5.83E-11
PAN2	0.6230	5.27E-10
PAN3	0.6946	6.39E-13
PANK4	0.6367	1.67E-10
PAOX	0.6042	2.34E-09
PAPLN	0.6687	8.95E-12
PAQR8	0.7575	2.74E-16
PARP1	0.7587	2.30E-16
PARP10	0.8238	3.64E-21
PARP12	0.6655	1.22E-11
PARP15	0.7723	3.10E-17
PARP16	0.6532	3.88E-11
PARP8	0.8367	2.33E-22
PARVG	0.8195	8.66E-21
PASK	0.8198	8.15E-21
PATL2	0.7821	6.75E-18
PAX5	0.7794	1.03E-17
PAXBP1	0.6325	2.40E-10
PAXX	0.7682	5.74E-17
PBK	0.7524	5.60E-16
PBX4	0.6973	4.77E-13
PCED1A	0.8067	9.82E-20
PCED1B	0.7732	2.70E-17
PCLAF	0.7192	3.93E-14
PCNA	0.7006	3.34E-13
PCNX2	0.7077	1.51E-13
PCNX3	0.6897	1.08E-12
PCNX4	0.6175	4.93E-10
PCP2	0.8520	6.59E-24
PCSK7	0.7304	1.01E-14
PCYOX1L	0.8717	3.48E-26
PDCD11	0.6234	5.11E-10

PDCL3P4	0.7669	7.04E-17
PDE6B	0.8571	1.82E-24
PDE6G	0.6990	3.96E-13
PDE7A	0.8121	3.61E-20
PELP1	0.7244	2.11E-14
PGAM1P8	0.6551	3.25E-11
PGAP2	0.7323	7.93E-15
PGAP3	0.6029	2.59E-09
PGBD2	0.6869	1.45E-12
PGBD4	0.7800	9.46E-18
PGBD4P1	0.7630	1.25E-16
PGGHG	0.7751	2.03E-17
PGM2L1	0.6402	1.23E-10
PHACTR1	0.6238	4.95E-10
PHBP5	0.6483	6.03E-11
PHC1	0.8107	4.74E-20
PHF12	0.8036	1.74E-19
PHF19	0.8005	3.02E-19
PHF6	0.7822	6.62E-18
PHF8	0.6437	9.05E-11
PHIP	0.6320	2.49E-10
PHKG2	0.7925	1.20E-18
PHLDB3	0.7807	8.46E-18
PHTF2	0.6792	3.19E-12
PI4KA	0.7368	4.45E-15
PIANP	0.7240	2.21E-14
PIAS1	0.6191	7.26E-10
PIH1D1	0.6554	3.15E-11
PIK3AP1	0.6515	4.51E-11
PIK3CD	0.9438	9.68E-40
PIK3CG	0.6071	1.88E-09
PIK3R5	0.7037	2.36E-13
PIM2	0.8121	3.61E-20
PIP4K2A	0.7051	2.03E-13
PIP4K2C	0.6278	3.56E-10
PITPNM1	0.7784	1.22E-17
PKIA	0.6820	2.40E-12

PKMYT1	0.6415	1.10E-10
PLA2G2D	0.6843	1.88E-12
PLA2G4B	0.6611	1.85E-11
PLAAT4	0.7205	3.40E-14
PLAC8	0.7499	7.85E-16
PLCB2	0.8240	3.47E-21
PLCH2	0.7975	5.09E-19
PLCXD2	0.8351	3.33E-22
PLD4	0.8231	4.16E-21
PLEC	0.6244	4.71E-10
PLEKHA2	0.7029	2.56E-13
PLEKHA3P1	0.6336	2.19E-10
PLEKHB1	0.9081	1.35E-31
PLEKHN1	0.6895	1.10E-12
PLEKHO1	0.7851	4.15E-18
PLK1	0.6381	1.48E-10
PLPP5	0.6540	3.60E-11
PLPP6	0.7748	2.12E-17
PLXNC1	0.7040	2.29E-13
PM20D2	0.6077	1.78E-09
PMCH	0.7825	6.32E-18
PMF1	0.6554	0.00E+00
PNN	0.7607	1.74E-16
PNOC	0.6680	9.57E-12
PNPLA6	0.6209	6.26E-10
POC1B	0.6683	0.00E+00
POGLUT1	0.8535	4.56E-24
POLA2	0.6669	1.07E-11
POLD1	0.7794	1.04E-17
POLDIP3	0.6498	0.00E+00
POLG2	0.7366	4.61E-15
POLR2J2	0.6961	5.41E-13
POLR2KP1	0.6257	4.23E-10
POLRMT	0.7145	6.90E-14
POMGNT2	0.6237	0.00E+00
POU2AF1	0.8204	7.20E-21
POU2F2	0.7448	1.56E-15

POU3F1	0.6291	3.18E-10
POU4F1	0.6628	1.58E-11
PPAN	0.6760	4.37E-12
PPHLN1	0.7392	3.30E-15
PPIAL4C	0.7794	1.04E-17
PPIAL4G	0.7316	8.67E-15
PPIAL4H	0.7500	7.79E-16
PPIAP45	0.7852	4.09E-18
PPIL2	0.6774	3.78E-12
PPM1J	0.7284	1.30E-14
PPM1K	0.7487	9.32E-16
PPM1M	0.8051	1.33E-19
PPM1N	0.7689	5.19E-17
PPP1CA	0.8088	6.69E-20
PPP1R18	0.6819	2.41E-12
PPP1R21	0.6186	3.43E-10
PPP1R35	0.7345	6.05E-15
PPP1R3E	0.6351	1.92E-10
PPP1R9B	0.6781	3.53E-12
PPP2R2B	0.6324	2.41E-10
PPP4R3A	0.7956	7.15E-19
PPP6R1	0.8524	5.94E-24
PPWD1	0.6052	2.18E-09
PQBP1	0.6950	6.13E-13
PRAMENP	0.8028	2.01E-19
PRDM10	0.6253	0.00E+00
PRDM15	0.7246	2.07E-14
PRDM7	0.6471	6.73E-11
PRDM8	0.6232	5.17E-10
PREX1	0.7557	3.52E-16
PRKCA	0.7018	2.90E-13
PRKCB	0.8580	1.46E-24
PRKCQ	0.8253	2.68E-21
PRKCZ	0.8506	9.23E-24
PRKXP1	0.7629	1.27E-16
PRM1	0.7049	2.07E-13
PRMT1	0.7392	3.29E-15

PRMT6	0.6378	1.51E-10
PROC	0.6872	1.39E-12
PROCA1	0.6643	1.37E-11
PROSER3	0.7201	3.55E-14
PRPF19	0.6570	0.00E+00
PRPF38A	0.6007	5.27E-09
PRPF38B	0.7873	2.89E-18
PRPF39	0.6746	5.04E-12
PRPS2	0.7775	1.40E-17
PRPSAP2	0.7220	2.84E-14
PRR13	0.6149	1.01E-09
PRR14	0.7692	5.01E-17
PRR19	0.6168	8.73E-10
PRR22	0.7717	3.40E-17
PRRC2C	0.7241	2.19E-14
PRSS1	0.6127	1.21E-09
PSD	0.6861	1.57E-12
PSD4	0.8886	1.80E-28
PSIP1	0.8252	2.71E-21
PSMB10	0.7303	1.02E-14
PSMB8	0.7068	1.66E-13
PSMD10P1	0.8372	2.11E-22
PSME1	0.7434	1.89E-15
PSME2	0.7469	1.18E-15
PSTPIP1	0.8376	1.93E-22
PTK2B	0.9328	9.41E-37
PTPN2	0.7385	3.58E-15
PTPN22	0.8200	7.72E-21
PTPN6	0.8571	1.80E-24
PTPN7	0.8569	1.94E-24
PTPRC	0.8632	3.71E-25
PTPRCAP	0.8251	2.76E-21
PTPRJ	0.6427	9.92E-11
PTTG1	0.7680	5.99E-17
PUM2	0.6200	1.68E-10
PUS1	0.6075	1.82E-09
PUS7L	0.6160	7.31E-10

PVALB	0.7806	8.55E-18
PVRIG	0.8005	3.04E-19
PWWP2A	0.6326	2.38E-10
PXK	0.6913	0.00E+00
PXYLP1	0.7454	0.00E+00
PYCARD	0.6714	6.87E-12
PYGO1	0.6802	0.00E+00
PYHIN1	0.7786	1.17E-17
PYM1	0.6494	5.46E-11
QPCTL	0.6516	4.46E-11
QSOX2	0.7988	4.09E-19
R3HDM2	0.6167	8.79E-10
R3HDM4	0.6514	4.54E-11
RAB11FIP2	0.6292	0.00E+00
RAB11FIP4	0.8930	4.11E-29
RAB19	0.6401	1.24E-10
RAB33A	0.8017	2.44E-19
RAB37	0.8306	8.83E-22
RAB39B	0.8336	4.58E-22
RAB5B	0.6398	0.00E+00
RAB8A	0.7146	6.83E-14
RABEP2	0.8082	7.49E-20
RABGAP1L	0.9157	5.15E-33
RABL2A	0.6275	3.62E-10
RABL2B	0.6139	1.10E-09
RAC2	0.8394	1.27E-22
RACK1	0.6605	1.97E-11
RAD23BP1	0.6964	5.27E-13
RAD52	0.6738	5.45E-12
RAD9A	0.6277	3.58E-10
RADX	0.8210	6.37E-21
RALGPS2	0.8352	3.22E-22
RANBP6	0.6724	6.23E-12
RANP9	0.7789	1.11E-17
RAP1GAP	0.6843	1.88E-12
RAP1GAP2	0.7961	6.59E-19
RAP2C	0.6547	3.36E-11

RAPGEF6	0.7453	1.48E-15
RASA2	0.7620	1.43E-16
RASA4CP	0.7328	7.50E-15
RASAL1	0.7933	1.05E-18
RASAL3	0.8185	1.05E-20
RASGEF1A	0.8233	4.04E-21
RASGRP1	0.8122	3.56E-20
RASGRP2	0.7856	3.82E-18
RASSF2	0.6381	1.47E-10
RASSF5	0.8311	7.90E-22
RASSF7	0.6408	1.17E-10
RAVER1	0.7009	3.22E-13
RBCK1	0.6952	5.97E-13
RBL1	0.6931	7.47E-13
RBL2	0.7821	6.71E-18
RBM10	0.7154	6.18E-14
RBM11	0.6678	9.81E-12
RBM19	0.8212	6.08E-21
RBM22	0.6244	4.72E-10
RBM23	0.6228	5.35E-10
RBM38	0.7184	4.37E-14
RBM39	0.6144	1.06E-09
RBM4B	0.7213	3.09E-14
RBMX	0.7545	4.18E-16
RBP5	0.6869	1.44E-12
RCAN3	0.7338	6.62E-15
RCC1	0.6993	3.82E-13
RCC2	0.7701	4.32E-17
RCSD1	0.7123	8.90E-14
RECQL5	0.7647	9.75E-17
REG4	0.7728	2.87E-17
RELCH	0.6766	4.10E-12
RELL2	0.8367	2.32E-22
RELT	0.6546	3.41E-11
REPS1	0.6785	3.42E-12
RESF1	0.8159	1.75E-20
RFC4	0.8425	6.25E-23

RFC5	0.6691	8.67E-12
RFPL2	0.6255	4.28E-10
RFWD3	0.7519	5.99E-16
RFX5	0.7426	2.09E-15
RFXANK	0.6300	2.95E-10
RGL4	0.7855	3.87E-18
RGS10	0.7893	2.07E-18
RGS14	0.8540	4.02E-24
RGS19	0.7826	6.18E-18
RGS7	0.7327	7.52E-15
RHBDF2	0.7145	6.85E-14
RHNO1	0.7819	6.96E-18
RHOF	0.6707	7.41E-12
RHOG	0.6656	1.21E-11
RHOH	0.7629	1.27E-16
RHOT1P1	0.6127	1.20E-09
RHOV	0.7352	5.53E-15
RHPN1	0.6885	1.22E-12
RIC3	0.8986	5.51E-30
RICTOR	0.7894	2.04E-18
RIMBP3	0.7473	1.13E-15
RIMBP3B	0.6356	1.83E-10
RINL	0.9067	2.38E-31
RIOX1	0.6434	9.29E-11
RIPOR2	0.8550	3.07E-24
RMC1	0.7008	3.23E-13
RMI2	0.8298	1.05E-21
RNA5SP180	0.7789	1.11E-17
RNA5SP241	0.8011	2.72E-19
RNASEH2B	0.7514	6.39E-16
RNASET2	0.8730	2.36E-26
RNF103	0.7720	0.00E+00
RNF113A	0.8191	9.27E-21
RNF166	0.7817	7.23E-18
RNF167	0.7919	1.34E-18
RNF213	0.7579	2.58E-16
RNF216	0.7967	5.92E-19

RNF220	0.6313	0.00E+00
RNF31	0.6529	3.97E-11
RNF38	0.6465	0.00E+00
RNF43	0.7307	9.73E-15
RNF44	0.8911	7.85E-29
RNFT2	0.6207	6.35E-10
RNGTT	0.6721	6.41E-12
RNMT	0.6921	8.32E-13
RPL10	0.6225	5.51E-10
RPL10A	0.6034	2.50E-09
RPL11	0.7147	6.73E-14
RPL12	0.6552	3.21E-11
RPL13	0.7646	9.86E-17
RPL13A	0.8034	1.81E-19
RPL14	0.7209	3.23E-14
RPL15	0.7295	1.13E-14
RPL17	0.6504	4.97E-11
RPL18	0.7605	1.79E-16
RPL18A	0.6634	1.49E-11
RPL19	0.7744	2.25E-17
RPL21	0.6649	1.29E-11
RPL23A	0.7806	8.55E-18
RPL23AP42	0.6559	3.03E-11
RPL26	0.6301	2.93E-10
RPL27A	0.7375	4.11E-15
RPL28	0.8327	5.60E-22
RPL3	0.7514	6.42E-16
RPL30	0.7277	1.41E-14
RPL31	0.6503	5.05E-11
RPL32	0.7944	8.80E-19
RPL32P29	0.6925	7.99E-13
RPL34	0.6593	2.20E-11
RPL36	0.7643	1.03E-16
RPL36A	0.7491	8.84E-16
RPL37	0.7849	4.28E-18
RPL38	0.7405	2.77E-15
RPL39	0.6742	5.24E-12

RPL3P4	0.7886	2.35E-18
RPL4	0.6605	1.96E-11
RPL4P1	0.7994	3.66E-19
RPL5	0.7092	1.26E-13
RPL6	0.7954	7.41E-19
RPL7P51	0.7844	4.63E-18
RPL8	0.7831	5.75E-18
RPLP1	0.7099	1.17E-13
RPS10	0.6250	4.47E-10
RPS11	0.8184	1.08E-20
RPS12	0.7149	6.56E-14
RPS14	0.7221	2.80E-14
RPS15	0.7567	3.07E-16
RPS15A	0.7014	3.05E-13
RPS16	0.6804	2.81E-12
RPS18	0.6631	1.54E-11
RPS19	0.8371	2.12E-22
RPS2	0.8144	2.33E-20
RPS20P32	0.6229	5.30E-10
RPS21	0.6802	2.86E-12
RPS23	0.7073	1.58E-13
RPS24P17	0.7133	7.93E-14
RPS27	0.8099	5.43E-20
RPS27A	0.6231	5.25E-10
RPS28	0.6435	9.27E-11
RPS28P7	0.6928	7.70E-13
RPS2P24	0.6349	1.95E-10
RPS2P36	0.6885	1.22E-12
RPS3	0.8055	1.23E-19
RPS3A	0.7165	5.43E-14
RPS3AP30	0.6768	4.05E-12
RPS4Y2	0.7497	8.08E-16
RPS5	0.6171	8.54E-10
RPS6	0.7899	1.87E-18
RPS6KA1	0.6788	3.29E-12
RPS6KB2	0.7283	1.31E-14
RPS7	0.6233	5.16E-10

RPS8	0.6818	2.43E-12
RPSA	0.7723	3.12E-17
RPSAP39	0.6642	1.38E-11
RPSAP41	0.6949	6.21E-13
RPSAP46	0.6789	3.27E-12
RPSAP53	0.6089	1.62E-09
RRM2	0.6453	7.86E-11
RRP7BP	0.6501	5.11E-11
RSBN1L	0.7416	2.40E-15
RSPH9	0.7167	5.29E-14
RSPRY1	0.6435	0.00E+00
RSRP1	0.6331	2.27E-10
RTKN2	0.7824	6.40E-18
RTL10	0.7796	1.01E-17
RTP4	0.6712	7.06E-12
RUBCN	0.7005	3.36E-13
RUBCNL	0.8333	4.92E-22
RUFY4	0.8317	6.97E-22
RUNX2	0.7486	9.48E-16
RUNX3	0.7940	9.44E-19
S100PBP	0.7605	1.79E-16
S1PR4	0.7618	1.48E-16
SAAL1	0.6788	3.32E-12
SACS	0.6623	1.66E-11
SAFB	0.6576	2.58E-11
SAMD1	0.6847	1.81E-12
SAMD10	0.8173	1.32E-20
SAMD14	0.6027	2.62E-09
SAMD3	0.8218	5.45E-21
SAMD9	0.8743	1.61E-26
SAP25	0.8695	6.48E-26
SARAF	0.6486	5.86E-11
SARDH	0.7681	5.87E-17
SART1	0.6650	1.29E-11
SART3	0.6921	8.37E-13
SASH3	0.8483	1.63E-23
SBF1	0.7451	1.51E-15

SBK1	0.9073	1.87E-31
SCIMP	0.6294	3.09E-10
SCML4	0.8068	9.69E-20
SCT	0.7086	1.36E-13
SCX	0.6301	2.92E-10
SCYGR4	0.6410	1.15E-10
SEC11C	0.6505	4.96E-11
SEC31B	0.6356	1.84E-10
SEC61A2	0.6670	1.06E-11
SECISBP2	0.7267	1.60E-14
SEL1L3	0.7150	6.47E-14
SELENOKP3	0.7761	1.74E-17
SELL	0.8065	1.02E-19
SELPLG	0.8186	1.04E-20
SEMA4A	0.6065	1.96E-09
SEMA4B	0.6287	3.28E-10
SEMA4D	0.9248	6.60E-35
SEMA7A	0.7728	2.89E-17
SENP1	0.6596	0.00E+00
SEPTIN1	0.8117	3.89E-20
SEPTIN6	0.8427	5.97E-23
SEPTIN9	0.7729	2.86E-17
SERPINA9	0.7724	3.07E-17
SERPINB9	0.6720	6.51E-12
SET	0.6490	5.64E-11
SETDB1	0.6568	2.76E-11
SETP9	0.7291	1.19E-14
SETX	0.6849	1.78E-12
SF3A2	0.6944	6.53E-13
SF3B1	0.7085	1.37E-13
SFI1	0.7913	1.48E-18
SFMBT2	0.7427	2.07E-15
SFXN1	0.7387	3.52E-15
SGF29	0.6598	2.09E-11
SGO1	0.6475	6.47E-11
SGSM2	0.7984	4.41E-19
SGSM3	0.7737	2.53E-17

SH2B2	0.6011	2.96E-09
SH2D1A	0.8453	3.31E-23
SH2D2A	0.6491	5.60E-11
SH2D3A	0.8267	1.99E-21
SH3BP1	0.8426	6.11E-23
SH3GLB2	0.6357	1.82E-10
SHD	0.7577	2.68E-16
SHFL	0.7693	4.94E-17
SHISAL2A	0.8088	6.72E-20
SHKBP1	0.6934	7.27E-13
SHMT2	0.7140	7.32E-14
SIGIRR	0.6989	4.00E-13
SIGLEC10	0.7930	1.11E-18
SIGLEC8	0.7052	1.99E-13
SIGMAR1	0.6005	5.34E-09
SINHCAF	0.7380	3.83E-15
SIPA1	0.8450	3.51E-23
SIPA1L3	0.7317	8.58E-15
SIRPB3P	0.7749	2.10E-17
SIRPG	0.7894	2.03E-18
SIRT6	0.6127	1.21E-09
SIRT7	0.8381	1.70E-22
SIT1	0.8012	2.66E-19
SKAP1	0.8101	5.28E-20
SLA2	0.8311	7.99E-22
SLAIN1	0.7191	4.00E-14
SLAMF1	0.8223	4.88E-21
SLAMF6	0.8072	9.02E-20
SLC10A3	0.6907	0.00E+00
SLC12A3	0.8201	7.69E-21
SLC12A9	0.7875	2.82E-18
SLC15A2	0.7874	2.87E-18
SLC16A13	0.6102	1.47E-09
SLC16A6	0.6171	8.54E-10
SLC16A9	0.6093	1.58E-09
SLC1A2	0.8280	1.53E-21
SLC22A17	0.6331	2.27E-10

SLC23A1	0.6403	1.22E-10
SLC23A2	0.6268	0.00E+00
SLC23A3	0.6754	4.62E-12
SLC25A22	0.7922	1.28E-18
SLC25A38	0.7122	8.96E-14
SLC25A45	0.7109	1.04E-13
SLC25A47P1	0.7080	1.45E-13
SLC2A1	0.6397	1.29E-10
SLC2A6	0.7411	2.55E-15
SLC35B2	0.6098	2.00E-09
SLC35C2	0.7470	1.18E-15
SLC35D1	0.6090	2.21E-09
SLC35E2B	0.6339	2.12E-10
SLC35F2	0.7728	2.90E-17
SLC35F3	0.8244	3.23E-21
SLC38A1	0.9108	4.35E-32
SLC38A5	0.8183	1.10E-20
SLC39A10	0.8515	7.45E-24
SLC45A3	0.7176	4.77E-14
SLC51A	0.6737	5.49E-12
SLC5A5	0.7345	6.00E-15
SLC7A11	0.6041	2.37E-09
SLC9A3	0.7693	4.92E-17
SLC9A3R1	0.6707	7.38E-12
SLC9A7	0.6992	3.86E-13
SLCO5A1	0.8284	1.40E-21
SLFN12L	0.7639	1.09E-16
SLFN13	0.6554	3.16E-11
SMARCA4	0.8337	4.54E-22
SMARCC1	0.6105	1.82E-09
SMC6	0.6223	5.57E-10
SMCHD1	0.7941	9.25E-19
SMG8	0.6165	6.45E-10
SMG9	0.7092	1.26E-13
SMIM24	0.6781	3.55E-12
SMIM5	0.7324	7.87E-15
SMPD2	0.7284	1.30E-14

SMPD5	0.8008	2.89E-19
SMURF2	0.6472	0.00E+00
SNAI3	0.7572	2.88E-16
SNAPC2	0.6119	1.51E-09
SNCB	0.6339	2.12E-10
SNRNP200	0.6863	1.53E-12
SNRNP40	0.6723	6.31E-12
SNRPA	0.7457	1.39E-15
SNRPD2	0.6498	5.25E-11
SNRPN	0.7653	8.90E-17
SNX20	0.8848	6.35E-28
SNX22	0.8277	1.62E-21
SNX29P1	0.7892	2.11E-18
SNX29P2	0.8145	2.26E-20
SOAT2	0.7528	5.28E-16
SOCS2P2	0.7789	1.11E-17
SON	0.6107	1.42E-09
SORCS1	0.7700	4.43E-17
SORL1	0.6679	9.65E-12
SOWAHD	0.7131	8.12E-14
SOX8	0.6516	4.48E-11
SP100	0.6224	5.53E-10
SP110	0.8354	3.13E-22
SP140	0.8435	4.96E-23
SP140L	0.8035	1.76E-19
SP3	0.6750	0.00E+00
SP4	0.7701	4.34E-17
SPAG5	0.6216	5.94E-10
SPATA13	0.7841	4.89E-18
SPATA19	0.6665	1.11E-11
SPATA48	0.7292	1.18E-14
SPATC1	0.7890	2.18E-18
SPG11	0.7579	2.59E-16
SPIB	0.8204	7.25E-21
SPIC	0.8342	4.04E-22
SPINDOC	0.6677	9.89E-12
SPINK2	0.7679	6.05E-17

SPINT2	0.7924	1.23E-18
SPN	0.7771	1.49E-17
SPNS3	0.7584	2.40E-16
SPOCK2	0.8785	4.55E-27
SPOP	0.6578	0.00E+00
SPOUT1	0.7370	4.35E-15
SPTSSB	0.6145	1.05E-09
SRC	0.6188	3.17E-10
SREBF2	0.6666	1.10E-11
SRMS	0.7966	6.03E-19
SRPK1	0.6033	2.51E-09
SRRM2	0.6991	3.91E-13
SRRT	0.7997	3.51E-19
SRSF1	0.7413	2.51E-15
SRSF2	0.6232	5.19E-10
SRSF6	0.6253	4.36E-10
SRSF9	0.6842	1.91E-12
SSH3	0.6510	0.00E+00
SSRP1	0.6812	0.00E+00
SSTR3	0.8903	1.04E-28
SSXP10	0.6567	2.80E-11
ST6GAL1	0.7564	3.21E-16
ST8SIA1	0.8768	7.80E-27
STAG3	0.7294	1.15E-14
STAMBPL1	0.6991	3.92E-13
STAP1	0.8381	1.72E-22
STAT4	0.7334	6.95E-15
STAT6	0.7224	2.68E-14
STIM2	0.7864	3.37E-18
STK10	0.7174	4.89E-14
STK11IP	0.7388	3.46E-15
STK17B	0.6131	1.17E-09
STK26	0.6317	2.56E-10
STK4	0.8607	7.08E-25
STMN1P1	0.6496	5.37E-11
STMN3	0.8345	3.78E-22
STRBP	0.9180	1.82E-33

STRIP2	0.7322	8.07E-15
STX16	0.6175	8.22E-10
STX16-NPEPL1	0.7053	1.98E-13
STX2	0.6107	1.77E-09
STXBP2	0.8842	7.68E-28
SUGP2	0.6911	9.29E-13
SULT1A3	0.6906	9.82E-13
SUMO2P17	0.6601	2.04E-11
SUPT16H	0.6494	0.00E+00
SUPT20H	0.7091	1.28E-13
SUPT5H	0.7611	1.63E-16
SUSD3	0.9126	1.98E-32
SUSD4	0.8403	1.05E-22
SV2A	0.6523	4.20E-11
SWSAP1	0.6266	3.92E-10
SYK	0.6565	2.85E-11
SYMPK	0.8127	3.23E-20
SYNE4	0.7808	8.33E-18
SYNGAP1	0.7469	1.18E-15
SYNGR1	0.6622	0.00E+00
SYNGR3	0.7850	4.19E-18
SYNPO2L	0.7485	9.51E-16
SYNRG	0.6529	3.98E-11
SYS1	0.7744	0.00E+00
SYT2	0.7186	4.26E-14
SYTL1	0.8134	2.80E-20
TACC3	0.8038	1.69E-19
TADA1	0.6022	4.57E-09
TADA3	0.6780	0.00E+00
TAF6	0.6190	2.96E-10
TAGAP	0.8729	2.45E-26
TAPBP	0.6376	1.54E-10
TAS2R4	0.6297	3.03E-10
TASOR	0.6752	4.73E-12
TATDN2	0.6329	0.00E+00
TAZ	0.6184	7.66E-10
TBC1D10C	0.8135	2.74E-20

TBC1D22A	0.6352	0.00E+00
TBC1D22B	0.6559	0.00E+00
TBC1D26	0.7683	5.69E-17
TBC1D27P	0.7936	9.98E-19
TBC1D32	0.6179	7.96E-10
TBC1D3L	0.6670	1.06E-11
TBCC	0.8008	2.87E-19
TBRG1	0.6555	3.12E-11
TBRG4	0.7682	5.81E-17
TBX10	0.6375	1.56E-10
TCAF2	0.7300	1.07E-14
TCF3	0.7014	3.05E-13
TCF7	0.7882	2.51E-18
TCIRG1	0.6651	1.27E-11
TCL1A	0.8244	3.19E-21
TCL1B	0.7260	1.74E-14
TDP1	0.6422	1.04E-10
TDRD7	0.6373	0.00E+00
TEC	0.6275	3.63E-10
TEP1	0.7299	1.08E-14
TEPP	0.6764	4.20E-12
TEPSIN	0.7091	1.28E-13
TESK2	0.6137	1.12E-09
TESPA1	0.8322	6.28E-22
TET2	0.6332	0.00E+00
TET3	0.7544	4.24E-16
TEX35	0.7873	2.89E-18
TEX9	0.6620	1.70E-11
TFAP2E	0.7471	1.15E-15
TFB1M	0.7135	7.75E-14
TFR2	0.7951	7.77E-19
TGFB1	0.7183	4.38E-14
TGIF2	0.7008	3.24E-13
THA1P	0.6837	2.00E-12
THAP11	0.6050	3.47E-09
THAP12P5	0.6038	2.42E-09
THAP7	0.6473	6.57E-11

THEM4	0.7753	1.95E-17
THOC2	0.7241	2.19E-14
THOC6	0.6989	4.01E-13
THOP1	0.6063	2.00E-09
TIA1	0.7276	1.42E-14
TIAM1	0.7918	1.37E-18
TICRR	0.6288	3.27E-10
TIFAB	0.7854	3.94E-18
TIGD1	0.8435	4.99E-23
TIGIT	0.8132	2.93E-20
TIMM17B	0.6071	1.88E-09
TJP3	0.8678	1.03E-25
TLE4	0.6368	1.65E-10
TLR10	0.7959	6.74E-19
TLR6	0.8199	8.01E-21
TM9SF4	0.6654	0.00E+00
TMBIM7P	0.6950	6.10E-13
TMC6	0.7089	1.31E-13
TMC8	0.8251	2.76E-21
TMED8	0.6724	0.00E+00
TMEM101	0.6017	4.80E-09
TMEM102	0.7343	6.20E-15
TMEM123	0.6783	3.48E-12
TMEM134	0.6181	7.84E-10
TMEM151B	0.8004	3.09E-19
TMEM156	0.7966	6.02E-19
TMEM161B	0.6798	2.99E-12
TMEM170A	0.6159	9.35E-10
TMEM178B	0.7097	1.20E-13
TMEM191A	0.8624	4.56E-25
TMEM229B	0.7931	1.09E-18
TMEM248	0.7191	0.00E+00
TMEM260	0.6157	9.52E-10
TMEM265	0.6664	1.12E-11
TMEM272	0.8243	3.30E-21
TMEM71	0.7270	1.54E-14
TMEM79	0.6539	3.62E-11

TMEM86B	0.8501	1.05E-23
TMEM9	0.6747	0.00E+00
TMIGD2	0.7804	8.90E-18
TMPO	0.9129	1.79E-32
TMPRSS13	0.7842	4.81E-18
TMPRSS6	0.7965	6.08E-19
TMX3	0.6250	4.48E-10
TNFAIP8L2	0.8503	9.97E-24
TNFRSF13B	0.7740	2.40E-17
TNFRSF13C	0.6206	6.40E-10
TNFRSF17	0.7511	6.67E-16
TNFRSF18	0.6990	3.98E-13
TNFRSF25	0.6845	1.84E-12
TNFRSF9	0.8357	2.93E-22
TNFSF11	0.7939	9.58E-19
TNFSF8	0.6085	1.67E-09
TNIK	0.8327	5.60E-22
TNK1	0.7591	2.17E-16
TNK2	0.7898	1.90E-18
TNNT2	0.7753	1.97E-17
TOE1	0.6553	3.20E-11
TOGARAM2	0.6794	3.12E-12
TOMM34	0.6438	9.02E-11
TONSL	0.7687	5.38E-17
TOP1MT	0.7015	3.02E-13
TOP2A	0.7802	9.05E-18
TOP2B	0.7449	1.55E-15
TOP3B	0.6638	1.43E-11
TOPBP1	0.6742	5.26E-12
TOR2A	0.6503	5.01E-11
TOX	0.7852	4.07E-18
TP53	0.7735	2.60E-17
TPD52	0.6135	1.13E-09
TPM3P9	0.6034	2.48E-09
TPP2	0.6462	7.26E-11
TPR	0.7098	1.18E-13
TRABD	0.7120	9.19E-14

TRAC	0.8078	8.05E-20
TRADD	0.6479	6.27E-11
TRAF1	0.8102	5.12E-20
TRAF2	0.7456	1.41E-15
TRAF3IP3	0.8020	2.31E-19
TRAF5	0.8646	2.50E-25
TRAFD1	0.7396	3.13E-15
TRAJ12	0.7789	1.11E-17
TRAJ3	0.7789	1.11E-17
TRAJ31	0.7789	1.11E-17
TRAJ33	0.7789	1.11E-17
TRAJ48	0.7789	1.11E-17
TRAJ57	0.7789	1.11E-17
TRAJ9	0.7789	1.11E-17
TRANK1	0.6447	8.30E-11
TRAPPC2	0.8256	2.51E-21
TRAT1	0.8197	8.32E-21
TRAV10	0.7670	6.93E-17
TRAV1-1	0.7725	3.04E-17
TRAV1-2	0.7698	4.55E-17
TRAV12-1	0.7853	4.00E-18
TRAV12-2	0.8196	8.46E-21
TRAV12-3	0.8017	2.45E-19
TRAV13-1	0.8007	2.92E-19
TRAV13-2	0.8227	4.50E-21
TRAV14DV4	0.8118	3.80E-20
TRAV16	0.8250	2.84E-21
TRAV17	0.8337	4.52E-22
TRAV18	0.7533	4.97E-16
TRAV19	0.8443	4.16E-23
TRAV2	0.7851	4.14E-18
TRAV20	0.7978	4.85E-19
TRAV21	0.8161	1.67E-20
TRAV22	0.8183	1.09E-20
TRAV23DV6	0.7962	6.42E-19
TRAV24	0.7340	6.40E-15
TRAV25	0.8109	4.50E-20

TRAV26-1	0.8097	5.68E-20
TRAV26-2	0.7728	2.87E-17
TRAV27	0.7921	1.30E-18
TRAV29DV5	0.8005	3.04E-19
TRAV3	0.8269	1.92E-21
TRAV30	0.7508	6.95E-16
TRAV34	0.7539	4.54E-16
TRAV35	0.7780	1.29E-17
TRAV36DV7	0.7963	6.34E-19
TRAV38-1	0.8006	2.96E-19
TRAV38-2DV8	0.8041	1.59E-19
TRAV39	0.7956	7.14E-19
TRAV4	0.7975	5.10E-19
TRAV40	0.6590	2.25E-11
TRAV41	0.7957	7.06E-19
TRAV5	0.7192	3.97E-14
TRAV6	0.7835	5.40E-18
TRAV8-1	0.7819	6.96E-18
TRAV8-2	0.7983	4.49E-19
TRAV8-3	0.7825	6.36E-18
TRAV8-4	0.8121	3.61E-20
TRAV8-6	0.7855	3.85E-18
TRAV9-2	0.7950	7.92E-19
TRBC1	0.8007	2.90E-19
TRBC2	0.7646	9.90E-17
TRBJ1-6	0.7789	1.11E-17
TRBJ2-1	0.7789	1.11E-17
TRBV1	0.8294	1.13E-21
TRBV10-1	0.7799	9.56E-18
TRBV10-2	0.7899	1.86E-18
TRBV10-3	0.7880	2.58E-18
TRBV11-1	0.8047	1.42E-19
TRBV11-3	0.7993	3.74E-19
TRBV12-1	0.7789	1.11E-17
TRBV12-3	0.8110	4.48E-20
TRBV12-4	0.8120	3.71E-20
TRBV12-5	0.7984	4.39E-19

TRBV13	0.7953	7.46E-19
TRBV14	0.7738	2.48E-17
TRBV15	0.8372	2.08E-22
TRBV18	0.7956	7.17E-19
TRBV19	0.8073	8.84E-20
TRBV2	0.8222	5.03E-21
TRBV20-1	0.7926	1.19E-18
TRBV21-1	0.7856	3.84E-18
TRBV23-1	0.7667	7.18E-17
TRBV25-1	0.7714	3.56E-17
TRBV27	0.8081	7.61E-20
TRBV28	0.7752	1.98E-17
TRBV29-1	0.8071	9.20E-20
TRBV30	0.7865	3.30E-18
TRBV3-1	0.7938	9.63E-19
TRBV4-1	0.7726	3.00E-17
TRBV5-1	0.7923	1.25E-18
TRBV5-4	0.7904	1.73E-18
TRBV5-5	0.7897	1.95E-18
TRBV5-6	0.8269	1.91E-21
TRBV6-1	0.7853	4.00E-18
TRBV6-2	0.8393	1.32E-22
TRBV6-4	0.7690	5.14E-17
TRBV6-5	0.8227	4.56E-21
TRBV6-6	0.7972	5.37E-19
TRBV7-1	0.7585	2.38E-16
TRBV7-2	0.7903	1.75E-18
TRBV7-3	0.7127	8.46E-14
TRBV7-4	0.7143	7.03E-14
TRBV7-6	0.8247	3.00E-21
TRBV7-7	0.7650	9.31E-17
TRBV7-9	0.8234	3.93E-21
TRBV9	0.7224	2.69E-14
TREML1	0.7478	1.04E-15
TREML2	0.6474	6.55E-11
TRERF1	0.6582	2.44E-11
TREX2	0.6969	4.99E-13

TRGC1	0.6480	6.18E-11
TRGC2	0.7106	1.08E-13
TRGV3	0.7302	1.03E-14
TRGV4	0.7713	3.63E-17
TRIM11	0.7759	1.79E-17
TRIM14	0.7827	6.07E-18
TRIM21	0.7134	7.81E-14
TRIM28	0.8739	1.80E-26
TRIM31	0.6089	1.62E-09
TRIM38	0.7410	2.59E-15
TRIM46	0.6126	1.22E-09
TRIM59	0.9145	8.63E-33
TRIM60P18	0.7206	3.35E-14
TRIM62	0.7229	2.53E-14
TRMT1	0.8409	9.03E-23
TRMT13	0.6362	1.74E-10
TRMT2A	0.6494	5.44E-11
TRMT2B	0.7243	2.15E-14
TRMU	0.6231	5.24E-10
TRPM5	0.7694	4.85E-17
TRPM7	0.6094	1.57E-09
TRRAP	0.7451	1.51E-15
TSC22D4	0.8460	2.76E-23
TSEN54	0.7909	1.58E-18
TSPAN32	0.7954	7.41E-19
TSPAN33	0.7486	9.41E-16
TSPAN5	0.6235	5.04E-10
TSPEAR	0.7461	1.31E-15
TSPOAP1	0.7034	2.43E-13
TSPYL4	0.6691	0.00E+00
TTC13	0.6648	1.31E-11
TTC16	0.8047	1.44E-19
TTC22	0.8698	5.93E-26
TTC24	0.7950	7.95E-19
TTC27	0.6798	0.00E+00
TTC31	0.6017	2.83E-09
TTC39B	0.7871	3.01E-18

TTC9	0.6925	8.01E-13
TTI1	0.6073	1.85E-09
TTN	0.7781	1.27E-17
TTYH2	0.6055	2.12E-09
TUBA4A	0.8294	1.13E-21
TUBB7P	0.7849	4.30E-18
TUBGCP2	0.6491	5.62E-11
TUBGCP4	0.6158	7.57E-10
TUBGCP6	0.7726	2.99E-17
TUT4	0.8691	7.17E-26
TUT7	0.6613	1.83E-11
TVP23A	0.7669	7.06E-17
TXK	0.8104	4.98E-20
TYK2	0.6730	5.89E-12
U2AF2	0.8199	7.93E-21
UBA52	0.6962	5.36E-13
UBA7	0.8012	2.66E-19
UBASH3A	0.8164	1.59E-20
UBD	0.7096	1.21E-13
UBE2C	0.7258	1.78E-14
UBE2I	0.6110	1.72E-09
UBE2Q1	0.6037	2.44E-09
UBE2T	0.6774	3.81E-12
UBE2Z	0.6225	0.00E+00
UBIAD1	0.6519	0.00E+00
UBTF	0.6080	1.75E-09
UBTFL2	0.7782	1.26E-17
UBXN11	0.6409	1.16E-10
UHRF1	0.7456	1.41E-15
UHRF2	0.7307	9.72E-15
UIMC1	0.6501	5.12E-11
ULK2	0.6406	0.00E+00
ULK3	0.6420	1.06E-10
UNC13D	0.8021	2.26E-19
UNC5CL	0.7497	8.07E-16
UNC93B1	0.6155	9.68E-10
UNK	0.6236	5.04E-10

UPB1	0.7469	1.18E-15
UPK3A	0.7153	6.24E-14
UPK3BL2	0.6699	7.95E-12
USF1	0.6481	6.15E-11
USP1	0.7384	0.00E+00
USP10	0.6882	1.26E-12
USP11	0.8346	3.72E-22
USP15	0.6270	3.78E-10
USP20	0.8073	8.86E-20
USP21	0.6404	1.21E-10
USP34	0.6044	2.31E-09
UTP18	0.6105	1.44E-09
UTP20	0.6133	1.21E-09
UTP25	0.6751	0.00E+00
UXS1	0.6869	1.45E-12
UXT	0.6779	3.63E-12
VAMP1	0.7911	1.53E-18
VAMP8	0.6163	9.10E-10
VANGL2	0.8159	1.75E-20
VAV1	0.8760	9.82E-27
VAV2	0.7254	1.87E-14
VAV3	0.8312	7.75E-22
VDR	0.6214	6.03E-10
VEZF1	0.6534	0.00E+00
VILL	0.7561	3.33E-16
VN1R9P	0.7295	1.13E-14
VPREB3	0.7795	1.02E-17
VPS16	0.6634	1.49E-11
VPS28	0.6218	5.81E-10
VRTN	0.7571	2.89E-16
VSIG1	0.7664	7.57E-17
WAPL	0.6087	1.65E-09
WAS	0.8707	4.66E-26
WASH2P	0.7427	2.08E-15
WASH3P	0.6550	3.26E-11
WASH6P	0.7853	4.00E-18
WASH9P	0.6727	6.05E-12

WBP1LP1	0.7471	1.15E-15
WDFY4	0.7478	1.05E-15
WDR33	0.6143	1.06E-09
WDR34	0.6111	1.37E-09
WDR37	0.7876	2.77E-18
WDR5	0.6641	0.00E+00
WDR54	0.8271	1.85E-21
WDR59	0.7117	9.53E-14
WDR5B	0.6425	1.01E-10
WDR6	0.7533	4.92E-16
WDR74	0.6774	3.79E-12
WDR75	0.6060	2.05E-09
WDR76	0.7355	5.27E-15
WDR89	0.6486	5.86E-11
WDR97	0.7297	1.10E-14
WFDC21P	0.7738	2.49E-17
WHRN	0.7948	8.21E-19
WIPF1	0.7103	1.12E-13
WNT10A	0.7431	1.96E-15
WNT7A	0.6476	6.38E-11
WRAP53	0.7228	2.56E-14
WRNIP1	0.6871	1.41E-12
XAB2	0.6029	2.60E-09
XCL2	0.6428	9.77E-11
XCR1	0.7244	2.11E-14
XKR6	0.7527	5.37E-16
XKR8	0.6140	1.08E-09
XPO6	0.7511	6.66E-16
XYLT2	0.6473	6.61E-11
YDJC	0.9350	2.67E-37
YWHABP1	0.6322	2.44E-10
ZAP70	0.7881	2.54E-18
ZBED5	0.7651	9.18E-17
ZBED6CL	0.7461	1.32E-15
ZBP1	0.8150	2.07E-20
ZBTB10	0.7019	0.00E+00
ZBTB24	0.6779	3.62E-12

ZBTB25	0.7563	3.25E-16
ZBTB26	0.6516	4.46E-11
ZBTB32	0.7302	1.03E-14
ZBTB39	0.6713	0.00E+00
ZBTB40	0.7303	1.02E-14
ZBTB48	0.6517	4.41E-11
ZBTB49	0.6003	3.15E-09
ZBTB5	0.7200	3.60E-14
ZBTB6	0.6339	0.00E+00
ZC3H12D	0.8062	1.09E-19
ZC3H18	0.6192	7.20E-10
ZC3HAV1	0.7125	8.68E-14
ZCCHC18	0.7028	2.60E-13
ZCCHC3	0.8315	7.21E-22
ZCCHC7	0.7953	7.51E-19
ZCCHC8	0.7154	6.21E-14
ZDBF2	0.6923	0.00E+00
ZDHHC13	0.7513	6.56E-16
ZDHHC16	0.6639	0.00E+00
ZDHHC23	0.6695	8.33E-12
ZDHHC6	0.7644	1.02E-16
ZFC3H1	0.6202	6.65E-10
ZFP62	0.7377	3.97E-15
ZFPM1	0.7176	4.77E-14
ZFR2	0.6127	1.21E-09
ZFYVE27	0.6780	3.57E-12
ZGLP1	0.6914	8.96E-13
ZHX2	0.7183	4.38E-14
ZMIZ2	0.7650	9.24E-17
ZMYND19	0.6666	1.09E-11
ZNF101	0.8218	5.48E-21
ZNF107	0.7967	5.90E-19
ZNF12	0.7231	2.48E-14
ZNF121	0.6427	9.90E-11
ZNF124	0.7551	3.86E-16
ZNF14	0.7633	1.20E-16
ZNF141	0.8179	1.17E-20

ZNF146	0.6839	0.00E+00
ZNF157	0.6829	2.18E-12
ZNF165	0.6710	7.17E-12
ZNF169	0.6704	7.57E-12
ZNF184	0.6154	8.25E-10
ZNF195	0.6081	1.74E-09
ZNF202	0.6694	8.40E-12
ZNF211	0.7427	2.07E-15
ZNF224	0.6386	1.42E-10
ZNF225	0.6534	0.00E+00
ZNF230	0.6780	3.57E-12
ZNF264	0.6095	1.55E-09
ZNF266	0.7902	1.78E-18
ZNF276	0.7804	8.82E-18
ZNF292	0.7770	1.52E-17
ZNF296	0.8118	3.81E-20
ZNF316	0.6699	7.96E-12
ZNF317	0.7440	1.74E-15
ZNF318	0.7185	4.28E-14
ZNF335	0.7554	3.68E-16
ZNF337	0.6441	8.75E-11
ZNF33B	0.6067	1.93E-09
ZNF354C	0.6285	0.00E+00
ZNF37BP	0.7364	4.74E-15
ZNF382	0.7137	7.55E-14
ZNF394	0.6164	8.99E-10
ZNF430	0.6905	9.89E-13
ZNF439	0.8520	6.60E-24
ZNF469	0.6399	0.00E+00
ZNF485	0.6728	6.01E-12
ZNF486	0.6458	0.00E+00
ZNF512	0.7048	2.08E-13
ZNF525	0.7422	2.21E-15
ZNF529	0.7660	8.01E-17
ZNF540	0.7173	4.93E-14
ZNF548	0.7238	2.28E-14
ZNF549	0.6384	1.45E-10

ZNF557	0.6776	0.00E+00
ZNF558	0.6953	5.95E-13
ZNF568	0.6135	1.17E-09
ZNF578	0.6308	2.77E-10
ZNF585B	0.6147	9.51E-10
ZNF586	0.8211	6.25E-21
ZNF589	0.7146	6.83E-14
ZNF594	0.7292	1.17E-14
ZNF600	0.6821	2.37E-12
ZNF606	0.6885	1.21E-12
ZNF619P1	0.7789	1.11E-17
ZNF627	0.6421	0.00E+00
ZNF655	0.7762	1.72E-17
ZNF671	0.7571	2.89E-16
ZNF681	0.7348	5.79E-15
ZNF683	0.6611	1.86E-11
ZNF692	0.8199	7.88E-21
ZNF700	0.7838	5.09E-18
ZNF708	0.7330	7.25E-15
ZNF710	0.7836	5.32E-18
ZNF711	0.6183	7.72E-10
ZNF736	0.6215	5.95E-10
ZNF738	0.6114	1.34E-09
ZNF74	0.6587	0.00E+00
ZNF76	0.7938	9.69E-19
ZNF764	0.7198	3.67E-14
ZNF767P	0.6253	4.38E-10
ZNF786	0.6692	8.55E-12
ZNF80	0.6568	2.76E-11
ZNF815P	0.7348	5.78E-15
ZNF830	0.7359	5.05E-15
ZNF831	0.8337	4.52E-22
ZNF84	0.6329	0.00E+00
ZNF853	0.6256	0.00E+00
ZNF860	0.7514	6.40E-16
ZNF862	0.6750	4.84E-12
ZNF875	0.6391	1.36E-10

ZNF879	0.6741	5.29E-12
ZNF92	0.7192	3.95E-14
ZNRF3	0.6552	0.00E+00
ZWINT	0.6178	8.06E-10

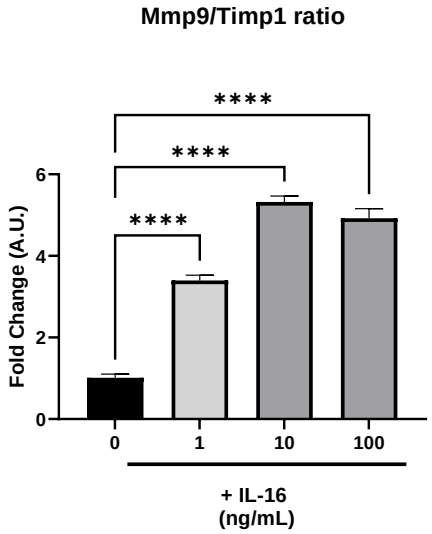

Figure S1. MMP9/TIMP1 ratio

3T3-L1 mature adipocytes were treated with increasing doses of IL-16. Data are represented as relative mRNA level (arbitrary units (A.U.)), relative to dose 0 ng/mL of IL-16, and expressed as mean±SEM; n=4. Data were analyzed by ordinary one-way ANOVA followed by uncorrected Fisher LSD, *p<0.05, **p<0.01, ***p<0.001, ****p<0.0001.

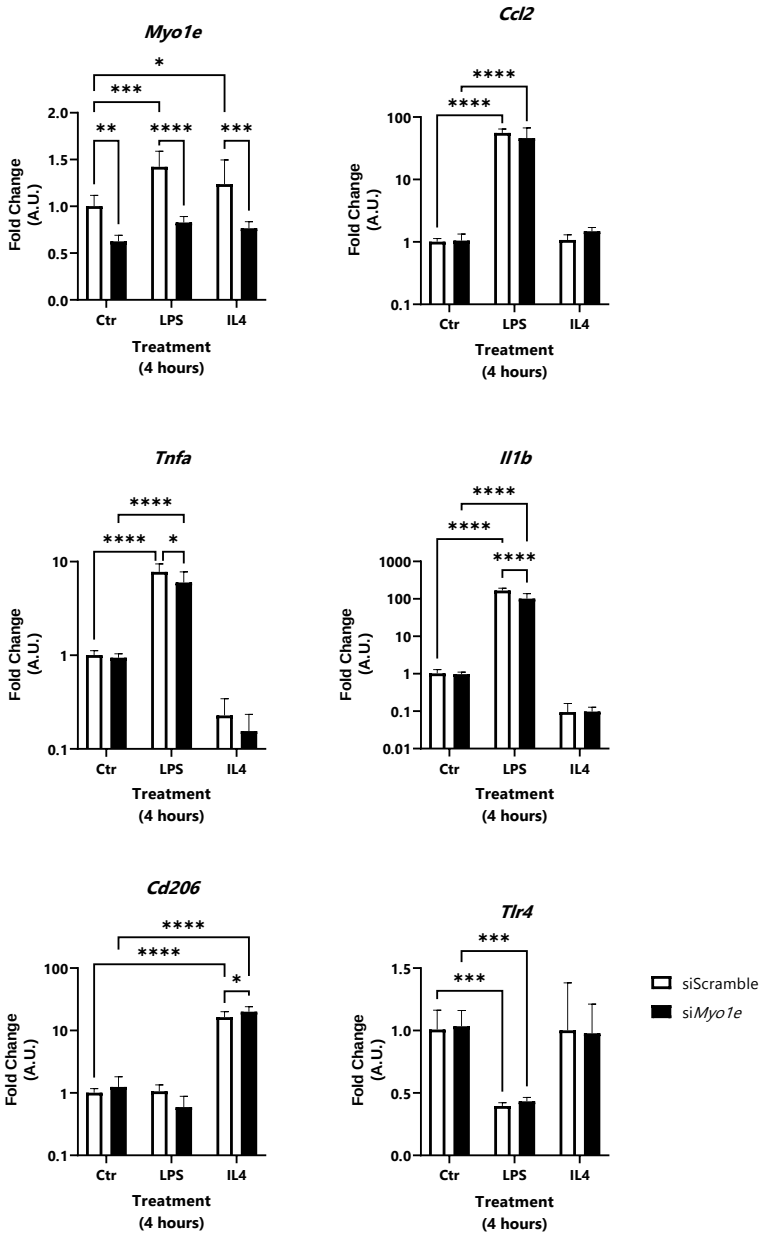

Figure S2. M1 and M2 polarization markers of RAW264.7 transfected with Myo1e siRNA.

Cells were transfected and then, treated with medium (control), 60 ng/mL LPS or 40 ng/mL IL-4 for 4 h. Data are represented as relative mRNA level (arbitrary units (A.U.)), relative to control group. Data represent mean±SEM (n=4). Data were analyzed by ordinary one-way ANOVA followed by uncorrected Fisher LSD, *p<0.05, **p<0.01, ***p<0.001, ****p<0.0001.

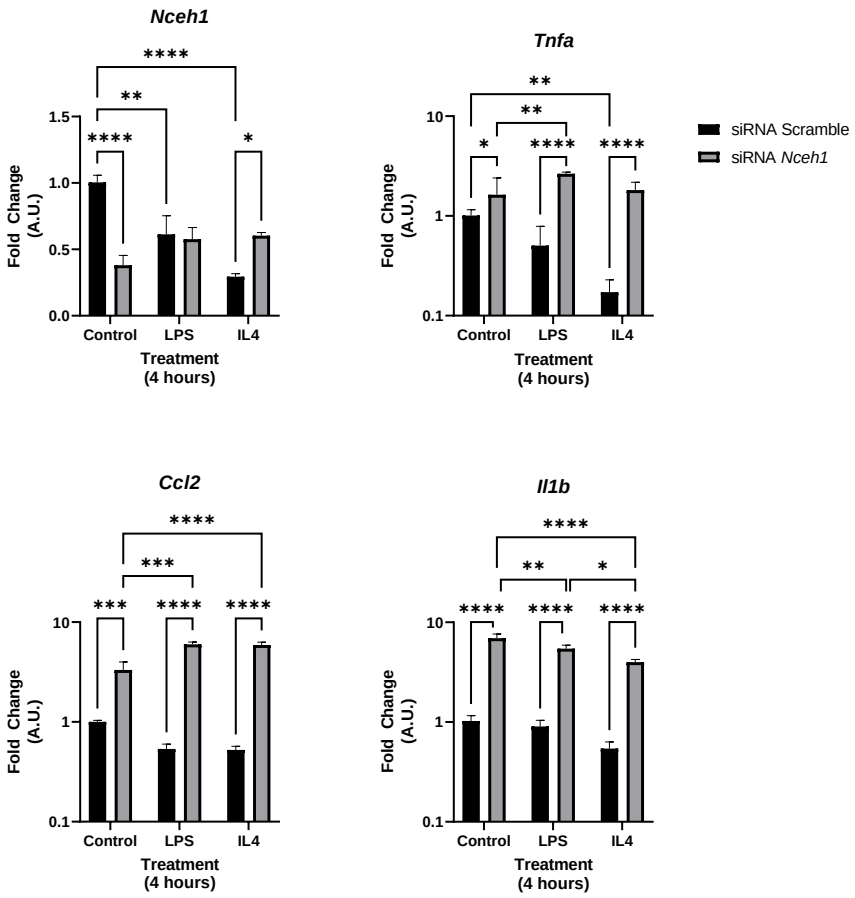

Figure S3. M1 and M2 polarization markers of RAW264.7 transfected with *Nceh1* siRNA.

Cells were transfected and then, treated with medium (control), 60 ng/mL LPS or 40 ng/mL IL-4 for 4 h. Data are represented as relative mRNA level (arbitrary units (A.U.)), relative to control group. Data represent mean±SEM (n=4). Data were analyzed by ordinary one-way ANOVA followed by uncorrected Fisher LSD, *p<0.05, **p<0.01, ***p<0.001, ****p<0.0001.